PHASE BEHAVIOR OF MULTIRESPONSIVE MICROGEL DISPERSIONS

A Dissertation
Presented to
The Academic Faculty

By

Saet Byul Debord

In Partial Fulfillment
Of the Requirements for the Degree
Doctor of Philosophy in the School of Chemistry and Biochemistry

Georgia Institute of Technology

May, 2006

PHASE BEHAVIOR OF MULTIRESPONSIVE MICROGEL DISPERSIONS

Approved by:

Dr. L. Andrew Lyon
School of Chemistry and Biochemistry
Georgia Institute of Technology

Dr. Victor Breedveld
School of Chemical and Biomolecular engineering
Georgia Institute of Technology

Dr. Thomas Orlando
School of Chemistry and Biochemistry
Georgia Institute of Technology

Dr. Mohan Srinivasarao
School of Polymer, Textile, and Fiber Engineering
Georgia Institute of Technology

Dr. Marcus Weck
School of Chemistry and Biochemistry
Georgia Institute of Technology

Date Approved: Nov., 21, 2005

Acknowledgements

The journey that I traveled the past few years at Tech was hard and there are many people to whom I would like to show my appreciatiation. I would like to thank my advisor Dr. L. Andrew Lyon for his support and encouragement. I believe that I had a great opportunity to work for a wonderful scientist and learned a lot from him. He is not only intelligent but also loves science. Most of all, he has a positive attitude and patience so that he helped me to accomplish many things under imperfect conditions. Also, I would like to show my appreciation to Dr. Victor Breedveld for helping me understand physics and give me generous advice. I deeply appreciate that my parents encouraged me to be a scientist and support me to move forward into a bigger world. Without their encouragement and support, I would not have been able to accomplish this much. I would like to thank my sister and brother because they are good friends and continue to pray for me. I would like to thank the Lyon group members: Ashlee and Courtney for their intelligent advice on science and grammar (I really appreciate your help). Johnny and Bart for showing endless enthusiasm toward something other than just science (usually sports). Christine and Caroline for encouraging me to be positive. Ryan for helping me out while I was gone. Neetu, Hyungie, Jonseong and other former members for being good friends. Jun, Ray, Jae-Kyu and Vivek for helping me survive the world of rheology. I would like to thank God that he gives me all of these opportunities and wonderful people specially my husband, Justin. Justin, I would like to thank for your support-intellectually, emotionally, and spiritually. For the past years, we have gone through difficult times since we were separated. But through every trial you have been always a devoted husband and a good father. I really appreciate that you took care of our son so

that I can finish this journey. I owe you a lot and I will always be there for you. I love you, I miss you, and I will see you soon.

TABLE OF CONTENTS

ACKNOWLEDGEMENTS iii

LIST OF TABLES viii

LIST OF FIGURES xi

SUMMARY xii

LIST OF ABBREVIATIONS xiii

CHAPTER 1: Introduction 1

1.1 Colloidal Dispersions 1

1.2 Colloidal crystals and Their Applications 2

1.3 Interaction Potentials and Phase Diagrams of Colloidal Particles 3

1.3.1 Hard Sphere and Soft Sphere Systems 4
1.3.2 Lennard-Jones Potential 6
1.3.3 Yukawa Potential 7
1.3.4 DLVO Theory 9
1.3.5 Colloidal Dispersions with Other Interactions 11

1.4 Kinetics of Crystallization 12

1.5 Microgel Particles as a New Building Block of Colloidal Self-Assemblies 12

1.5.1 Responsive Microgels 13
1.5.2 Preparation and Characterization of Microgels 15
1.5.3 Responsive Microgels : New Building Block for Colloidal Crystals 16

References 18

CHAPTER 2: Influence of Particle Volume Fraction on Packing in Responsive Microgel Colloidal Crystals 30

2.1 Introduction 30

2.2 Experimental 32

2.3 Results and Discussion 35

2.4 Conclusions 47

References 47

CHAPTER 3: Shift Factor Determination 52

3.1 Introduction 52

3.2 Experimental 56

3.3 Results and Discussion 60

3.4 Conclusions 68

References 68

CHAPTER 4: Effect of Attractive Interaction on the Phase Behavior of pH Responsive Microgel Assemblies 71

4.1 Introduction 71

4.2 Experimental 73

4.3 Results and Discussion 77

4.4 Conclusions 90

References 90

CHAPTER 5: Crystallization Evolution of pH Responsive Microgel Dispersions 94

5.1 Introduction 94

5.2 Experimental 97

5.3 Results and Discussion 98

5.5 Conclusions 124

References 125

CHAPTER 6: Phase Behavior of Charged pH Responsive Colloidal Dispersions 128

6.1 Introduction 128

6.2 Experimental 131

6.3 Results and Discussion 132

6.4 Conclusions 141

References 142

APPENDIX A 146

LIST OF TABLES

Table **Page**

3.3-1 Average relative viscosity and its standard deviation of *p*NIPAm-*co*-AAc microgel dispersions in pH 3.0 (15 mM) buffer solution 63

3.3-2 Average relative viscosity and its standard deviation of *p*NIPAm-*co*-AAc microgel dispersions in pH 3.85 (15 mM) buffer solution 63

3.3-3 Average relative viscosity and its standard deviation of *p*NIPAm-*co*-AAc microgel dispersions in pH 6.5 (100 mM) buffer solution 63

3.3-4 The shift factors and confidence range at 90 % confidence level of *p*NIPAm-*co*-AAc microgel dispersions of different pH at 22 °C and 25 °C 67

3.3-5 Shift factor ratio, volume ratio and shift factor (*k'*) calculated from volume ratio of *p*NIPAm-*co*-AAc microgel dispersions of different pH at 22 °C 67

3.3-6 Shift factor ratio, volume ratio and shift factor (*k'*) calculated from volume ratio of *p*NIPAm-*co*-AAc microgel dispersions of different pH at 25 °C 67

4.3-1 The center-to-center distance of various effective volume fraction microgel dispersion calculated from *g(r)* 87

6.3-1 The center-to-center distance calculated from *g(r)* 137

LIST OF FIGURES

Figure **Page**

1.3-1 Equilibrium hard-sphere phase diagram 6

1.5-1 Chemical structures of N-isopropylacrylamide, N,N'-methylene (bisacrylamide), and acrylic acid 14

1.5-2 A volume phase transition behavior from *p*NIPAm-*co*-AAc microgels in 1 mM ionic strength solutions. 15

2.2-1 Method of microgel crystal assembly for microscope observation 35

2.3-1 Photo correlation spectroscopy as a function of temperature for *p*NIPAm-*co*-AAc microgel particles at pH 3.56 and pH 4.96 37

2.3-2 Series of optical sections of laser scanning confocal microscopy images of fluorescein-dyed *p*NIPAm-*co*-AAc microgel colloidal crystal 39

2.3-3 Differential interference contrast microscopy images of colloidal crystals assembled from *p*NIPAm-*co*-AAc microgel particles 43

2.3-4 Differential interference contrast microscopy images of colloidal crystals assembled from *p*NIPAm microgel particles 46

3.2-1 A volume phase transition behavior from *p*NIPAm-*co*-AAc microgels 57

3.3-1 Shear viscosity of *p*NIPAm-*co*-AAc microgel dispersions as a function of shear rate at 22 °C and at 25 °C 62

3.3-2 The relative viscosity of microgels vs. microgel concentration in weight percent plot 66

4.3-1 Photographs of *p*NIPAm-*co*-AAc dispersions in rectangular glass tubes at pH 3.85 79

4.3-2 Photographs of *p*NIPAm-*co*-AAc dispersions in rectangular glass tubes at pH 3.0 80

4.3-3 Differential interference contrast microscopy images of colloidal dispersions assembled from *p*NIPAm-*co*-AAc microgels dispersed in pH 3.85 buffer solution. 83

4.3-4 Particle trajectories of *p*NIPAm-*co*-AAc microgel assemblies dispersed in pH 3.85 buffer solution. 84

4.3-5 (a) MSD vs. lag time plots of microgel assemblies dispersed in pH 3.85 buffer as effective volume fraction changes. (b) Radial distribution function of the same microgel dispersions as (a). 87

4.3-6 Photographs of microgel dispersions of ϕ_{eff}= 0.57 in glass tubes at pH 3.85 as the crystal is heated. 89

4.3-7 Photographs of microgel dispersions of ϕ_{eff}= 0.53 in glass tubes at pH 3.0 as the crystal is heated. 89

5.3-1 Photographs of *p*NIPAm-*co*-AAc dispersions in a rectangular glass tube upon aging. These photographs were taken from ϕ_{eff} = 0.48 ($\phi_{eff,calculated}$ =0.38) microgel dispersion at pH 3.85. 100

5.3-2 Photographs of *p*NIPAm-*co*-AAc dispersions in a rectangular glass tube upon aging. These photographs were taken from ϕ_{eff} = 0.53 microgel dispersion at pH 3.0. 101

5.3-3 DIC images and trajectories of pH 3.85 *p*NIPAm-*co*-AAc microgel dispersion at ϕ_{eff}=0.48 ($\phi_{eff,calculated}$ =0.38). 104

5.3-4 The MSD evolution of *p*NIPAm-*co*-AAc microgel dispersions at pH 3.85 upon aging. The movies were recorded at 25 mm from the ends. 108

5.3-5 The MSD evolution of *p*NIPAm-*co*-AAc microgel dispersions at pH 3.85 upon aging. The movies were recorded at 12.5 mm from the ends. 109

5.3-6 The MSD evolution of *p*NIPAm-*co*-AAc microgel dispersions at pH 3.0 upon aging. The movies were recorded at 25 mm from the ends. 110

5.3-7 The MSD evolution of *p*NIPAm-*co*-AAc microgel dispersions at pH 3.0 upon aging. The movies were recorded at 12.5 mm from the ends. 111

5.3-8 The MSD evolution of *p*NIPAm microgel dispersions upon aging. 112

5.3-9 Radial distribution of microgel assemblies over time. ϕ_{eff} = 0.48 ($\phi_{eff,calculated}$ =0.38), at pH=3.85. 113

5.3-10 Particle trajectories of *p*NIPAm-*co*-AAc microgels at the interface of crystal and fluid. The microgel are dispersed in pH 3.85 buffer solution. 116

5.3-11 Radial distribution of day 0 sample at different positions. Microgels are redispersed in pH=3.85 buffer solution and have ϕ_{eff} = 0.48 ($\phi_{eff,calculated}$ =0.38). 117

5.3-12 Crystal growth of *p*NIPAm-*co*-AAc microgels at the interface of crystal and fluid. (a) 0 minute, (b) 5 minutes after (a), and (c) 10 minutes after (a). 118

5.3-13 The MSD vs, lag time plot calculated from different positions over time. 119

5.3-14 Melting transition of microgel dispersions of ϕ_{eff}= 0.57 in a glass tube at pH 3.85 at day 0. 122

5.3-15 Melting transition of microgel dispersions of ϕ_{eff}= 0.57 in a glass tube at pH 3.85 at day 1. 122

5.3-16 Melting transition of microgel dispersions of ϕ_{eff}= 0.57 in a glass tube at pH 3.85 at day 9. 123

5.3-17 Melting transition of microgel dispersions of ϕ_{eff}= 0.53 in a glass tube at pH 3.0 at day 7. 123

6.3-1 DIC micrograph images of *p*NIPAm-*co*-AAc microgels (R_h = 450 nm at 22 °C) dispersed in pH 6.5 buffer solution. At 25 mm. 135

6.3-2 Particle trajectories of *p*NIPAm-*co*-AAc microgels (R_h = 450 nm at 22 °C) dispersed in pH 6.5 buffer solution. At 25 mm. 136

6.3-3 The radial distribution function of the responsive microgel dispersions at pH 6.5. ϕ_{eff}= 0.66, ϕ_{eff}= 0.59, ϕ_{eff}= 0.56, ϕ_{eff}= 0.52, ϕ_{eff}= 0.50 and ϕ_{eff}= 0.45. 137

6.3-4 The MSD evolution of microgel dispersions upon aging at 25 mm from the end 139

6.3-5 The MSD evolution of microgel dispersions upon aging at 12.5 mm from the end 140

SUMMARY

In this thesis, pH and thermo-responsive microgels, poly-(N-isopropylacrylamide)-*co*-acrylic acid) (*p*NIPAm-*co*-AAc), are utilized as a building block for colloid crystals. The pH responsivity allows us to tune the effective interaction between particles and to explore the phase behavior of such microgel dispersions under different conditions. Chapter 1 presents brief introduction for colloidal crystals, their interactions and phase behaviors. Also, responsive microgels are introduced as a new building block to prepare colloidal crystals. Chapter 2 describes the particle concentration effect on the phase diagram of *p*NIPAm-*co*-AAc microgel assemblies. In chapter 3, the shift factors of *p*NIPAm-*co*-AAc microgel dispersions at different pHs are determined. These shift factors allow one to calculate the effective volume fraction of each sample. In chapter 4, the effect of attractive interaction on the phase behavior of *p*NIPAm-*co*-AAc dispersions is discussed. The attractive interaction is achieved by changing the pH of dispersions close to the pK_a of microgel. The phase diagram is obtained and further quantative analyses are performed at pH << pK_a and at pH close to the pK_a. Chapter 5 details the phase evolution of *p*NIPAm-*co*-AAc microgel dispersions in the presence of weak cooperative interactions. More quantative analysis is utilized to see the evolution and this evolution helps to understand the energetics of the system. Finally, the last chapter explores the phase behavior of *p*NIPAm-*co*-AAc microgels redispersed in pH >> pK_a. At pH >> pK_a, microgels are charged and the effective interaction between particles are different from the previous chapters.

LIST OF ABBREVIATIONS

AAc	Acrylic acid
AFA	4-Aminofluorescein
A_H	Hamaker constant
APS	Ammonium persulfate
BIS	*N, N'* Methylenebisacrylamide
CLSM	Confocal laser scanning microscopy
d	diameter of colloidal particles
D	Diffusion coefficient
DIC	Differential image contrast
ε	Dielectric constant
e	Electronic charge
EDC/EDAC	1-[3-(dimethylamino)propyl]-3-ethylcarbodiimide HCl
g(r)	Radial distribution function
η	Viscosity
η_0	Solvent viscosity
k_B	Boltzmann's constant
LCST	Lower critical solution temperature
MSD	Mean square displacement
NHS	*N*-Hydroxysuccinimide
NIPAm	N-Isopropylacrylamide
ϕ	Volume fraction

ϕ_{eff}	Effective volume fraction
PBS	Phosphate Buffered Saline
PBG	Photonic band gap
PCS	Photon correlation spectroscopy
PEG	Poly(ethylene glycol)
*p*NIPAm	Poly *N*-Isopropylacrylamide
*p*NIPAm-*co*-AAc	Poly(*N*-isopropylacrylamide-*co*-acrylic acid)
r	Interparticle distance
R_h	Hydrodynamic radius
SDS	Sodium dodecyl sulfate
T	Absolute temperature
TBAm	Tert-butyl acrylamide
$U(r)$	Interparticle potential
$U_{HS}(r)$	Hard sphere interparticle potential
$U_{DLVO}(r)$	DLVO pair potential
$U_{vdW}(r)$	van der Waals pair potential
UV-VIS	Ultraviolet-visible spectroscopy
VPT	Volume phase transition
VPTT	Volume phase transition temperature
Z	Charge on the particle

CHAPTER 1

Introduction

The intention of this chapter is to introduce colloidal dispersions, the interaction potentials that govern different colloidal dispersions, colloidal phase behavior, colloidal crystallization kinetics and finally responsive hydrogel microparticles (microgels) as a new building block for colloidal crystals. These materials will be introduced and the relevant literature will be discussed. The chapter will conclude with a brief discussion of the intended application of responsive microgels for this research project.

1.1 Colloidal Dispersions

Colloidal dispersions are composed of mesoscopic solutes (the dispersed phase), i.e. species with sizes 1 nm ~ 1 μm, dispersed into a solvent whose molecules are much smaller in size (so called dispersion medium, typically of atomic or molecular dimensions).[1] Here the mesoscopic solutes can be spheres, ellipsoidal particles, rods or plates, but this thesis will only cover spherical particles for convenience. Depending on the dispersed phases and dispersion media, the type of colloidal dispersions can be varied. In addition to solutes and dispersion medium, colloidal dispersions may contain other, smaller species such as short polymeric chains, ions dissociated from salts, etc.

Colloidal dispersions have been used in foods,[2] paints,[3] coatings,[4, 5] papers,[6] cosmetics,[7] and pharmaceutics[8-10] for a long time. It was not until relatively recently that colloidal dispersions have been studied extensively for their fundamental properties as

well as applications. The following section will cover crystalline colloidal arrays and their applications.

1.2 Colloidal Crystals and Their Applications

Colloidal crystals are ordered arrays of colloidal particles. Colloidal crystals can be prepared artificially, but they also occur naturally. The example of the naturally formed colloidal crystal is the precious gem opal, which is formed by sedimentation of silicate particles.[11-13] The process of colloidal crystallization has been intensively studied, leading to the development of several methods to prepare high quality crystals. These techniques include slow sedimentation,[14-16] centrifugation,[17-19] controlled drying method,[20-22] colloidal epitaxy,[23, 24] depletion-induced crystallization,[25, 26] physical confinement[27, 28] and electrophoretic deposition.[29, 30]

The periodicity of the assembly makes Bragg diffractions appear in the visible part of the spectrum as a beautiful iridescence, which can be described by Bragg's law.

$$m\lambda = 2nd\sin\theta \qquad (1\text{-}1)$$

where λ is the Bragg wavelength, m is the diffraction order, d is the interlayer spacing, θ is the diffraction angle and n is the composite refractive index. Here, the color i.e. the wavelength of diffracted light of the colloidal crystals can be systematically changed by varying interlayer spacing. The interlayer spacing can be tuned by changing the size of particles[21] or changing the edge to edge particle spacing.[31-33]

These assemblies have found potential applications in a wide range of areas, including sensors,[34, 35] optical filters,[36] switches,[33, 37] and photonic crystals. Here, the photonic crystal applications will be reviewed briefly. A photonic crystal is a periodic structure fabricated from materials having different dielectric constants. Light traveling through such crystals experiences a periodic variation of the refractive index, analogous to the periodic potential energy of an electron in atomic crystals. Since the concept of photonic crystals was proposed independently by John[36] and Yablonovitch,[38] huge effort has been devoted to develop materials and structures that could support and expand their initial hypotheses.[39-44] Colloidal crystals created via self-assembly offer an alternative route to fabricating periodical dielectric materials rather than lithographic methods.[45]

1.3 Interaction Potentials and the Phase Diagrams of Colloidal Particles

Due to relatively slow diffusion and a large enough length scale to be seen under an optical microscope, colloidal dispersions are good model systems for the study of fundamental problems of condensed matter physics such as crystal nucleation, phase behavior, and interaction potentials. On top of this experimental accessibility, the magnitude and length scales of the interparticle potential can be varied systematically. This tunability makes colloidal dispersions an excellent model system for investigating phase behavior of colloidal dispersions. Also recent developments in digital image processing combined with video microscopy[46-50] provide excellent tools for studying colloidal dispersions. Confocal laser scanning microscopy (CLSM) is specially useful as it enables to study the structure and dynamics of colloidal particles on a single particle level in three-dimensional (3D) real space.[23, 51-55]

Numerous experimental and theoretical studies have explored the interaction potential[56-58] and phase behavior[59-61] of colloidal dispersions. In this section, the interparticle potential that governs the phase behavior will be reviewed.

1.3.1 Hard Sphere and Soft Sphere Systems

In a hard sphere system, two particles do not interact with each other until they are in contact. Since they are incompressible like two billiard balls, when they approach too close, they strongly repel due to steric repulsion i.e. the repulsive interaction becomes infinite.

$$U_{HS}(r) = \begin{cases} 0 & r \geq d \\ \infty & r \leq d \end{cases} \qquad (1\text{-}2)$$

where U_{HS}(r) is hard sphere interparticle potential, d is diameter, and r is interparticle distance.

Since the attractive interaction between spheres is negligible, enthalpy does not play a role in determining the phase behavior of colloidal dispersions. As a result, the crystallization is driven by entropy and occurs at a concentration where the decrease in the global (or configurational) entropy of the system is more than offset by the increase in the local (or free-volume) entropy. Theoretical as well as experimental results reveal that the face-centered cubic (fcc) structure is the lowest free energy configuration for colloids with repulsive electrostatic,[62, 63] hard sphere,[15, 51] and attractive van der Waals potentials.[64, 65] Also, it is known that fcc structure has a maximum particle fill fraction of 74%.[66]

In many experiments, polymer latex particles are used as hard sphere-like particles. Usually, colloidal stability in the solution is a problem, i.e. without stabilization colloidal particles tend to aggregate due to van der Waals attractive force. To achieve the hard sphere limit, most research groups 1) match the refractive indices (or dielectric constant) of the sphere and the solvent so that van der Waals attraction between the spheres are almost the same as those between a sphere and the solvent,[53] 2) graft polymer chains to the sphere to suppress the effect of van der Waals interaction (steric stabilized).[59, 67]

Sterically stabilized polymethylmethacrylate (PMMA) spheres behave as hard sphere-like polymer latex particles. Interaction potential studies showed that PMMA reveal model hard sphere behavior i.e. short ranged steric repulsion between two particles.[59] And phase behavior studies show that hard sphere-like colloidal particle dispersions undergo disorder to order transition with increasing particle concentrations,[16, 59, 68] the volume fraction (ϕ) where freezing and melting occur is near that predicted via computer simulations for theoretically hard spheres.[66] Fig. 1.3-1 illustrates the phase diagram of hard spheres. Here, the particle dispersion below ϕ of 0.494 shows a disordered fluid phase, where particle positions are not correlated over long distances. In the region between ϕ of 0.494 and 0.545, liquid-solid coexistence is observed. Above 0.545 volume fraction, dispersions are solid phase where particle motion and position are highly correlated over long distances. Under these conditions, the particles tend to enter a kinetically trapped glassy phase with increasing particle concentration.[52, 69-73] A number of theoretical calculations and experimental measurements have been done to predict the maximum volume fraction for glassy phase, obtaining ~ 0.64.[74]

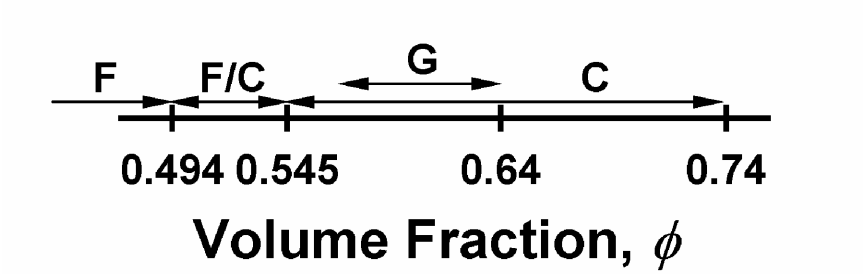

Figure 1.3-1 Equilibrium hard-sphere phase diagram. F: fluid, F/C: coexistence of fluid and crystal, C: crystal, and G: glassy phase.

Unlike the hard sphere interactions of stabilized latexes (such as PS, PMMA, and silica), star polymers,[75-82] polyelectrolyte stars,[83-86] ionic gels[87, 88] and cross-linked particles dispersed in good solvent[89] provide a different system that can be used to examine the effects of interparticle interactions and phase behavior of spheres due to their softness i.e. particles are interpenetrable and deformable. This softness is due to steric and/or compressive forces related to dangling chains on the particle surface and change interaction potential i.e. the slope of the repulsive interaction is less steep. Because particle deformation and deswelling can lead to high particle concentration, it is possible to have effective volume fractions greater than 0.74.[90, 91] One interesting feature of the phase behavior of soft spheres is that depending on the particle softness and density a wider variety of phases such as body-centered orthogonal (bco), and diamond crystals were theoretically predicted.[79]

1.3.2 Lennard-Jones Potential

When a spontaneously forming electric dipole on one molecule induces on a neighboring molecule another dipole which tends to align itself with the former, there

exists an attractive force between the particles namely the van der Waals interaction (so called dispersion force). For neutral particles, the effective interaction is determined in equilibrium by means of an attracting van der Waals force and a repelling force due to impenetrable nature. The total interparticle potential is obtained by summing the attractive and repulsive potentials. The potential resulting from these attractive and repulsive interactions is called the Lennard-Jones potential (LJ potential or '6-12' potential) and is described by the following equation:

$$U_{LJ}(r) = 4\varepsilon_{LJ}\left[\left(\frac{d_C}{r}\right)^{12} - \left(\frac{d_C}{r}\right)^{6}\right] \qquad (1\text{-}3)$$

Here, r is the interparticle distance, d_c is the hard sphere diameter of a particle and ε_{LJ} is the depth of the attractive well which is scaled by k_BT. The term $1/r^{12}$, dominating at short distance, models the repulsion between particles when they are brought very close to each other. The term $1/r^6$, dominating at longer distance, constitute the attractive part. A $1/r^6$ attraction originates from van der Waals dispersion forces, which are due to dipole-dipole interactions. Due to the simplicity, many groups use LJ potential for model interaction to predict structure and phase of colloidal dispersions.[92]

1.3.3 Yukawa Potential

In suspension, charged colloids are surrounded by a cloud of counter-ions. This counter-ion double layer screens the pure Coulomb interaction between the colloids. The

hard-core Yukawa potential (screened-Coulombic repulsion) is a standard model to describe this electrostatic repulsions between charged particles in suspension.

$$\beta U_Y(r) = \begin{cases} \infty & r \le d \\ \beta\varepsilon \dfrac{\exp(-\kappa(r-d))}{r/d} & r \ge d \end{cases} \quad (1\text{-}4)$$

$$\kappa = \left(\sum_i n_i z_i^2 / k_B T \varepsilon_0 \varepsilon \right)^{1/2} \quad (1\text{-}5)$$

Here, d is hard-core diameter, βε is the potential in units of k_BT, e is the electronic charge, z_i is the charge on the particle, ε is the dielectric constant of the medium, and κ^{-1} is the Debye-Hückel screening length.

In charge stabilized dispersions, the magnitude of the interparticle potential and the range of repulsive interaction can be tuned by varying salt (electrolyte) concentration, volume fraction, the charge on the particle, etc.[53, 93, 94] The easy tunability of the interparticle potential makes charged colloidal dispersions an excellent model system for studies of phase transition and ordering phenomenon. For example, at low ionic strength, the repulsion is long ranged, producing crystalline phase at volume fraction as low as 0.1 %.[1] Increasing ionic strength yields short ranged repulsive interaction, the attractive component of the potential being negligible. This results in an increase in the freezing point volume fraction to near that for ideal hard spheres.[95] There are some interesting reports observed in charged spheres such as reentrance of phases, exotic phases etc. Under suitable circumstances a reentrant such as bcc → fcc → bcc transition was predicted as salt was added.[95] According to a theoretical calculation, the phase diagram of

charged colloids exhibits exotic phases such as body-centered-orthorhombic (bco), body-centered-tetragonal (bct) in addition to the more common face-centered-cubic (fcc).[96]

1.3.4 DLVO Theory

It is known that the van der Waals attraction of microscopic dipoles scales as $-r^{-6}$. For the van der Waals interaction (U_{vdW}) between two large spheres is as follows.

$$U_{vdW} = -\frac{A_H}{6}\left[\frac{2a^2}{r^2-4a^2} + \frac{2a^2}{r^2} + \ln\left(\frac{r^2-4a^2}{r^2}\right)\right] \qquad (1\text{-}6)$$

Here A_H is the Hamaker constant, r is center-to-center distance and a is the particle radius. The Hamaker constant can be expressed as;

$$A_H = \frac{3h\nu\left(n_1+n_2\right)^2\left(n_1-n_2\right)^2}{16\sqrt{2}\left(n_1^2+n_2^2\right)^{3/2}} \qquad (1\text{-}7)$$

where h is Plank's constant, ν is a characteristic frequency and n_1, n_2 are the optical refractive indices of the colloids and the solvent, respectively. This van der Waals force leads to irreversible aggregation of unprotected particles and it is desirable to suppress its magnitude. Common mechanisms for reducing the effect of van der Waals attraction are steric stabilization and charge stabilization as mentioned earlier.

The standard theory of interaction between charged colloidal particles is explained by Deryagin-Landau-Verwey-Overbeek (DLVO) theory. The DLVO potential

includes (i) steric repulsion due to finite diameter of the colloidal spheres (ii) screened Coulombic repulsion (or Yukawa repulsion) with the screening length given by Debye-Hückel screening length and (iii) short-range (a few nm typically) van der Waals attraction.[97]

$$U_{DLVO}(r) = U_{HS}(r) + U_{Y}(r) + U_{vdW}(r) \qquad (1\text{-}8)$$

The relative strengths of these contributions can be varied by changing the solvent, salt concentration, or temperature. For example, adding salt to a dispersion decreases Debye-Hückel screening length, hence the van der Waals attraction becomes relatively more pronounced causing reversible vapor-liquid coexistence or irreversible flocculation if salt concentration is high enough.[98] Conversely, decreasing the salt concentration makes the screened-Coulombic repulsion larger, thereby stabilizing the suspensions by masking the van der Waals attractions. This describes well a first-order fluid-to-crystal transition upon increasing the colloidal density and the existence of colloidal crystals at low effective volume fraction.[1]

In many studies, the DLVO formulation avoids complexity originated from the solvent and ions. Despite the simplified approximations, the DLVO theory has been successful in explaining some experimental data as the model for colloidal electrostatic interactions.[57, 99, 100] However some extremely low salt concentration dispersions do not behave as DLVO theory predicts; for example large stable voids in colloidal fluid,[101, 102] anomalously small lattice constants in colloidal crystals[103, 104] and unusual fluid/crystal coexistence have been observed.[55, 56, 105-108] To explain the long-range interaction between

charge-stabilized colloidal suspensions, Sogami-Ise introduced long-range pairwise attractions mediated by counterion distributions.[109, 110] However, very recent direct interaction measurements show that the Sogami-Ise theory does not correctly describe the interactions between unconfined pairs of particles.[99] The existence and behavior of superheated colloidal crystals suggest that many-body effects may contribute an attractive component to the pairwise interactions between charged particles.[56, 111]

1.3.5 Colloidal Dispersions with Other Interactions

When free non-adsorbing short polymer chains (or small particles) are introduced into colloidal particle dispersions, a short-ranged attractive interaction known as depletion force is generated. The physical origin of this interaction in polymer/large colloid mixture or small colloid/large colloid mixture is due to osmotic depletion effect. When two large particles approach each other, polymer chains (or small particles) are expelled out from the region in between two large particles. The osmotic pressure due to small spheres in the depletion region is lower than that in the outer regions. This imbalance of the osmotic pressure results in an effective attractive interaction between the large particles. This eventually leads to an entropically driven phase separation. As a result of the attractive interaction between large particles, the large particles form glassy or crystalline phases.[112-114] A similar mechanism explains the attraction of large spheres towards a wall or steps.[115, 116]

1.4 Kinetics of Crystallization

The kinetics of crystallization of colloidal dispersions has been the subject of study due to the ability of the dispersions to mimic molecular crystallization, and due to the relatively easy experimental accessibility for their size and slow diffusion. The models based on classical nucleation theory have been employed to analyze nucleation kinetic data. In the case of dispersions of particles with long-ranged screened Coulombic interactions, the crystal size in found to increase linearly with time,[117] whereas, for the particles with hard-sphere-like interactions, the size of the crystals increases with the square root in time.[118] These and other studies have enhanced understanding of crystallization kinetics.[15, 119, 120] However, since steady state nucleation rate was generally assumed in these works, comparisons between experimental results and model calculation showed discrepancies that cannot be attributed to approximation in theory or uncertainties in experiments.[118, 121]

Model calculations by the Zukoski group suggest that nucleation rate, crystal growth velocity and induction time are affected by the decrease in the background monomer volume fraction as crystallization progresses.[122] Also, it is observed that above the melting point volume fraction, crystal growth appears to be suppressed by high nucleation rate.[123, 124] These studies explained the crystallization mechanisms of hard sphere colloidal particles that can help to understand crystallization of soft spheres.

1.5 Microgel Particles as a New Building Block of Colloidal Self-Assemblies

1.5.1 Responsive Microgels

Hydrogels are water-swollen cross-linked polymer network where majority of volume is occupied by water. Hydrogels can undergo solvation changes in response to the application of an external stimulus, such as temperature,[125-127] ionic strength,[128, 129] pH,[126, 130, 131] metal ions[132] etc. Most intensively studied microgels are based on thermoresponsive *poly*(N-isopropylacrylamide) (*p*NIPAm) or related co-polymers that are cross-linked.[133] The structures of the NIPAm, cross-linking agent (BIS), and co-polymer (AAc) are shown in Fig. 1.5-1. Below its characteristic lower critical solution temperature (LCST) which is ~ 31 °C for *p*NIPAm, *p*NIPAm hydrogel exists in a solvated state (or swollen state). In its swollen state, water molecules inside of the hydrogel form hydrogen bonding with amide groups in the polymer network. Also, other water molecules inside the polymer network tend to form structured clusters (structured water) to minimize the energy. As the hydrogel is heated, the hydrogen bonding between water and nitrogen on amide groups gets weaker. When the hydrogel is heated above LCST, the hydrogen bonding between water and amide groups breaks and water molecules are expelled resulting in collapses of polymer chains. This macromolecular shrinkage of *p*NIPAm also released a large amount of structured water resulting in an increase in entropy. This transition is usually referred to as the volume phase transition (VPT), where the hydrogel undergoes a transition from a swollen to a de-swollen network. Similarly, cross-linked micron-sized hydrogels, microgels, undergo a reversible VPT.[133, 134]

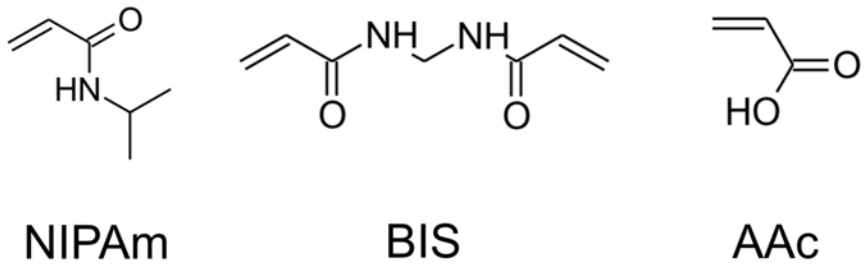

Figure 1.5-1 Chemical structures of N-isopropylacrylamide (NIPAm), N,N'-methylene (bisacrylamide) (BIS), and acrylic acid (AAc), monomers frequently used to form responsive hydrogels.

To tune the LCST and other properties, a variety of co-polymers such as acrylic acid, dimethylaminoethylmethacrylate, allylamine, vinyl laurate etc are used.[135-143] In this thesis, acrylic acid will be mainly discussed and used as co-monomer to prepared poly(*N*-isopropylacrylamide-*co*-acrylic acid) (*p*NIPAm-*co*-AAc). Acrylic acid possesses an ionizable carboxylic acid group with a pK_a of ~4.5. Below the pK_a, the moiety is protonated and has little to no effect on the volume phase transition temperature. Above the pK_a, the moiety is deprotonated and exerts an effect on the hydrogel via the hydrophilic nature of the anion, Coulombic repulsion and osmotic swelling due to counterion influx (Donnan potential).[144, 145] As a result, first the microgels above pK_a uptake more water resulting in larger hydrodynamic radius. Secondly, the Coulombic repulsion in the polymer network resists the shrinking so that the volume phase transition temperature is shifter toward higher temperature than ~ 31 °C. Figure1-3 displays volume phase transition behaviors of *p*NIPAm-*co*-AAc microgels dispersed in different pH buffer solutions. At pH 3.5, most acrylic acid groups in the polymer network are protonated, i.e. microgel is relatively neutral. As a result, the microgel dispersed in 15 mM pH 3.5 buffer aqueous solution undergoes phase transition at ~ 31 °C as observed in *p*NIPAm

microgels. At pH 6.5, however, since ~99 % acrylic acid groups in the microgel are protonated, the R_h of microgel is larger and the volume phase transition temperature is shifted toward higher temperature.

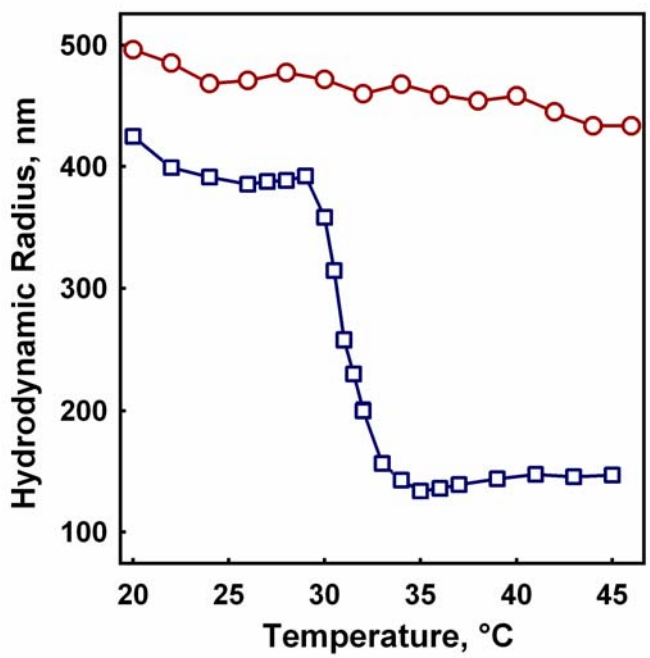

Figure 1.5-2 A volume phase transition behavior from *p*NIPAm-*co*-AAc microgels. As the temperature is increased the microgels undergo a deswelling transition, going from solvent swollen to deswollen at pH 3.5 (blue squares) and pH 6.5 (red circles).

1.5.2 Preparation and Characterization of Microgels

The microgels described in this work were synthesized by precipitation polymerization resulting in relatively mono-disperse spheres.[146, 147] Using this method, the resultant particle size can be continuously varied from ~50-nm to 1-μm diameter by controlling the surfactant and initiator concentrations while maintaining low polydispersities. The size and size distribution of the microgel particles are determined by

photon correlation spectroscopy (PCS also known as dynamic light scattering, DLS) and static light scattering (SLS). DLS is a tool for studying the time dependence of light scattering, while with SLS, the average intensity in examined. DLS monitors the fluctuations in the scattered light intensity as a function of a time and this intensity fluctuation vs. time is plotted as an autocorrelation function. The diffusion coefficient can be calculated and hydrodynamic radius (R_h) can be calculated using the Stokes-Einstein relationship.[148]

$$R_h = \frac{k_B T}{6\pi\eta D} \tag{1-9}$$

Here, k_B is Boltzmann's constant, T is the absolute temperature, η is the solvent viscosity and D is the diffusion coefficient.

1.5.3 Responsive Microgels : New Building Block for Colloidal Crystals.

Responsive microgels have gained great interest as model colloidal particles for investigating soft sphere phase behavior, since *p*NIPAm-based microgels have several excellent characteristics to utilize for colloidal crystals. First, since majority of volume is water, the density of microgels are similar to dispersion medium, water, sedimentation does not play a significant role in crystallization. Secondly, in the swollen state, since the refractive index of *p*NIPAm-based microgel is close to water, the contribution from van der Waals attraction is negligible. Thirdly, the thermoresponsive property of *p*NIPAm-based microgels makes the crystals processible by simply heating and cooling. Finally, since the softness and/or chemical properties of microgels can be easily modified by

simply varying cross-linker concentration[149] or introducing co-monomers as mentioned earlier, the interaction potential between colloidal particles can be tuned.

The assembly of colloidal crystals from *p*NIPAm microgels has been reported previously by our group[90, 91, 146] and others. A number of groups have investigated the rheological properties,[149-151] phase behavior,[151-155] optical properties[90, 146, 156] and crystallization kinetices[157] of *p*NIPAm microgel dispersions.

In this thesis, very complex phase behaviors of microgel dispersions will be investigated. We utilize *p*NIPAm-*co*-AAc microgels as a building block for soft sphere colloidal self-assemblies. The microgels utilized for this research have the source for weak attractive interactions[158, 159] as well as soft repulsive interactions[150]. Since microgels are dispersed in good solvent, water, they can be deformed i.e. showing soft sphere interactions. Incorporating the co-monomer, acrylic acid (AAc), can introduce to the *p*NIPAm microgels the source of attractive interactions and this interaction can be tuned by changing pH. The rest of the thesis is organized as follows: In chapter 2, we present the effective volume fraction effect on packing *p*NIPAm-*co*-AAc microgel dispersions. The shift factors of *p*NIPAm-*co*-AAc microgel dispersions are determined by rheology experiments in chapter 3. Here, we chose three different pHs, pH 3.0, 3.85 and 6.5 to see the phase behavior of fully protonated, partially protonated and fully deprotonated conditions respectively. The phase diagrams depending on pHs of the dispersions are discussed in chapter 4. In chapter 5, we investigate the phase evolution of microgel dispersions to understand the energetics of *p*NIPAm-*co*-AAc microgel dispersions. Finally, in chapter 6, the phase diagram and the phase evolution of pH 6.5 dispersions are discussed.

References

(1) W. B. Russel, D. A. Saville and W. R. Schowalter *Colloidal Dispersions*; Cambridge University Press: Cambridge, 1989.

(2) Gel trapping of dense colloids, B. Laxton Peter and C. Berg John *J. colloid interface sci.*, *285*, 152.

(3) Some unusual properties of colloidal dispersions, R. V. Williamson *J. Phys. Chem.* **1931**, *35*, 354.

(4) SnO2 thin films prepared by dip-coating from microwave synthesized colloidal suspensions, E. Michel, D. Chaumont and D. Stuerga *J. Colloid Interface Sci.* **2003**, *257*, 258.

(5) TiO2 coatings on silicon carbide and carbon fibre substrates by electrophoretic deposition, A. R. Boccaccini, P. Karapappas, J. M. Marijuan and C. Kaya *J. Mater. Sci.* **2004**, *39*, 851.

(6) Paper whiteners. I. Titania coated silica, W. P. Hsu, R. Yu and E. Matijevic *J. Colloid Interface Sci.* **1993**, *156*, 56.

(7) Interfacial and colloidal properties of cosmetic emulsions containing fatty alcohol and fatty alcohol polyglycol ethers, F. Schambil, F. Jost and M. J. Schwuger *Prog. Colloid Polym. Sci.* **1987**, *73*, 37.

(8) The use of colloidal microgels as a (trans)dermal drug delivery system, V. C. Lopez, J. Hadgraft and M. J. Snowden *Int. J. Pharm.* **2005**, *292*, 137.

(9) Fabrication of novel colloidosome microcapsules with gelled aqueous cores, O. J. Cayre, P. F. Noble and V. N. Paunov *J. Mater. Chem.* **2004**, *14*, 3351.

(10) Fabrication of novel types of colloidosome microcapsules for drug delivery applications, V. N. Paunov, P. F. Noble, O. J. Cayre, R. G. Alargova and O. D. Velev *MRS Proc.* **2005**, *845*, 279.

(11) Diffraction of light by opals, J. V. Sanders *Acta Crystallogr., Sect. A* **1968**, *24*, 427.

(12) Close-packed structures of spheres of two different sizes. I. Observations on natural opal, J. V. Sanders *Philos. Mag., [Part] A* **1980**, *42*, 705.

(13) Structure of opals, J. V. Sanders *J. Phys., Colloq.* **1985**, 1.

(14) Colloidal crystals, P. Pieranski *Contemp. Phys.* **1983**, *24*, 25.

(15) Classical growth of hard-sphere colloidal crystals, B. J. Ackerson and K. Schaetzel *Phys. Rev. E* **1995**, *52*, 6448.

(16) Structure of crystals of hard colloidal spheres, P. N. Pusey, W. Van Megen, P. Bartlett, B. J. Ackerson, J. G. Rarity and S. M. Underwood *Phys. Rev. Lett.* **1989**, *63*, 2753.

(17) Controlled growth of hard-sphere colloidal crystals, Z. D. Cheng, W. B. Russell and P. M. Chaikin *Nature* **1999**, *401*, 893.

(18) Self-assembly of colloidal crystals, A. D. Dinsmore, J. C. Crocker and A. G. Yodh *Curr. Opin. Colloid Interface Sci.* **1998**, *3*, 5.

(19) Centrifugal compression of crystal-like structures of seionized colloidal spheres, T. Okubo *J. Am. Chem. Soc.* **1990**, *112*, 5420.

(20) Two-dimensional crystallization, N. D. Denkov, O. D. Velev, P. A. Kralchevsky, I. B. Ivanov, H. Yoshimura and K. Nagayama *Nature* **1993**, *361*, 26.

(21) Single-crystal colloidal multilayers of controlled thickness, P. Jiang, J. F. Bertone, K. S. Hwang and V. L. Colvin *Chem. Mat.* **1999**, *11*, 2132.

(22) Observations of latex particle two-dimensional-crystal nucleation in wetting films on mercury, glass, and mica, A. S. Dimitrov, C. D. Dushkin, H. Yoshimura and K. Nagayama *Langmuir* **1994**, *10*, 432.

(23) Template-directed colloidal crystallization, A. van Blaaderen, R. Rue and P. Wiltzius *Nature* **1997**, *385*, 321.

(24) Nanoparticle-mediated epitaxial assembly of colloidal crystals on patterned substrates, W. Lee, A. Chan, M. A. Bevan, J. A. Lewis and P. V. Braun *Langmuir* **2004**, *20*, 5262.

(25) Star-polymers as depleting agents of colloidal hard spheres, J. Dzubiella, C. N. Likos and H. Lowen *Europhys. Lett.* **2002**, *58*, 133.

(26) Depletion-induced colloidal crystals at a wall characterized by small-angle X-ray diffraction, X. Xian, A. V. Petukhov, M. M. E. Snel, I. P. Dolbnya, D. G. A. L. Aarts, G. J. Vroege and H. N. W. Lekkerkerker *J. Appl. Crystallogr.* **2003**, *36*, 597.

(27) Macroporous membranes with highly ordered and three-dimensionally interconnected spherical pores, S. H. Park and Y. Xia *Adv. Mater.* **1998**, *10*, 1045.

(28) Monodispersed colloidal spheres: Old materials with new applications, Y. N. Xia, B. Gates, Y. D. Yin and Y. Lu *Adv. Mater.* **2000**, *12*, 693.

(29) Size control of monodispersed Pt nanoparticles and their 2D organization by electrophoretic deposition, T. Teranishi, M. Hosoe, T. Tanaka and M. Miyake *J. Phys. Chem. B* **1999**, *103*, 3818.

(30) Formation of ordered 2-dimensional gold colloid lattices by electrophoretic deposition, M. Giersig and P. Mulvaney *J. Phys. Chem.* **1993**, *97*, 6334.

(31) Colloidal crystals with tunable colors and their use as photonic papers, H. Fudouzi and Y. Xia *Langmuir* **2003**, *19*, 9653.

(32) Diffraction of visible light by ordered monodisperse silica-poly(methyl acrylate) composite films, J. M. Jethmalani and W. T. Ford *Chem. Mater.* **1996**, *8*, 2138.

(33) Thermally switchable periodicities and diffraction from mesoscopically ordered materials, J. M. Weissman, H. B. Sunkara, A. S. Tse and S. A. Asher *Science* **1996**, *274*, 959.

(34) Photonic crystal carbohydrate sensors: Low ionic strength sugar sensing, S. A. Asher, V. L. Alexeev, A. V. Goponenko, A. C. Sharma, I. K. Lednev, C. S. Wilcox and D. N. Finegold *J. Am. Chem. Soc.* **2003**, *125*, 3322.

(35) Polymerized colloidal crystal hydrogel films as intelligent chemical sensing materials, J. H. Holtz and S. A. Asher *Nature* **1997**, *389*, 829.

(36) Strong localization of photons in certain disordered dielectric superlattices, S. John *Phys. Rev. Lett.* **1987**, *58*, 2486.

(37) Optically nonlinear Bragg diffracting nanosecond optical switches, G. Pan, R. Kesavamoorthy and S. A. Asher *Phys. Rev. Lett.* **1997**, *78*, 3860.

(38) Inhibited spontaneous emission in solid-state physics and electronics, E. Yablonovitch *Phys. Rev. Lett.* **1987**, *58*, 2059.

(39) Optical Properties of planar colloidal crystals: Dynamical diffraction and the scalar wave approximation, D. M. Mittleman, J. F. Bertone, P. Jiang, K. S. Hwang and V. L. Colvin *J. Chem. Phys.* **1999**, *111*, 345.

(40) Preparation of photonic crystals made of air spheres in titania, J. Wijnhoven and W. L. Vos *Science* **1998**, *281*, 802.

(41) Photonic Band-Structure - the Face-Centered-Cubic Case, E. Yablonovitch and T. J. Gmitter *Phys. Rev. Lett.* **1989**, *63*, 1950.

(42) Large-scale synthesis of a silicon photonic crystal with a complete three-dimensional bandgap near 1.5 micrometres, A. Blanco, E. Chomski, S. Grabtchak, M. Ibisate, S. John, S. W. Leonard, C. Lopez, F. Meseguer, H. Miguez, J. P. Mondia, G. A. Ozin, O. Toader and H. M. van Driel *Nature* **2000**, *405*, 437.

(43) Inhibited light propagation and broadband reflection in photonic air-sphere crystals, M. S. Thijssen, R. Sprik, J. Wijnhoven, M. Megens, T. Narayanan, A. Lagendijk and W. L. Vos *Phys. Rev. Lett.* **1999**, *83*, 2730.

(44) Band spectroscopy of colloidal photonic crystal films, H. Miguez, V. Kitaev and G. A. Ozin *Appl. Phys. Lett.* **2004**, *84*, 1239.

(45) Synthesis of inorganic materials with complex form, S. Mann and G. A. Ozin *Nature* **1996**, *382*, 313.

(46) Methods of digital video microscopy for colloidal studies, J. C. Crocker and D. G. Grier *J. Coll. Inter. Sci.* **1996**, *179*, 298.

(47) The microscopic dynamics of freezing in supercooled colloidal fluids, D. G. Grier and C. A. Murray *J. Chem. Phys.* **1994**, *100*, 9088.

(48) Kinetics of crystal growth in charged colloidal suspensions, T. Palberg, M. Wuerth, J. Schwarz and P. Leiderer *Prog. Colloid Polym. Sci.* **1995**, *98*, 6.

(49) Martensitic transition in a confined colloidal suspension, J. A. Weiss, D. W. Oxtoby, D. G. Grier and C. A. Murray *J. Chem. Phys.* **1995**, *103*, 1180.

(50) Video microscopy of colloidal suspensions and colloidal crystals, P. Habdas and E. R. Weeks *Curr. Opinion in Coll. & Inter. Sci.* **2002**, *7*, 196.

(51) Real-space imaging of nucleation and growth in colloidal crystallization, U. Gasser, E. R. Weeks, A. Schofield, P. N. Pusey and D. A. Weitz *Science* **2001**, *292*, 258.

(52) Real-Space Structure of Colloidal Hard-Sphere Glasses, A. Vanblaaderen and P. Wiltzius *Science* **1995**, *270*, 1177.

(53) A new colloidal model system to study long-range interactions quantitatively in real space, C. P. Royall, M. E. Leunissen and A. van Blaaderen *J. Phys.: Condens. Matter* **2003**, *15*, S3581.

(54) Three-dimensional direct imaging of structural relaxation near the colloidal glass transition, E. R. Weeks, J. C. Crocker, A. C. Levitt, A. Schofield and D. A. Weitz *Science* **2000**, *287*, 627.

(55) Novel crystallization process in dilute ionic colloids, H. Yoshida, J. Yamanaka, T. Koga, N. Ise and T. Hashimoto *Langmuir* **1998**, *14*, 569.

(56) Like-charge attractions in metastable colloidal crystallites, A. E. Larsen and D. G. Grier *Nature* **1997**, *385*, 230.

(57) Microscopic measurement of the pair interaction potential of charge-stabilized colloid, J. C. Crocker and D. G. Grier *Phys. Rev. Lett.* **1994**, *73*, 352.

(58) Colloids: A surprisingly attractive couple, D. G. Grier *Nature* **1998**, *393*, 621.

(59) Phase behaviour of concentrated suspensions of nearly hard colloidal spheres, P. N. Pusey and W. van Megen *Nature* **1986**, *320*, 340.

(60) Phase transitions in soft matter systems, H. Lowen, M. Watzlawek, C. N. Likos, M. Schmidt, A. Jusufi, H. Graf, A. R. Denton and C. von Ferber *AIP Conference Proc.* **2000**, *519*, 140.

(61) The experimental phase diagram of charged colloidal suspensions, Y. Monovoukas and A. P. Gast *J. Colloid Interface Sci.* **1989**, *128*, 533.

(62) Solid-liquid coexistence in the adhesive hard sphere system, S. J. Smithline and A. D. J. Haymet *J. Chem. Phys.* **1985**, *83*, 4103.

(63) Complete phase diagram of a charged colloidal system: a synchrotron x-ray scattering study, E. B. Sirota, H. D. Ou-Yang, S. K. Sinha, P. M. Chaikin, J. D. Axe and Y. Fujii *Phys. Rev. Lett.* **1989**, *62*, 1524.

(64) Solid-liquid coexistence in the adhesive hard sphere system, S. J. Smithline and A. D. J. Hayment *J. Chem. Phys.* **1985**, *83*, 4103.

(65) On the solid-fluid interface of adhesive spheres., D. W. Marr and A. P. Gast *J. Chem. Phys.* **1993**, *99*, 2024.

(66) Melting transition and communal entropy for hard spheres, W. G. Hoover and F. H. Ree *J. Chem. Phys.* **1968**, *49*, 3609.

(67) Sterically stabilized colloidal particles as model hard spheres, S. M. Underwood, J. R. Taylor and W. van Megen *Langmuir* **1994**, *10*, 3550.

(68) Observation of a glass transition in suspensions of spherical colloidal particles, P. N. Pusey and W. Van Megen *Phys. Rev. Lett.* **1987**, *59*, 2083.

(69) Phase behavior of small attractive colloidal particles, D. Rosenbaum, P. C. Zamora and C. F. Zukoski *Phys. Rev. Lett.* **1996**, *76*, 150.

(70) The glass paradigm for colloidal glasses, gels, and other arrested states driven by attractive interactions., K. A. Dawson *Curr. Opin. Colloid Interface Sci.* **2002**, *7*, 218.

(71) Subdiffusion and the cage effect studied near the colloidal glass transition, E. R. Weeks and D. A. Weitz *Chem. Phys.* **2002**, *284*, 361.

(72) Properties of cage rearrangements observed near the colloidal glass transition, E. R. Weeks and D. A. Weitz *Phys. Rev. Lett.* **2002**, *89*, 095704/1.

(73) Direct visualization of ageing in colloidal glasses, R. E. Courtland and E. R. Weeks *J. Phys.: Condens. Matter* **2003**, *15*, S359.

(74) Is random close packing of spheres well defined?, S. Torquato, T. M. Truskett and P. G. Debenedetti *Phys. Rev. Lett.* **2000**, *84*, 2064.

(75) Star polymers viewed as ultrasoft colloidal particles, C. N. Likos, H. Lowen, M. Watzlawek, B. Abbas, O. Jucknischke, J. Allgaier and D. Richter *Phys. Rev. Lett.* **1998**, *80*, 4450.

(76) Effective interactions in soft condensed matter physics, C. N. Likos *Phys. Rep.* **2001**, *348*, 267.

(77) Ordering phenomena of star polymer solutions approaching the .THETA. state, C. N. Likos, H. Lowen, A. Poppe, L. Willner, J. Roovers, B. Cubitt and D. Richter *Phys. Rev. E: Stat. Phys., Plasmas, Fluids, Relat. Interdiscip. Top.* **1998**, *58*, 6299.

(78) Star polymers: from conformations to interactions to phase diagrams, C. N. Likos and H. M. Harreis *Condens. Matter. Phys.* **2002**, *29*, 173.

(79) Phase diagram of star polymer solutions, M. Watzlawek, C. N. Likos and H. Lowen *Phys. Rev. Lett.* **1999**, *82*, 5289.

(80) Partial structure factors in star polymer/colloid mixtures, J. Stellbrink, J. Allgaier, D. Richter, A. Moussaid, A. B. Schofield, W. C. K. Poon, P. N. Pusey, P. Lindner, J. Dzubiella, C. N. Likos and H. Lowen *Appl. Phys. A* **2002**, *74*, S355.

(81) Effective interactions between star polymers and colloidal particles, A. Jusufi, J. Dzubiella, C. N. Likos, C. von Ferber and H. Lowen *Los Alamos National Laboratory, Preprint Archive, Condensed Matter* **2000**, 1.

(82) Phase transitions in colloidal suspensions and star polymer solutions, H. Lowen, M. Watzlawek, C. N. Likos, M. Schmidt, A. Jusufi and A. R. Denton *J. Phys.: Condens. Matter* **2000**, *12*, A465.

(83) Counterion-induced entropic interactions in solutions of strongly stretched, osmotic polyelectrolyte stars, A. Jusufi, C. N. Likos and H. Lowen *J. Chem. Phys.* **2002**, *116*, 11011.

(84) Interactions and Phase Behavior of Polyelectrolyte Star Solutions, C. N. Likos, N. Hoffmann, A. Jusufi and H. Lowen *J. Phys.: Condens. Matter* **2003**, *15*, S233.

(85) Structure and phase behavior of polyelectrolyte star solutions, N. Hoffmann, C. N. Likos and H. Lowen *J. Chem. Phys.* **2004**, *121*, 7009.

(86) Counterion penetration and effective eletrostatic interactions in solutions of polyelectrolyte stars and Microgels, A. R. Denton *Phys. Rev. E* **2003**, *67*, 011804/1.

(87) Ionic microgels as model systems for colloids with an ultrasoft electrosteric repulsion: structure and thermodynamics, D. Gottwald, C. N. Likos, G. Kahl and H. Lowen *J. Chem. Phys.* **2005**, *122*, 074903/1.

(88) Phase behavior of ionic microgels, D. Gottwald, C. N. Likos, G. Kahl and H. Lowen *Phys. Rev. Lett.* **2004**, *92*, 680103/1.

(89) Equilibrium and shear induced nonequilibrium phase behavior of PMMA microgel spheres, S. E. Paulin, B. J. Ackerson and M. S. Wolfe *J. Colloid Interface Sci.* **1996**, *178*, 251.

(90) Color-tunable colloidal crystals from soft hydrogel nanoparticles, J. D. Debord, S. Eustis, S. B. Debord, M. T. Lofye and L. A. Lyon *Adv. Mater.* **2002**, *14*, 658.

(91) Influence of particle volume fraction on packing in responsive hydrogel colloidal crystals, S. B. Debord and L. A. Lyon *J. Phys. Chem. B* **2003**, *107*, 2927.

(92) Melting temperature of colloidal crystals of monodisperse silica spheres, T. Okubo *J. Chem. Phys.* **1992**, *96*, 2261.

(93) Order-disorder transition in colloidal suspensions, R. O. Rosenberg and D. Thirumalai *Phys. Rev. A: At., Mol., Opt. Phys.* **1987**, *36*, 5690.

(94) Ordering in charged colloidal dispersions and macroionic solutions: a density-functional approximation, P. Salgi and R. Rajagopalan *Langmuir* **1991**, *7*, 1383.

(95) The phase diagram of charged colloidal suspensions, D. Hone, S. Alexander, P. M. Chaikin and P. Pincus *J. Chem. Phys.* **1983**, *79*, 1474.

(96) Phase Diagram of Dipolar Hard and Soft Spheres: Manipulation of Colloidal Crystal Structures by an External Field, A.-P. Hynninen and M. Dijkstra *Phys. Rev. Lett.* **2005**, *94*, 138303/1.

(97) E. J. W. Verwey and J. T. Overbeek *Theory of the Stability of Lyphobic Colloids*; Elsevier: Amsterdam, 1948.

(98) Spinodal decomposition and the liquid-vapor equilibrium in charged colloidal dispersions, J. M. Victor and J. P. Hansen *J. Chem. Soc. Faraday Trans. II* **1985**, *81*, 43.

(99) When like charges attract: the effects of geometrical confinement on long-range colloidal interactions, J. C. Crocker and D. G. Grier *Phys. Rev. Lett.* **1996**, *77*, 1897.

(100) Brownian motion: A tool to determine the pair potential between colloid particles, K. Vondermassen, J. Bongers, A. Mueller and H. Versmold *Langmuir* **1994**, *10*, 1351.

(101) Void structure and vapor-liquid condensation in dilute deionized colloidal dispersions, H. Yoshida, N. Ise and T. Hashimoto *J. Chem. Phys.* **1995**, *103*, 10146.

(102) Void structure in colloidal dispersions, K. Ito, H. Yoshida and N. Ise *Science* **1994**, *263*, 66.

(103) Kossel line analysis on colloidal crystals in semidilute aqueous solutions, T. Yoshiyama, I. Sogami and N. Ise *Phys. Rev. Lett.* **1984**, *53*, 2153.

(104) Ordered structure in dilute solutions of highly charged polymer lattices as studied by microscopy. I. Interparticle distance as a function of latex concentration, N. Ise, T. Okubo, M. Sugimura, K. Ito and H. J. Nolte *J. Chem. Phys.* **1983**, *78*, 536.

(105) A surprisingly attractive couple, D. G. Grier *Nature* **1998**, *393*, 621.

(106) Pair interaction of charged colloidal spheres near a charged wall, S. H. Behrens and D. G. Grier *Phys. Rev. E* **2001**, *64*, 050401/1.

(107) Visible evidence for interparticle attraction in polymer latex dispersions, N. Ise, T. Okubo, K. Ito, S. Dosho and I. Sogami *Langmuir* **1985**, *1*, 176.

(108) How homogeneous are "homogeneous dispersions"? counterion-mediated attraction between like-charged species, N. Ise, T. Konishi and B. V. R. Tata *Langmuir* **1999**, *15*, 4176.

(109) On the electrostatic interaction in macroion solution, I. Sogami and N. Ise *J. Chem. Phys.* **1984**, *91*, 6320.

(110) Effective potential between charged spherical particles in dilute suspension., I. Sogami *Phys. Lett.* **1983**, *96A*, 199.

(111) Three-body forces between charged colloidal particles, C. Russ, H. H. von Grunberg, M. Dijkstra and R. van Roij *Phys. Rev. E* **2002**, *66*, 011402.

(112) Glasses in hard spheres with short-range attraction, K. N. Pham, S. U. Egelhaaf, P. N. Pusey and W. C. K. Poon *Phys. Rev. E* **2004**, *69*, 011503/1.

(113) "Unsticking" a colloidal glass, and sticking it again, W. C. K. Poon, K. N. Pham, S. U. Egelhaaf and P. N. Pusey *J. Phys.: Condensed Matter* **2003**, *15*, S269.

(114) Depletion-induced aggregation and colloidal phase separation, A. Milling and B. Vincent *Colloid-Polym. Interact.* **1999**, 147.

(115) Entropic control of particle motion using passive surface microstructures, A. D. Dinsmore, A. G. Yodh and D. J. Pine *Nature* **1996**, *383*, 239.

(116) Entropic confinement of colloidal spheres in corners on silicon substrates, A. D. Dinsmore and A. G. Yodh *Langmuir* **1999**, *15*, 314.

(117) Nucleation and growth of colloidal crystals, D. J. W. Aastuen, N. A. Clark, L. K. Cotter and B. J. Ackerson *Phys. Rev. Lett.* **1986**, *57*, 1733.

(118) Density fluctuations during crystallization of colloids, K. Schaetzel and B. J. Ackerson *Phys. Rev. E* **1993**, *48*, 3766.

(119) Homogeneous nucleation : theory adn experiment, D. W. Oxtoby *J. Phys.: Condens. Matter* **1992**, *4*, 7627.

(120) Enhancement of protein crystal nucleation by critical density fluctuations, P. R. ten Wolde and D. Frenkel *Science* **1997**, *277*, 1975.

(121) Comparison of experimental estimates and model predictions of protein crystal nucleation rates, N. M. Dixit, A. M. Kulkarni and C. F. Zukoski *Colloids and Surf., A* **2001**, *190*, 47.

(122) Nucleation rates and induction times during colloidal crystallization. Links between models and experiments, N. M. Dixit and C. F. Zukoski *Phys. Rev. E* **2002**, *66*, 051602/1.

(123) Observation of accelerated nucleation in dense colloidal fluids of hard sphere particles, J. L. Harland, S. I. Henderson, S. M. Underwood and W. van Megen *Phys. Rev. Lett.* **1995**, *75*, 3572.

(124) Crystallization kinetics of suspensions of hard colloidal spheres, J. L. Harland and W. van Megen *Phys. Rev. E* **1997**, *55*, 3054.

(125) Influence of polymerization conditions on the structure of temperature-sensitive poly(N-isopropylacrylamide) microgels, S. Meyer and W. Richtering *Macromolecules* **2005**, *38*, 1517.

(126) Graft copolymers that exhibit temperature-induced phase transitions over a wide range of pH, G. Chen and A. S. Hoffman *Nature* **1995**, *373*, 49.

(127) Globule-to-coil transition of a single homopolymer chain in solution, C. Wu and X. Wang *Phys. Rev. Lett.* **1998**, *80*, 4092.

(128) Photonic crystal chemical sensors: pH and ionic strength, K. Lee and S. A. Asher *J. Am. Chem. Soc.* **2000**, *122*, 9534.

(129) pH and ion-triggered volume response of anionic hydrogel microspheres, G. M. Eichenbaum, P. F. Kiser, S. A. Simon and D. Needham *Macromolecules* **1998**, *31*, 5084.

(130) Functional hydrogel structures for autonomous flow control inside microfluidic channels, D. J. Beebe, J. S. Moore, J. M. Bauer, Q. Yu, R. H. Liu, C. Devadoss and B. H. Jo *Nature* **2000**, *404*, 588.

(131) Colloidal copolymer microgels of N-isopropylacrylamide and acrylic acid: pH, ionic strength and temperature effects, M. J. Snowden, B. Z. Chowdhry, B. Vincent and G. E. Morris *Journal of the Chemical Society-Faraday Transactions* **1996**, *92*, 5013.

(132) Photonic crystal optrode sensor for detection of Pb2+ in high ionic strength environments, C. E. Reese and S. A. Asher *Anal. Chem.* **2003**, *75*, 3915.

(133) Temperature-sensitive aqueous microgels, R. Pelton *J. Colloid Interface Sci.* **2000**, *85*, 1.

(134) Poly(NIPAM) microgel particle de-swelling: a light scattering and small-angle neutron scattering study, H. M. Crowther, B. R. Saunders, S. J. Mears, T. Cosgrove, B. Vincent, S. M. King and G. E. Yu *Colloid Surf. A-Physicochem. Eng. Asp.* **1999**, *152*, 327.

(135) The effect of electrolyte on the colloidal properties of poly(N-isopropylacrylamide-co-dimethylaminoethylmethacrylate) microgel latexes, L. Zha, J. Hu, C. Wang, S. Fu and M. Luo *Colloid Polym. Sci.* **2002**, *280*, 1116.

(136) Novel gelling behavior of poly(N-isopropylacrylamide-co-vinyl laurate) microgel dispersions, L. S. Benee, M. J. Snowden and B. Z. Chowdhry *Langmuir* **2002**, *18*, 6025.

(137) Colloidal stability of a temperature-sensitive poly(N-isopropylacrylamide/2-acrylamido-2-methylpropanesulphonic acid) microgel, M. J. Garcia-Salinas, M. S. Romero-Cano and F. J. de las Nieves *J. Colloid Interface Sci.* **2002**, *248*, 54.

(138) Influence of charge density on the swelling of colloidal poly(N-isopropylacrylamide-co-acrylic acid) microgels, K. Kratz, T. Hellweg and W. Eimer *Colloids Surf., A* **2000**, *170*, 137.

(139) Charged thermosensitive microgels, T. Hoare and R. Pelton *Polym. Mater. Sci. Eng.* **2002**, *87*, 501.

(140) The coil-to-globule-to-brush transition of linear thermally sensitive poly(N-isopropylacrylamide) chains grafted on a spherical microgel, T. Hu, Y. You, C. Pan and C. Wu *J. Phys. Chem. B* **2002**, *106*, 6659.

(141) Synthesis and characterization of pH-responsive copolymer microgels with tunable volume phase transition temperatures, J. D. Debord and L. A. Lyon *Langmuir* **2003**, *19*, 7662.

(142) Controlled drug release from hydrogel nanoparticle networks, G. Huang, J. Gao, Z. Hu, J. V. St. John, B. C. Ponder and D. Moro *J. Controlled Release* **2004**, *94*, 303.

(143) PNIPAM-co-polystyrene core-shell microgels: structure, swelling behavior, and crystallization, T. Hellweg, C. D. Dewhurst, W. Eimer and K. Kratz *Langmuir* **2004**, *20*, 4330.

(144) Preparation of thermosensitive submicrometer gel particles with anionic and cationic charges, S. Ito, K. Ogawa, H. Suzuki, B. Wang, R. Yoshida and E. Kokufuta *Langmuir* **1999**, *15*, 4289.

(145) Charge controlled swelling of microgel particles, A. Fernandez-Nieves, A. Fernandez-Barbero, B. Vincent and F. J. de las Nieves *Macromolecules* **2000**, *33*, 2114.

(146) Thermoresponsive photonic crystals, J. D. Debord and L. A. Lyon *J. Phys. Chem. B* **2000**, *104*, 6327.

(147) Synthesis and characterization of multiresponsive core-shell microgels, C. D. Jones and L. A. Lyon *Macromolecules* **2000**, *33*, 8301.

(148) P. J. Flory *Principles of Polymer Chemistry*; Cornell University Press: London, 1953.

(149) Influence of crosslink density on rheological properties of temperature-sensitive microgel suspensions, H. Senff and W. Richtering *Colloid Polym. Sci.* **2000**, *278*, 830.

(150) Temperature sensitive microgel suspensions: Colloidal phase behavior and rheology of soft spheres, H. Senff and W. Richtering *J. Chem. Phys.* **1999**, *111*, 1705.

(151) Are thermoresponsive microgels model systems for concentrated colloidal suspensions? A rheology and small-angle neutron scattering study, M. Stieger, J. S. Pedersen, P. Lindner and W. Richtering *Langmuir* **2004**, *20*, 7283.

(152) Colloidal crystals made of poly(N-iospropylacrylamide) microgel particles, T. Hellweg, C. D. Dewhurst, E. Bruckner, K. Kratz and W. Eimer *Colloid Polym. Sci.* **2000**, *278*, 972.

(153) Phase behavior of thermally responsive microgel colloids, J. Wu, B. Zhou and Z. Hu *Phys. Rev. Lett.* **2003**, *90*, 048304/1.

(154) Interparticle potential and the phase behavior of temperature-sensitive microgel sispersions, J. Wu, G. Huang and Z. Hu *Macromolecules* **2003**, *36*, 440.

(155) Premelting at defects within bulk colloidal crystals, A. M. Alsayed, M. F. Islam, J. Zhang, P. J. Collings and A. G. Yodh *Science* **2005**, *309*, 1207.

(156) Optical properties of N-Isopropylacrylamide microgel spheres in water, J. Gao and Z. Hu *Langmuir* **2002**, *18*, 1360.

(157) Crystallization kinetics of thermosensitive colloids probed by transmission spectroscopy, S. Tang, Z. Hu, Z. Cheng and J. Wu *Langmuir* **2004**, *20*, 8858.

(158) A Simple functional representation of angular-dependent hydrogen-bonded systems. 1. Amide, carboxylic acid, and amide-carboxylic acid pairs, K. T. No, O. Y. Kwon and S. Y. Kim *J. Phys. Chem.* **1995**, *99*, 3478.

(159) Ionic hydrogen bond and ion solvation. 6. Interaction energies of the acetate Ion with organic molecules. Comparison of CH_3COO^- with Cl^-, CN^-, and SH^-, M. Meot-Ner *J. Am. Chem. Soc.* **1988**, *110*, 3854.

CHAPTER 2

Influence of Particle Volume Fraction on Packing in Responsive Microgel Colloidal Crystals

2.1 Introduction

Predictions that omnidirectional bandgap[1, 2] should be observable in opal-inspired materials have stimulated investigations into the materials science and optical physics of self-assembled photonic materials.[3-7] The building blocks for such materials are often spherical colloidal particles, which (as in natural opals)[8-10] assemble into diffractive cubic close packed structures and hence are excellent templates for the synthesis of slightly more advanced diffractive periodic dielectric structures such as inverse opals.[5, 11, 12] However, before this relatively recent interest in opaline photonic structures, dispersions and suspensions of spherical colloidal particles had been studied extensively as models for condensed matter phase behavior.[13-15]

Due to their simple interaction potential, numerous studies have investigated the phase behavior of hard sphere systems. The hard sphere system is governed by steric repulsive interactions where the particles form ordered structures to maximize the configurational entropy. Thus, the phase of hard spheres is mainly determined by effective volume faction (ϕ) of the dispersion.[16] The basic phase diagram that governs hard sphere behavior is fairly well understood and is illustrated in figure 1.3-1 in the chapter 1. The fluid phase exists below volume fractions (ϕ) of ~0.494, where monodispersed hard spheres adopt a state wherein particle motions and positions are

correlated, yet no long-range order exists. The freezing point of the system occurs at ϕ=0.494, with the melting point being ϕ=0.545. Between these two values of ϕ, there exists a phase separated coexistence between the fluid and crystal phases. Above ϕ=0.545 and continuing to the maximum density of ϕ=0.74 the thermodynamically preferred state is that of a crystalline assembly, although under many conditions a kinetically-trapped jammed or glassy state may result, which is generally considered to exist between ϕ=0.58 and ϕ=0.64.[15, 17]

Although many of these investigations have utilized particles that display interaction potentials that are dominated by hard-sphere repulsion, others have probed the interplay of soft interactions, and the influence of such potentials on the resultant phase diagram.[18-23] Star polymers,[18, 19, 22] ionic microgels,[24-26] and latex particles dispersed in a good solvent[21, 27] were used as model systems for studying the soft sphere interactions. These studies theoretically predicted more exotic phase behavior such as body-centered orthogonal (bco) structure and diamond crystal structure due to the *soft* repulsive interaction.[24, 25] Finally, the appearance of attractive interactions (which lead to an unusual fluid/crystal phase coexistence) in systems designed to have purely repulsive interactions have been an area of recent intense interest.[28-32]

In this chapter, we describe the phase behavior of aqueous dispersions of spherical, submicron-sized microgel particles.[33-35] The building blocks for these dispersions are spherical microgels composed of the pH and thermoresponsive polymer poly-*N*-isopropylacrylamide-*co*-acrylic acid (*p*NIPAm-*co*-AAc) lightly cross-linked with *N*,*N*'-methylenebis(acrylamide) (BIS). Such particles are typically referred to as microgels or hydrogel particles, as *p*NIPAm is water-soluble at room temperature. Thus,

loosely cross-linked particles of the polymer tend to swell dramatically in aqueous media. As a result of this extreme degree of solvent swelling, such particles might be expected to display a soft interaction potential. Indeed, others have indirectly illustrated the presence of a soft (concentration-dependent) interaction potential in *p*NIPAm particles and shown the influence of this softness on the crystallization and melting behavior of entropic crystals.[23, 36] Additional interest with respect to these particle assemblies is the thermoresponsivity of *p*NIPAm. Below its characteristic lower critical solution temperature (LCST) of ~31 °C *p*NIPAm exists as a solvated random coil in aqueous media. However, above that temperature, the chains collapse to a hydrophobic globular state due to the entropically favored release of water from the polymer. For cross-linked microgels, this transition is typically referred to as the volume phase transition (VPT), where the particle undergoes a transition from a swollen to a deswollen network. Our group has utilized this VPT to create colloidal crystals from *p*NIPAm particles that are optically tunable by controlling the degree of particle hydration, and crystals that can be annealed *via* the VPT.[37, 38] The studies described below are designed to elucidate the influence of soft *and* weakly attractive particle interactions on the phase behavior of colloidal dispersions. Our results suggest that particles with such unique interaction potentials may offer new opportunities for the construction of periodic, self-assembled structures.

2.2 Experimental

Materials. N-isopropylacrylamide (NIPAm, Aldrich) was purified by recrystallization from hexane (J. T. Baker) prior to use. Acrylic acid (AAc), *N, N*'-

methylenebis(acrylamide) (BIS), ammonium persulfate (APS) and fluorescein disodium salt were purchased from Aldrich and used as received. All water used throughout this investigation was house distilled, deionized to a resistance of at least 18 M□ (Barnstead Thermolyne E-Pure system), and then filtered through a 0.2 □m filter for particulate removal.

Particle Synthesis. PNIPAm-*co*-AAc particles were prepared as follows. NIPAm (1.4 g) and 0.03 g of cross-linker (BIS) were dissolved in 100 mL of water and filtered to remove particulate matter. The mixture was transferred into a 250 mL round bottom flask and heated and kept at 70 °C under gentle nitrogen stream for 40 minutes. Then, 95 μL of AAc was added, followed by APS (0.05 g) to initiate polymerization. The reaction mixture was kept at 70 °C under nitrogen at least for 4 hours to complete the reaction. PNIPAm particles were synthesized by same method as the *p*NIPAm-*co*-AAc particle preparation. NIPAm (2.0 g) and BIS (0.04 g) were dissolved in 100 mL of water and filtered. The reaction mixture was transferred into 250 mL round bottom flask and heated in the same manner as above. APS (0.05 g) was added to initiate reaction. After synthesis, the hydrogel solution was filtered and purified by dialysis (Spectra/Por 7 dialysis membrane, MWCO 10,000) for at least 7 days. The hydrodynamic radius and size distribution of the hydrogel particles were characterized with photon correlation spectroscopy (PCS, Protein Solutions, Inc.) as described previously.[39-41] For these measurements, each sample was allowed to equilibrate at each temperature for 10 min. At each temperature 3 consecutive runs were performed where each run was composed of 15 individual radius measurements using a 60 sec integration time for each measurement.

In general, PCS-determined polydispersities fall below 20%. However, it should be noted that this "effective" polydispersity probably reflects the presence of loosely-crosslinked chains at the particle surface, which contribute to the hydrodynamic radius but may not contribute greatly to crystallization, especially at high volume fractions. Thus, the relationship between PCS-determined polydispersites of hydrogel particles and crystallization thermodynamics/defect density is not clear at this point. Nonetheless, for this and previous studies,[37, 38, 40-42] it has been found that excellent crystallization is observed when the PCS-determined values lie below 20%.

Crystal Assembly. The figure 2.2-1 illustrates the sample preparation. To concentrate the particles into close contact, a hydrogel solution was centrifuged at 29 °C at a relative centrifugal force (RCF) 16,100 g for 1 hour. The ionic strength of the hydrogel solutions was adjusted ~1 mM with 0.1 M NaCl solution before centrifugation. For samples for confocal microscopic observation, a fluorescein disodium salt solution was added to the sample to a concentration of 2.8×10^{-5} M. After centrifugation, the supernatant water was removed to isolate the particle pellet. Diluted crystal samples were prepared by adding H_2O to the pellet in the centrifuge tube while maintaining the ionic strength of samples at ~1 mM with a 0.1 M NaCl solution. To control the extent of AAc protonation, the pH of the samples was adjusted to ~3.8 with 0.01 M HCl. After dilution, the crystals were transferred into Vitrotube borosilicate rectangular capillaries (0.1 mm × 2.0 mm × 50 mm) by capillary action and annealed between room temperature and 35 °C at least 15 times. The samples were placed in the room temperature for several days before observation.

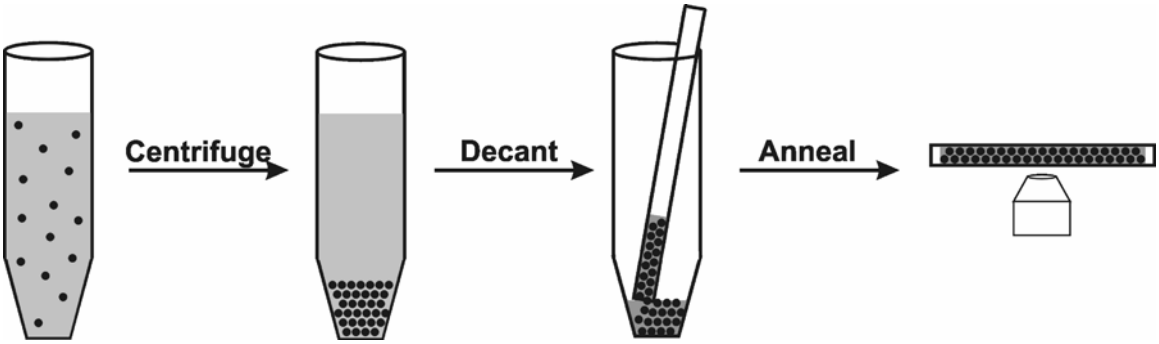

Figure 2.2-1 Method of microgel colloidal crystal assembly for microscope observation.

Microscopy. An Olympus IX 70 inverted microscope equipped with a high numerical aperture, oil immersion 100× objective (N.A.=1.30) was utilized to obtain Differential interference contrast (DIC) images of microgel arrays. Images were captured using a black and white CCD camera (PixelFly, Cooke Corporation). For confocal laser scanning microscopic (LCSM) images, a Leica confocal microscope (Ar^+ laser, 488 nm excitation line) was used. The emission in the range from 500 nm to 650 nm was used to detect fluorescence from the fluorescein dye.

2.3 Results and Discussion

As described above, these particles display both pH and temperature responsivity in that the degree of particle swelling is tunable with these stimuli; Figure 2.3-1 illustrates this responsivity in the form of temperature-dependent PCS data. This technique allows for determination of the particle translational diffusion coefficient in dilute solution, which can then be converted to a hydrodynamic radius (R_h) *via* the Stokes-Einstein equation.[43] These data show that below the characteristic VPT temperature the particles are solvent swollen, a state that exists due to favorable hydrogen bonding interactions

between water and the NIPAm amide groups. The temperature responsivity of the particles manifests itself as a large decrease in particle size upon traversing the VPT temperature. This is an entropically favored volume phase transition, where release of water from the polymer network increases the entropy of the system; a concomitant hydrophobic aggregation of the *p*NIPAm chains occurs thereby resulting in the observed particle size decrease. Although this particular manuscript does not directly deal with the influence of pH on *p*NIPAm-*co*-AAc particle packing, it is worth illustrating the effect pH can have on the particle behavior. Specifically, deprotonation of the AAc groups has a large influence on the degree of swelling. As shown in figure 2.3-1, the particle radius at 25 °C increases from ~410 nm at pH 3.56 to ~530 nm at pH 4.96, reflecting the deprotonation of the AAc groups (pK_a= 4.5), which causes an increase in the Donnan potential and osmotic pressure inside the particles.[39, 44-47] At pH values further above the pK_a, the particles swell further due to complete deprotonation. However, light scattering data for these particles under those conditions are somewhat unreliable, as the refractive index contrast between the highly swollen particles and the solvent is too small for an adequate scattering intensity to be observed. The ability of the particles to swell in response to pH is illustrative of the chain conformation in the protonated particles. Although the particles are network polymers where the chain conformation is somewhat restricted by crosslinks, some degree of a random coil chain conformation is present when the AAc groups are protonated. In other words, the elastic swelling limit of the network does not solely limit the degree of swelling at low pH. However, AAc deprotonation and the resultant increase of the Donnan potential causes the polymer chains to stretch more towards a polyelectrolyte-like (rod-like) conformation and the

network is thus swollen towards its elastic limit. As a result of the pH induced swelling, the magnitude of the size change at the VPT temperature is significantly decreased, as the Coulombic repulsion between neighboring chains decreases the propensity for chain aggregation to occur. This is further evidenced by an increase in the VPT temperature and a broadening of that transition. deprotonation of the AAc groups (pK_a)

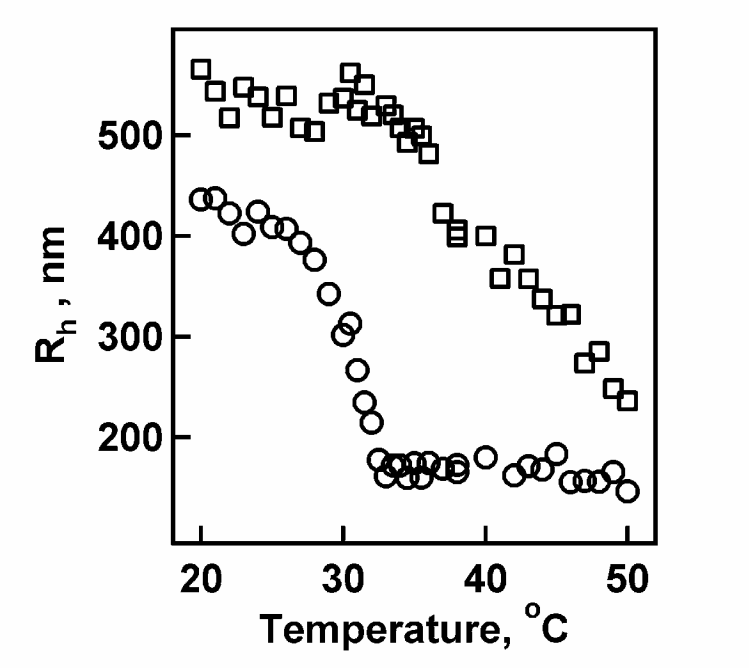

Figure 2.3-1 Photon correlation spectroscopy as a function of temperature for *p*NIPAm-*co*-AAc microgel particles at pH 3.56 (circles) and pH 4.96 (squares). The pH increase induces deprotonation of the AAc groups and hence particle swelling with a concomitant phase transition shift.

Figure 2.3-2 shows series of optical sections taken of a crystal assembled from fluorescein-loaded particles. In this sample, the fluorescein was added to the particle solution prior to centrifugation; the water:particle partition coefficient of the fluorescein lies to the side of the particles, thereby providing fluorescence contrast between the particles and the interstices. Analysis by laser scanning confocal microscopy of

fluorescently dyed crystals indicates that the particles are arranged in a three dimensional FCC lattice with 111 planes facing the wall of the capillary. The degree of particle contact can be estimated by measuring the microgel center-to-center distances from either the confocal or DIC images. These measurements yield distances on the order of ~700 nm. As described above, dilute solution PCS measurements of these microgels reveal a size of 820 nm in diameter, in close agreement with the measured center-to-center distances. The small difference in the size between the two methods may be explained by a slight compression of the microgels during centrifugation and crystallization or by experimental differences between the PCS-measured hydrodynamic radius and microscopy-observed radius. However, it is unwise to ascribe too much quantitative value to these measurements, as the translational diffusion coefficient can be significantly perturbed by dangling chains on the particle surface; the exact relationship between the microscopically observed and spectroscopically determined hydrogel particle sizes is not well-defined. Nonetheless, we have previously demonstrated that large degrees of particle compression are possible in similar materials,[37, 38] so it may indeed be the case that the assembly shown in figure 2.3-2 is comprised of particles that are slightly dehydrated relative to their size in dilute solution. It should further be noted, as we have discussed in previous publications,[37, 38] that the thermoresponsivity of the particles allows us to circumvent the kinetically trapped glassy phase during this assembly process. The relatively inelegant and harsh method of assembly used here (centrifugation) would not be expected to yield the thermodynamically preferred particle arrangement, but should instead yield large regions of kinetically-trapped glassy phase. However, shrinking the particles by raising the sample above the VPT temperature causes an increase in the

particle translational diffusion coefficient (as evidenced by the change in sample viscosity), thereby allowing for assembly of the close-packed thermodynamic product at the expense of the kinetically trapped structure.

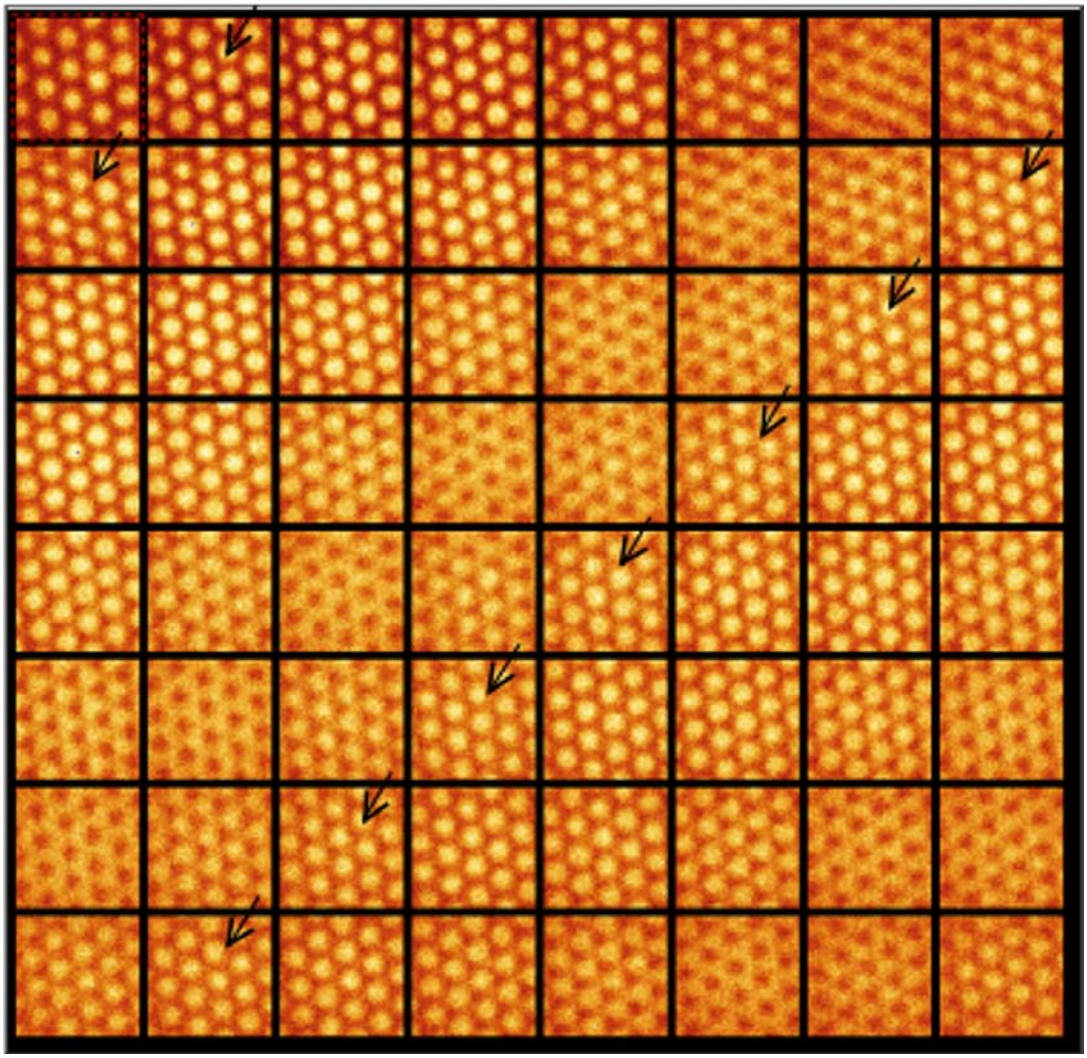

Figure 2.3-2 Series of optical sections of laser scanning confocal microscopy images of fluorescein-dyed *p*NIPAm-*co*-AAc microgel colloidal crystal. Arrows are placed at the exact same location in each image to illustrate the ABCAB…packing in the crystals. The image size is 3.1 μm × 3.1 μm × 7.7 μm.

To better understand the influence of particle concentration on crystal packing, a series of particle dispersions were prepared over a decade-wide range of concentrations (0.66-6.6 w/w% polymer). It is worthwhile noting that these samples were diluted following centrifugation prior to loading into capillaries as opposed to the successive dilution of pre-formed crystals. Any crystallization observed following dilution should not be the result of any templating or "memory" effects. That is, each sample should represent the thermodynamically preferred phase at that volume fraction and should not be influenced by crystallization that occurred when the system was at a higher concentration. All samples were prepared at a pH of 3.8, where ~18% of the AAc groups are protonated. Furthermore, the ionic strength was held constant at 1 mM, where the Debye-Hückel screening length is <10 nm; electrostatic repulsion should not contribute significantly to packing in these dispersions. Thus, if we consider the highest concentration sample to have a 74% fill fraction, the investigated concentration range should span the hard sphere phase diagram from the crystalline region (ϕ=0.494 to 0.74) to the fluid region (below ϕ=0.494). Representative images obtained for these samples are shown in Figure 2.3-3; the polymer weight percentages are indicated on each image along with the "effective" volume fraction (ϕ_{eff}). This effective volume fraction is estimated from the polymer mass fraction using a treatment previously published by Senff and Richtering.[23, 48] In that work, the solvation degree of *p*NIPAm microgels was determined from rheology measurements as a function of crosslinker concentration and temperature. For example, using their data for ~2 mol-% crosslinked *p*NIPAm particles at 25 °C,[48] one would estimate the ϕ_{eff} for image *a* (6.6 w/w%) at 1.10. The fact that this number is greater than 74% (and indeed, greater than 100%) indicates that the particles

have been significantly compressed, as was suggested by the previously presented comparison of the particle sizes obtained from microscopy and PCS. It should be noted that these numbers are simply meant to convey an *estimate* of particle overpacking and hence the "softness" of the particles; it is probable that the absolute magnitude of these estimates are incorrect, given the slightly different synthetic conditions used to produce the microgels used in this study. Also indicated on each panel is the corresponding "hard sphere" particle volume fraction (ϕ) that one calculates if image *a* is defined as having a volume fraction of 0.74 (close packed).

An initial overview of this collection of images reveals the surprising result that the particles crystallize spontaneously even after being diluted 9-fold from the initial polymer concentration (ϕ_{HS}=0.08, ϕ_{eff}=0.12, w/w%=0.73, figure 2.3-3(*h*)). Indeed, only the highest dilution (10-fold dilution, image *i*) shows a disordered fluid phase. If the particles behaved as hard spheres with purely repulsive interaction potentials, the fluid phase should be observable even after a 2-fold dilution (ϕ_{HS}=0.37, 2.3-3(*b*)). If we further account for the softness of the particles, melting should at least be observable following a 3-fold dilution (ϕ_{eff}=0.37, 2.3-3(*c*)). In a sense, these observations are reminiscent of those related to long-range attractive forces in highly charged colloidal systems.[28-30, 32, 49] In those studies, particle solutions diluted far beyond the theoretically predicted (from DLVO theory) freezing point display an unexpected coexistence of crystalline and fluid phases. While the origins of the long range attractive interactions required for such phenomena remain a matter of debate, it is clear that such effects are typically observed only in highly confined systems and/or with highly charged spheres. Neither condition exists here so it is likely that a different force is influencing packing. Closer inspection of

the images in figure 2.3-3 indicates a far more unexpected behavior. In 2.3-3(*a*)-(*h*), no fluid phase is observable and the particles remain closely packed in spite of dilution because *the particles themselves have grown in size*. Indeed, in 2.3-3(*h*), the center-to-center distance is ~1.5 μm, which is ~1.8-times larger than the particle diameter measured in dilute solution by PCS. Although dilution of the dispersion has occurred with respect to polymer w/w%, the particles have grown to maximize particle-particle contact, thus maintaining the assembly at a particle volume fraction that is higher than the freezing point. As with the aforementioned phase coexistence studies, our observations can only result from long-range attractive forces in the pair or multibody potential. Since there are no apparent entropic origins of the particle-particle attractive forces, it seems likely that the forces are of enthalpic origin. Examination of the chemical structure and morphology of the *p*NIPAm-*co*-AAc microgel particles suggests that the only possible attractive interactions are AAc-AAc and/or AAc-amide hydrogen bonding between the particles.[50] While it is expected that these interactions would be weak in an aqueous milieu, multiple interactions along the copolymer chain may be sufficient to stabilize the structure. Indeed, the interactions must not be exceedingly strong in this case, because if the particles were excessively "sticky", assembly of the colloidal crystal would be inhibited by particle-particle friction.

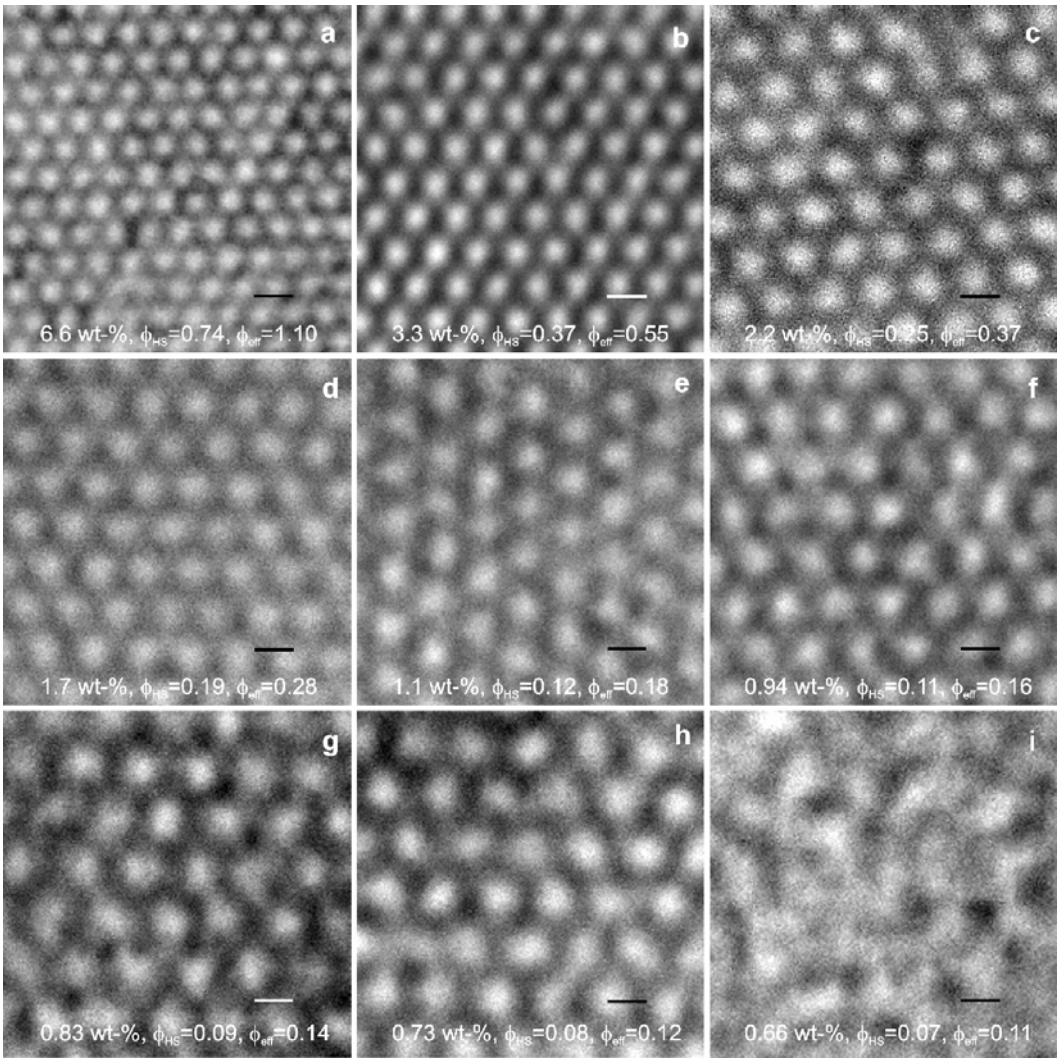

Figure 2.3-3 Differential interference contrast microscopy images of colloidal crystals assembled from *p*NIPAm-*co*-AAc microgel particles (R_h = 410 nm). The polymer concentrations in weight percent are indicated on each image, along with the hard sphere (ϕ_{HS}) and effective (ϕ_{eff}) particle volume fractions. See the text for details concerning these values. Scale bars = 1 μm.

A logical test of this hypothesis would be to study assembly as a function of pH, as hydrogen bonding involving AAc is only efficient at pH values below the pK_a of the acid. Above the pK_a, the *p*NIPAm-*co*-AAc system, with the particle center-to-center distance being less than the hydrodynamic diameter, reflecting compression of the particles during centrifugation. Decreasing the particle concentration by a factor of two (5.85 w/w%, ϕ_{HS}=0.37, ϕ_{eff}=0.98, image electrostatic repulsion should be dominant. In this case, such experiments do not clearly point to the origin of the effect, however. As described above, raising the pH above the pK_a causes extreme particle swelling and also increases the repulsive forces due to electrostatics. Therefore, similar packing effects may be observed at all pH values, where below the pK_a, hydrogen bonding enforces packing *via* attractive interactions, while above the pK_a, packing is enforced by electrostatic repulsion and charge-induced particle swelling. As a result of the complications presented by *p*NIPAm-*co*-AAc particles, the hydrogen-bonding hypothesis was tested using *p*NIPAm particles that do not contain AAc. Again, crystals were prepared by centrifugation of particle dispersions, with all dilutions being performed in the centrifuge tubes prior to capillary loading. In the case of the pNIPAm particles and centrifugation conditions used here, the original (undiluted) pellets were 11.7 w/w% polymer as opposed to the 6.6 w/w% concentration observed for *p*NIPAm-*co*-AAc. Despite this higher polymer concentration, particle assembly is still observed; the results are shown in figure 2.3-4. Again, both the effective (ϕ_{eff}) and hard sphere (ϕ_{HS}) volume fractions are indicated on each image, along with the wt-% polymer in the sample. Analysis of particle packing as a function of volume fraction reveals that efficient packing is observable over a more narrow range of particle concentrations. Figure 2.3-4(*a*) (11.7 w/w%, ϕ_{HS}=0.74,

ϕ_{eff}=1.96) shows a polycrystalline structure in the pNIPAm assembly (R_h=380 nm by PCS) as observed for the *p*NIPAm-*co*-AAc microgel dispersions, with the particle center-to-center distance being less than the hydrodynamic diameter. This reflects compression of the particle during centrifugation. Decreasing the volume fraction by a factor of two (5.85 w/w%, ϕ_{HS}=0.37, ϕ_{eff}=0.98, figure 2.3-4(*b*)) or three (3.9 w/w%, ϕ_{HS}=0.25, ϕ_{eff}=0.65, figure 2.3-4(*c*)) results in a crystalline assembly with increased particle spacing. Finally, dilution of the sample by a factor of four yields a disordered fluid phase with no evidence of strong particle interactions (2.93 w/w%, ϕ_{HS}=0.19, ϕ_{eff}=0.49, figure 2.3-4(*d*)). It is interesting to note that the effective volume fraction of the 4-fold diluted sample lies below the characteristic hard sphere freezing point. It is therefore not surprising that this image should show a fluid phase, since there are no apparent sources of attractive interparticle forces. These results suggest that while microgel particles pack efficiently at high volume fractions independent of the particle chemistry, the presence of AAc is required for crystal stability over a large range of concentrations. The particle-particle interaction potential is therefore strongly perturbed by the presence of AAc, with the attractive forces likely due to multiple hydrogen bonding interactions between the microgel particles.

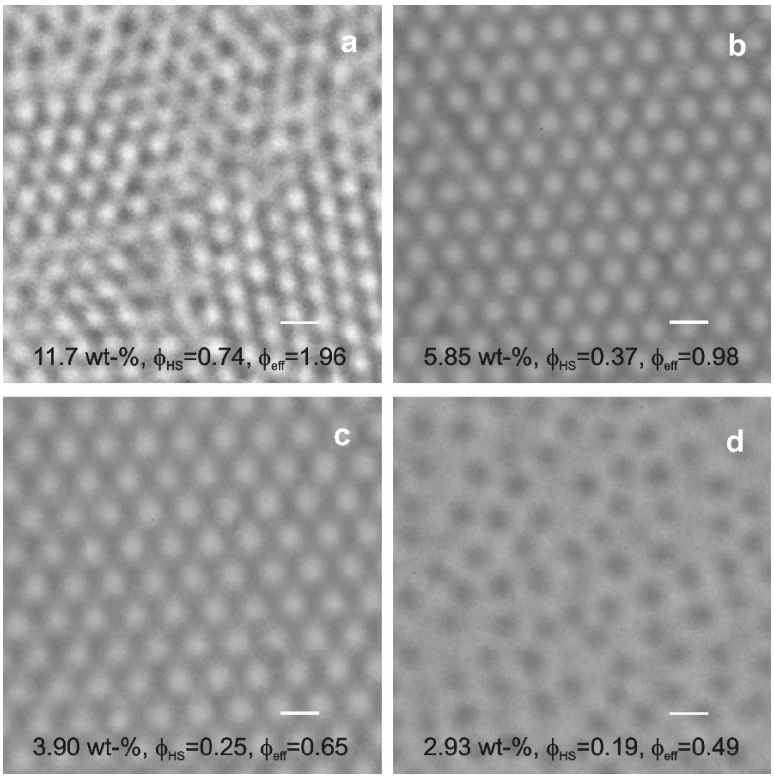

Figure 2.3-4 Differential interference contrast microscopy images of colloidal crystals assembled from *p*NIPAm microgel particles (R_h = 380 nm). The polymer concentrations in weight percent are indicated on each image, along with the hard sphere (ϕ_{HS}) and effective (ϕ_{eff}) particle volume fractions. See the text for details concerning these values. Scale bars = 1 μm.

2.4 Conclusions

In this chapter, the *p*NIPAm-*co*-AAc microgel dispersions over a broad range of concentration were investigated. At the highest packing density, the particles are overpacked, with the center-to-center distance being smaller than the hydrodynamic diameter as determined by PCS. Dilution of those samples by as low as ϕ_{eff}=0.12 is possible without observation of crystal melting and the center-to-center distance (d_{c-c}) calculated in low ϕ_{eff} crystals is larger than the hydrodynamic diameter determined by PCS. This broad range of crystalline assembly can only be due to a previously unidentified particle-particle attractive interaction, which causes particle swelling so as to maintain a close-packed structure. We propose that the origin of this attractive force is hydrogen bonding between the particles due to AAc dimerization and/or AAc-amide interactions. Hydrogen bonding is further implicated as being the origin of these forces as such attractive forces are apparently absent from particles lacking acrylic acid.

References

(1) Strong localization of photons in certain disordered dielectric superlattices, S. John *Phys. Rev. Lett.* **1987**, *58*, 2486.

(2) Inhibited spontaneous emission in solid-state physics and electronics, E. Yablonovitch *Phys. Rev. Lett.* **1987**, *58*, 2059.

(3) Tuning the photonic bandgap properties of crystalline arrays of polystyrene beads by annealing at elevated temperatures, B. Gates, S. H. Park and Y. Xia *Adv. Mater.* **2000**, *12*, 653.

(4) Preparation of photonic crystals made of air spheres in titania, J. Wijnhoven and W. L. Vos *Science* **1998**, *281*, 802.

(5) Synthesis of photonic crystals for optical wavelengths from semiconductor quantum dots, Y. A. Vlasov, N. Yao and D. J. Norris *Adv. Mater.* **1999**, *11*, 165.

(6) Optical properties of planar colloidal crystals: Dynamical diffraction and the scalar wave approximation, D. M. Mittleman, J. F. Bertone, P. Jiang, K. S. Hwang and V. L. Colvin *J. Chem. Phys.* **1999**, *111*, 345.

(7) Band spectroscopy of colloidal photonic crystal films, H. Miguez, V. Kitaev and G. A. Ozin *Appl. Phys. Lett.* **2004**, *84*, 1239.

(8) Diffraction of light by opals, J. V. Sanders *Acta Crystallogr., Sect. A* **1968**, *24*, 427.

(9) Structure of opals, J. V. Sanders *J. Phys., Colloq.* **1985**, 1.

(10) Close-packed structures of spheres of two different sizes. I. Observations on natural opal, J. V. Sanders *Philos. Mag., [Part] A* **1980**, *42*, 705.

(11) Single-crystal colloidal multilayers of controlled thickness, P. Jiang, J. F. Bertone, K. S. Hwang and V. L. Colvin *Chem. Mat.* **1999**, *11*, 2132.

(12) Structured porous materials via colloidal crystal templating: From inorganic oxides to metals, O. D. Velev and E. W. Kaler *Adv. Mater.* **2000**, *12*, 531.

(13) Diffraction of light by ordered suspensions, P. A. Hiltner and I. M. Krieger *J. Phys. Chem.* **1969**, *73*, 2386.

(14) Colloidal crystals, P. Pieranski *Contemp. Phys.* **1983**, *24*, 25.

(15) Phase behaviour of concentrated suspensions of nearly hard colloidal spheres, P. N. Pusey and W. van Megen *Nature* **1986**, *320*, 340.

(16) Phase behavior of concentrated suspensions of nearly hard colloidal spheres, P. N. Pusey and W. Van Megen *Nature* **1986**, *320*, 340.

(17) Is random close packing of spheres well defined?, S. Torquato, T. M. Truskett and P. G. Debenedetti *Phys. Rev. Lett.* **2000**, *84*, 2064.

(18) Star polymers viewed as ultrasoft colloidal particles, C. N. Likos, H. Lowen, M. Watzlawek, B. Abbas, O. Jucknischke, J. Allgaier and D. Richter *Phys. Rev. Lett.* **1998**, *80*, 4450.

(19) Phase diagram of star polymer solutions, M. Watzlawek, C. N. Likos and H. Lowen *Phys. Rev. Lett.* **1999**, *82*, 5289.

(20) Spherical microgel colloids - hard spheres from soft matter, E. Bartsch, S. Kirsch, P. Lindner, T. Scherer and S. Stolken *Ber. Bunsenges. Phys. Chem.* **1998**, *102*, 1597.

(21) Dynamic light scattering study of concentrated microgel solutions as mesoscopic model fo the glass transition in quasiatomic fluids, E. Bartsch, M. Antonietti, W. Schupp and H. Sillescu *J. Chem. Phys.* **1992**, *97*, 3950.

(22) Phase transitions in colloidal suspensions and star polymer solutions, H. Lowen, M. Watzlawek, C. N. Likos, M. Schmidt, A. Jusufi and A. R. Denton *J. Phys.: Condens. Matter* **2000**, *12*, A465.

(23) Temperature sensitive microgel suspensions: Colloidal phase behavior and rheology of soft spheres, H. Senff and W. Richtering *J. Chem. Phys.* **1999**, *111*, 1705.

(24) Ionic microgels as model systems for colloids with an ultrasoft electrosteric repulsion: Structure and thermodynamics, D. Gottwald, C. N. Likos, G. Kahl and H. Lowen *J. Chem. Phys.* **2005**, *122*, 074903/1.

(25) Phase behavior of ionic microgels, D. Gottwald, C. N. Likos, G. Kahl and H. Lowen *Phys. Rev. Lett.* **2004**, *92*, 680103/1.

(26) Charged colloids and polyelectrolytes: From statics to electrokinetics, H. Lowen, A. Esztermann, A. Wysocki, E. Allahyarov, R. Messina, A. Jusufi, N. Hoffmann, D. Gottwald, G. Kahl, M. Konieczny and C. N. Likos *J. Phys.* **2005**, *11*, 207.

(27) Equilibrium and shear induced nonequilibrium phase behavior of pmma microgel spheres, S. E. Paulin, B. J. Ackerson and M. S. Wolfe *J. Colloid Interface Sci.* **1996**, *178*, 251.

(28) A surprisingly attractive couple, D. G. Grier *Nature* **1998**, *393*, 621.

(29) Visible evidence for interparticle attraction in polymer latex dispersions, N. Ise, T. Okubo, K. Ito, S. Dosho and I. Sogami *Langmuir* **1985**, *1*, 176.

(30) Like-charge attractions in metastable colloidal crystallites, A. E. Larsen and D. G. Grier *Nature* **1997**, *385*, 230.

(31) Colloids: A surprisingly attractive couple, D. G. Grier *Nature* **1998**, *393*, 621.

(32) How homogeneous are "homogeneous dispersions"? Counterion-mediated attraction between like-charged species, N. Ise, T. Konishi and B. V. R. Tata *Langmuir* **1999**, *15*, 4176.

(33) Phase transitions in ionic gels, T. Tanaka, D. J. Fillmore, S.-T. Sun, I. Nishio, G. Swislow and A. Shah *Phys. Rev. Lett.* **1980**, *45*, 1636.

(34) Microgel particles as model colloids: Theory, properties and applications, B. R. Saunders and B. Vincent *Adv. Colloid Interface Sci.* **1999**, *80*, 1.

(35) Temperature-sensitive aqueous microgels, R. Pelton *J. Colloid Interface Sci.* **2000**, *85*, 1.

(36) Optical properties of n-isopropylacrylamide microgel spheres in water, J. Gao and Z. Hu *Langmuir* **2002**, *18*, 1360.

(37) Thermoresponsive photonic crystals, J. D. Debord and L. A. Lyon *J. Phys. Chem. B* **2000**, *104*, 6327.

(38) Color-tunable colloidal crystals from soft hydrogel nanoparticles, J. D. Debord, S. Eustis, S. B. Debord, M. T. Lofye and L. A. Lyon *Adv. Mater.* **2002**, *14*, 658.

(39) Synthesis and characterization of multiresponsive core-shell microgels, C. D. Jones and L. A. Lyon *Macromolecules* **2000**, *33*, 8301.

(40) Tunable swelling kinetics in core-shell hydrogel nanoparticles, D. Gan and L. A. Lyon *J. Am. Chem. Soc.* **2001**, *123*, 7511.

(41) Interfacial nonradiative energy transfer in responsive core-shell hydrogel nanoparticles, D. Gan and L. A. Lyon *J. Am. Chem. Soc.* **2001**, *123*, 8203.

(42) Influence of particle volume fraction on packing in responsive hydrogel colloidal crystals, S. B. Debord and L. A. Lyon *J. Phys. Chem. B* **2003**, *107*, 2927.

(43) R. Pecora *Dynamic light scattering*; Plenum Press: New York, 1985.

(44) Colloidal copolymer microgels of n-isopropylacrylamide and acrylic acid: Ph, ionic strength and temperature effects, M. J. Snowden, B. Z. Chowdhry, B. Vincent and G. E. Morris *J. Chem. Soc.-Faraday Trans.* **1996**, *92*, 5013.

(45) P. J. Flory *Principles of polymer chemistry*; Cornell University Press: London, 1953.

(46) Charge controlled swelling of microgel particles, A. Fernandez-Nieves, A. Fernandez-Barbero, B. Vincent and F. J. de las Nieves *Macromolecules* **2000**, *33*, 2114.

(47) Preparation of thermosensitive submicrometer gel particles with anionic and cationic charges, S. Ito, K. Ogawa, H. Suzuki, B. Wang, R. Yoshida and E. Kokufuta *Langmuir* **1999**, *15*, 4289.

(48) Influence of crosslink density on rheological properties of temperature-sensitive microgel suspensions, H. Senff and W. Richtering *Colloid Polym. Sci.* **2000**, *278*, 830.

(49) Pair interaction of charged colloidal spheres near a charged wall, S. H. Behrens and D. G. Grier *Phys. Rev. E* **2001**, *64*, 050401/1.

(50) A simple functional representation of angular-dependent hydrogen-bonded systems. 1. Amide, carboxylic acid, and amide-carboxylic acid pairs, K. T. No, O. Y. Kwon and S. Y. Kim *J. Phys. Chem.* **1995**, *99*, 3478.

CHAPTER 3

Shift Factor Determination

3.1 Introduction

Ideal solids show the simplest relation between force and deformation known as Hooke's law. The force is proportional to the deformation

$$\tau = G \cdot \gamma \qquad (3\text{-}1)$$

where τ is the force per unit area or stress, γ is the relative length change or strain and G is the constant of proportionality or elastic modulus.

On the other hand, ideal liquids follow Newton's law of viscosity, where the stress is proportional to the rate of deformation.

$$\tau = \eta \cdot \dot{\gamma} \qquad (3\text{-}2)$$

where η is the Newtonian viscosity and $\dot{\gamma}$ =dγ/dt.

Many materials obey the ideal laws shown above. However, some materials such as milk, blood, paints, and foods display behavior between the ideal solid and the ideal fluid. These materials are dispersions that consist of discrete particles randomly distributed in fluid media. The behavior between the ideal solid and the ideal fluid can be

the viscosity dependency on the shear rate (called non-Newtonian flow behavior) or complex rheological properties such as viscoelasticity (G', G") as a function of frequency (time) or temperature. Here G' is the storage modulus (elastic component) and G" that of loss modulus (viscous component).

There has been considerable effort in determining and understanding the rheological properties of colloidal dispersions since colloidal dispersions play an important role in many industrial applications. The majority of these works have concentrated on hard, repulsive particles such as polystyrene and silica particles.[1-5] Several studies have shown that the viscoelastic properties of concentrated dispersions are strongly dependent on volume fraction. Increases in volume fraction lead to a decrease in mean particle separation and consequently to a more elastic dispersion.[3, 6-8]

Many groups have investigated the interparticle interactions by studying viscoelastic properties, since the interaction between particles change rheological properties of colloidal dispersions. Paulin et al. modeled the interaction potential of concentrated poly(methymethacrylate) (PMMA) microgel dispersions as $\Psi(r) \propto 1/r^n$ which gives a power law behavior for the concentration dependence of the plateau modulus.[9] They investigated PMMA microgels and a power law exponent of 20 was obtained. The rheological data of plateau modulus showed the *p*NIPAm microgels have repulsive interaction of the order of $(1/r^{12})$,[10] and high frequency shear modulus data demonstrated that the repulsive interaction can be modeled in terms of a power law with an exponent 9.[11] These experiments revealed that *p*NIPAm microgels are best regarded as soft spheres. Unlike a dispersion of hard spheres, the effective volume fraction of the *p*NIPAm microgel dispersions changes with temperature since the thermoresponsive

microgel undergoes phase transition from swollen to collapse upon heating.[12] At low temperature, the storage modulus is higher than the loss modulus implying the microgel dispersions behave like viscoelastic solid. When the dispersions are heated, the dispersions become a viscoelastic liquid with higher loss modulus than storage modulus. This results show the viscoelastic properties and elasticity of thermoresponsive microgel dispersions decrease as the temperature is increased.[11, 13]

Adding a rigid sphere to a fluid changes the flow field and this hydrodymic disturbance increases the viscosity of the dispersion. The viscosity of hard sphere dispersions has been studied by Einstein and he found that the viscosity of dispersion increases by a fraction of the volume fraction of the dispersion.[14, 15]

$$\eta = \eta_S(1 + 2.5 \cdot \phi) \qquad (3\text{-}3)$$

where η is the viscosity of a dispersion, η_s is the solvent viscosity and ϕ is the volume fraction of particles. Here he assumed no interaction between particles.

The addition of particles not only increases the viscosity of dispersion but also introduces deviations from Newtonian behavior. In non-Newtonian fluid, the viscosity changes as shear rate changes. The viscosity decrease observed with increasing shear rate is called shear thinning. The opposite case is known as shear thickening. For both purely repulsive hard spheres[5, 9, 16] as well as electrically stabilized particles,[17] shear thinning is often observed in concentrated dispersions. Other rheological experiments showed that dilute and moderately concentrated *p*NIPAm dispersions behave like low-viscosity liquids at low shear rate and show shear thinning.[10, 13, 18]

Batchelor[19] and Brady and coworkers[20] took Brownian motion of particles into account to contribute to the relative viscosity of such dispersions in dilute solution. This Brownian motion plus hydrodynamic interaction introduces ϕ^2 term to the Einstein's results (3-3). As discussed in other references,[21, 22] it is important to take the quadratic term into account due to the hydrodynamic interaction between particles.

$$\eta_{rel} = 1 + 2.5\phi_{eff} + 5.9\phi_{eff}^2 \qquad (3\text{-}4)$$

where η_{rel} is solvent viscosity and ϕ_{eff} is effective volume fraction.

This expression can be utilized to determine the effective volume fraction of a colloidal dispersion. The volume fraction of rigid sphere particles is easily calculated as the ratio of total sphere volume to total sample volume. However, for microgels, due to the swollen nature of the particles it is not possible to make direct volume fraction calculations based on particle mass and density. A simple method to determine the effective volume fraction of colloidal dispersions is to measure a property, usually the viscosity, of dilute suspensions as a function of weight percent of suspensions.[2, 23-25] The relative viscosity as a function of weight percent of microgel dispersions can be plotted. The fitting for the relative viscosity vs. weight percent is fitted according to equation (3-4) where the effective volume fraction ϕ_{eff} is substituted by $\phi_{eff} = kc$. c is the concentration of the dispersion in weight/weight % and k is the shift factor for converting the concentration to the effective volume fraction. In soft sphere dispersions, it is possible to have volume fractions greater than 0.74, the maximum volume fraction for ideal hard

spheres, because large particle concentrations can lead to particle deformation and deswelling.

In the previous chapter, the shift factor of *p*NIPAm calculated by Richtering[10] was utilized to estimate the effective volume fraction of *p*NIPAm-*co*-AAc microgel dispersions. Since *p*NIPAm-*co*-AAc is more hydrophilic, the same mass of *p*NIPAm-*co*-AAc microgels tends to uptake more water than *p*NIPAm resulting in larger volume. On top of that, unlike *p*NIPAm microgels, the hydrodynamic radius of *p*NIPAm-*co*-AAc microgels is highly dependent on pH of dispersion solutions due to their pH responsivity. The shift factor of *p*NIPAm microgels will not give accurate effective volume fraction of pH responsive microgels. In this chapter, viscosity measurements of microgel dispersions as a function of weight percent and pH will be performed to determine shift factor of *p*NIPA*m*-*co*-AAc microgel dispersions for accurate effective volume fraction calculation.

3.2 Experimental

Microgel Samples Preparation The *p*NIPAm-*co*-AAc (90:10) microgel is synthesized by surfactant free precipitation polymerization as described in chapter 2. A different batch of *p*NIPAm-*co*-AAc microgels is used for this chapter, but properties including volume phase transition are the same. The hydrodynamic radius of *p*NIPAm-*co*-AAc microgels dispersed in pH 3.5 (10 mM) buffer solution at 25 °C is 324 nm.

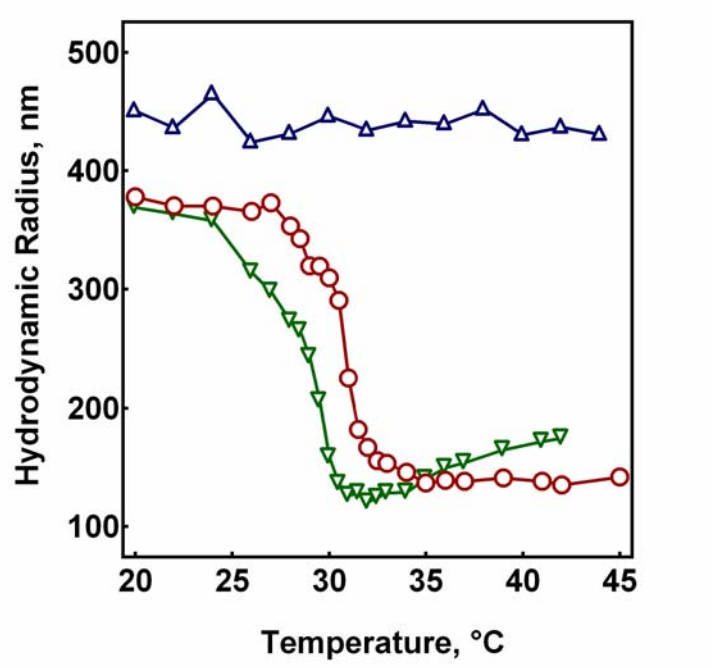

Figure 3.2-1 A volume phase transition behavior from *p*NIPAm-*co*-AAc microgels. As the temperature increases the microgels undergo a deswelling transition, going from solvent swollen to deswollen state at pH 3.0 (∇, upper triangle), pH 3.85 (○, circles) and pH 6.5 (Δ, triangle).

We describe the preparation of microgel dispersions for rheometry experiments. First, the *p*NIPAm-*co*-AAc microgel dispersion was freeze-dried over night then the freeze-dried microgel was redispersed in buffer solutions of desired pH. Buffer solutions of pH 3.0 (μ=15 mM), 3.85 (μ=15 mM), and 6.5 (μ=100 mM) were used for this project. Once the microgels are redispersed completely, the redispersed samples in 3.85, and 6.5 buffer solutions were centrifuged at 29 °C at a relative centrifugal force (RCF) 16,100 g for 1 hour. Microgels redispersed in pH 3.0 buffer solutions were centrifuged RCF 13,000 g at 4 °C for 30 minutes to avoid aggregation since the ionic strength of the dispersion is relatively high. The weight percent of the centrifuged pellet was determined by measuring the mass of centrifuged microgel pellets before and after freeze-drying

assuming that most of the water evaporates during freeze-drying process. The centrifuged pellet was diluted with buffer solution to achieve desired weight percent for the experiments, which is usually ~ 0.1 ~ 1.2 weight percent (w/w%). Once diluted, the samples were place on the shaker table over night to redisperse the microgels completely.

Rheological Measurements The viscosity measurement as a function of shear rate was carried out with a cone-plate rheometer (Physica, MCR300). The diameter of the cone and plate is 50 mm and the angle of the cone is 1 degree. The viscosity of a microgel dispersion was measured while the shear rate raised from 30 s^{-1} to 1000 s^{-1}. The viscosity vs. shear rate was measured at two different temperatures, 22 °C and 25 °C. Since the real room temperature in the lab is ~ 22 °C, the shift factor at 22 °C will be utilized in this thesis for volume fraction calculation.

Error Calculation Usually there is uncertainty associated with each of the individual measurements. Here, the combined effect on the quantity of interest will be evaluated through the propagation of errors analysis. Let's say Q is the desired property determined from n independently measurable quantities through the analytical expressions $Q = Q(x_1, x_2, x_3, \ldots, x_n)$. It is assumed that changes in variables, x_i, are due to random error and the errors involved in one variable do not affect those of any other. Then, the uncertainty or errors in the desired property, ε_Q, is expressed as follows. Here, ε is an *absolute* uncertainty in x_i and x_i is each of variables.

$$\varepsilon_Q^2 = \left(\frac{\partial Q}{\partial x_1}\right)^2 \varepsilon_{x_1}^2 + \left(\frac{\partial Q}{\partial x_2}\right)^2 \varepsilon_{x_2}^2 + \ldots + \left(\frac{\partial Q}{\partial x_n}\right)^2 \varepsilon_n^2 \qquad (3\text{-}3)$$

In this experiment, there are several variables which can contribute to the propagation of error. For both the errors of microgel dispersions for viscosity measurements and dispersions for phase behavior study (will be discussed in the chapters 4, 5, and 6), the following four steps will be included for uncertainty evaluation; measuring the mass of polymer pellet before and after freeze-drying to calculated weight percent of centrifuged microgel pellet, measuring the mass of centrifuged microgel pellet for each sample, measuring the mass of buffer solution for desired weight percent.

As an example, the error involved in pH 3.85 microgel dispersions will be calculated here. After the microgel crystal was prepared by centrifugation, the masses of the crystal before and after freeze-drying were measured. The masses of the crystal before and after were 0.0714 g and 0.0042 g, respectively. To get average, another sample was prepared and the masses before and after were 0.0586 g and 0.0031 g, respectively. The weight percent of the pH 3.85 crystal is 6.08 w/w% and since the balance reads to the level of 0.0001 g, the error here was calculated as follows.

$$error_1 = \left[\left(\frac{0.0001}{0.0042}\right)^2 + \left(\frac{0.0001}{0.0714}\right)^2\right]^{1/2} = 0.0237 \qquad (3\text{-}4)$$

$$error_2 = \left[\left(\frac{0.0001}{0.0031}\right)^2 + \left(\frac{0.0001}{0.0586}\right)^2\right]^{1/2} = 0.0320 \qquad (3\text{-}5)$$

Here error from taking average or adding is $error_{avg} = (error1^2 + error2^2)^{½} = 0.0398$ i.e. 3.98% of 6.08 w/w%. The next step is preparing samples by diluting the centrifuged microgel crystals with buffer solutions. For sample preparation, 0.0253 g of crystal was diluted with 0.7198 g of pH 3.85 buffer solution. Here, the error was calculated as follows.

$$error_3 = \left[\left(\frac{0.0001}{0.0253}\right)^2 + \left(\frac{0.0001}{0.7198}\right)^2\right]^{1/2} = 0.00396 \qquad (3\text{-}6)$$

The weight percent of this sample is calculated in the follow expression and shown at second row in table 3.3-2.

$$w/w\% = 6.08(w/w\%) \times \frac{0.0253(g)}{0.0253(g) + 0.7198(g)} = 0.2064(w/w\%) \quad (3\text{-}7)$$

The overall error for this process results from the multiplication and dividing process shown above. For the error calculation from the multiplication and dividing $error_{overall}$ = $error_{overall}$ = $(relative\ error_1^2 + relative\ error_2^2 + \ldots)^{½}$. Since $error_{avg}$ and *error3* are relative errors, the overall error is $error_{overall} = (error_{avg}^2 + error_3^2)^{½} = 0.0396$ i.e. 3.96% of 0.206 w/w% or 0.008 w/w%. Errors for all other samples were calculated in the same manner as described here and the results are in the parenthesis in the first columns in table 3.3-1~3.3-3.

3.3 Results and Discussion

Viscosity of dispersions as a function of shear rate was measured in the 0.1 ~ 1.2 w/w% range. Figure 3.3-1 shows the viscosity vs. shear rate plot of microgels dispersed

in pH 3.0, 3.85 and 6.5 buffer solutions. The viscosity was measured as shear rate increased as well as decreased and the viscosities obtained from both directions were almost identical. In figure 3.3-1, only viscosity as shear rate increases is plotted.

These plots are examples of microgel dispersions at each pH and the highest concentration from each pH was selected. It has been shown that thermoresponsive microgel dispersions show shear thinning at higher concentration and lower temperature than this experiments.[10, 18, 26] However, the microgel dispersions in these experiments display almost Newtonian behavior in this shear rate range due to low concentration. When the viscosity of each concentration at a certain pH is determined, the averaged viscosity over shear rate was used. The average relative viscosity and standard deviation of each samples are shown in tables 3.3-1~3.3-3. For all samples (not presented here), the viscosity of microgel dispersions at 25 °C is lower than one at 22 °C, since the deswelling of the microgels gives rise to decrease of the effective volume fraction and thus reduces the viscosity of the dispersions.[13, 27]

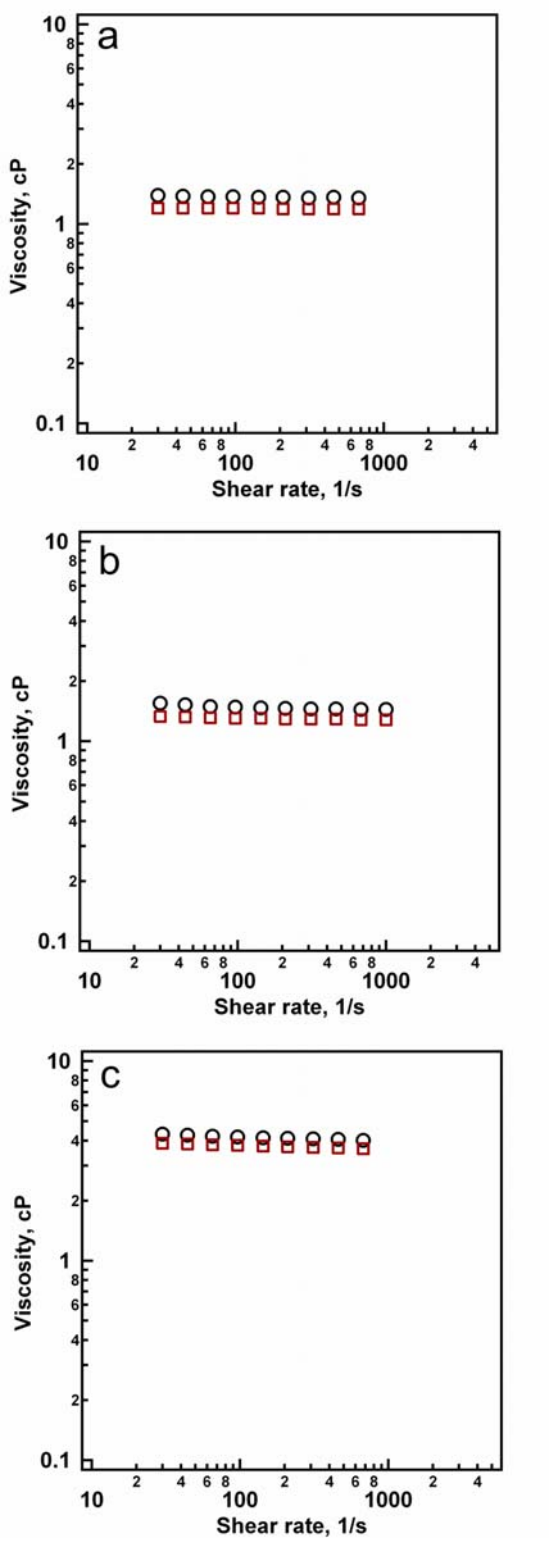

Figure 3.3-1 Shear viscosity of *p*NIPAm-*co*-AAc microgel dispersions as a function of shear rate at 22 °C (open circle) and at 25 °C (open square). The viscosities plotted here were measured as shear rate increased. Pannel (a) c=1.23 w/w%, pH 3.0, (b) c=1.13 w/w%, pH 3.85, and (c) c=1.09 w/w%, pH 6.5

Table 3.3-1 Average relative viscosity and its standard deviation (± sd) of *p*NIPAm-*co*-AAc microgel dispersions in pH 3.0 (15 mM) buffer solution.

Weight % (± absolute error)	η (± sd) at 22 °C	η (± sd) at 25 °C
0.098 (± 0.005)	1.030 (± 0.011)	1.011 (± 0.007)
0.182 (± 0.010)	1.062 (± 0.011)	1.039 (± 0.007)
0.592 (± 0.032)	1.193 (± 0.011)	1.135 (± 0.007)
0.790 (± 0.043)	1.263 (± 0.013)	1.192 (± 0.008)
1.123 (± 0.060)	1.487 (± 0.015)	1.366 (± 0.009)

Table 3.3-2 Average relative viscosity and its standard deviation (± sd) of *p*NIPAm-*co*-AAc microgel dispersions in pH 3.85 (15 mM) buffer solution.

Weight % (± absolute error)	η (± sd) at 22 °C	η (± sd) at 25 °C
0.095 (± 0.004)	1.054 (± 0.005)	1.043 (± 0.032)
0.206 (± 0.008)	1.081 (± 0.010)	1.048 (± 0.010)
0.427 (± 0.017)	1.210 (± 0.009)	1.185 (± 0.017)
0.680 (± 0.036)	1.389 (± 0.014)	1.303 (± 0.701)
0.914 (± 0.065)	1.586 (± 0.018)	1.485 (± 0.026)

Table 3.3-3 Average relative viscosity and its standard deviation (± sd) of *p*NIPAm-*co*-AAc microgel dispersions in pH 6.5 (100 mM) buffer solution.

Weight % (± absolute error)	η (± sd) at 22 °C	η (± sd) at 25 °C
0.107 (± 0.004)	1.074 (± 0.004)	1.050 (± 0.007)
0.134 (± 0.005)	1.072 (± 0.010)	1.062 (± 0.011)
0.211 (± 0.007)	1.113 (± 0.006)	1.104 (± 0.008)
0.253 (± 0.009)	1.133 (± 0.006)	1.116 (± 0.006)
0.434 (± 0.015)	1.263 (± 0.004)	1.237 (± 0.007)

In figure 3.3-2, the relative viscosity of *p*NIPAm-*co*-AAc microgel dispersions is plotted as a function of weight percent. Other than very low weight percent region, relative viscosities of higher pH dispersions are larger than ones of lower pH. This is due to the deprotonation of AAc groups in the microgel network at higher pH. The higher deprotonation of AAc groups leads microgels to swell. This swelling leads higher ϕ_{eff} resulting in relative viscosity. The lines represent fittings according to equation (3-4) with the effective volume fraction substituted by $\phi_{eff} = kc$. The shift factors (k) at different pH and temperatures are given in table 3.3-4. The shift factors have errors ranging from 3% to 10% with 90% confidence level. Since the errors from fitting are larger than errors from measuring (3% ~ 5%) and viscosity measurements (< 1%), the errors from fitting can be considered as major sources of errors in the shift factor determination.

The shift factors show the volume change of microgels and they tend to increase as pH (or protonation) of microgel dispersions increases. When the ratios k/k(pH 3.0) and $[R_h/R_h(\text{pH 3.0})]^3$ are compared, they do not agree well shown in table 3.3-5 and 3.3-6. Compared to the shift factors calculated from ratios $[R_h/R_h(\text{pH 3.0})]^3$, the shift factors obtained from viscosity measurements are higher at pH 3.85 and lower at pH 6.5. This disagreement may originate from different experimental conditions. Since R_h is measured under highly diluted condition, the interaction between particles can be considered to be negligible. However, for viscosity measurements, particles concentration is significantly higher than dynamic light scattering measurements. Samples for viscosity measurements in this chapter have approximately 10~100 times higher particles concentration than one for light scattering experiments. At pH 3.0, most AAc groups on the microgel particles are protonated so that the microgels do not have many charged groups for ion-dipole

interaction between deprotonated AAc and AAc or amides. Since there is a little interaction between particles, microgel dispersions at pH 3.0 most likely will obey equation (3-4) well. At pH 3.85, there is more ion-dipole interaction between particles and this attractive interaction may result in higher viscosity. As a result, the shift factors could be overestimated. At pH 6.5, further deprotonation of AAc leads microgels to highly charged species. The same charge on the microgels may give rise to repulsion between particles and lower relative viscosity. This lower relative viscosity would give smaller shift factor at pH 6.5.

In general, the shift factors determined by viscosity measurements show the volume change of microgels well. But for more accurate shift factor determination, better models to explain the rheological behavior of microgels dispersions with interactions need to be investigated.

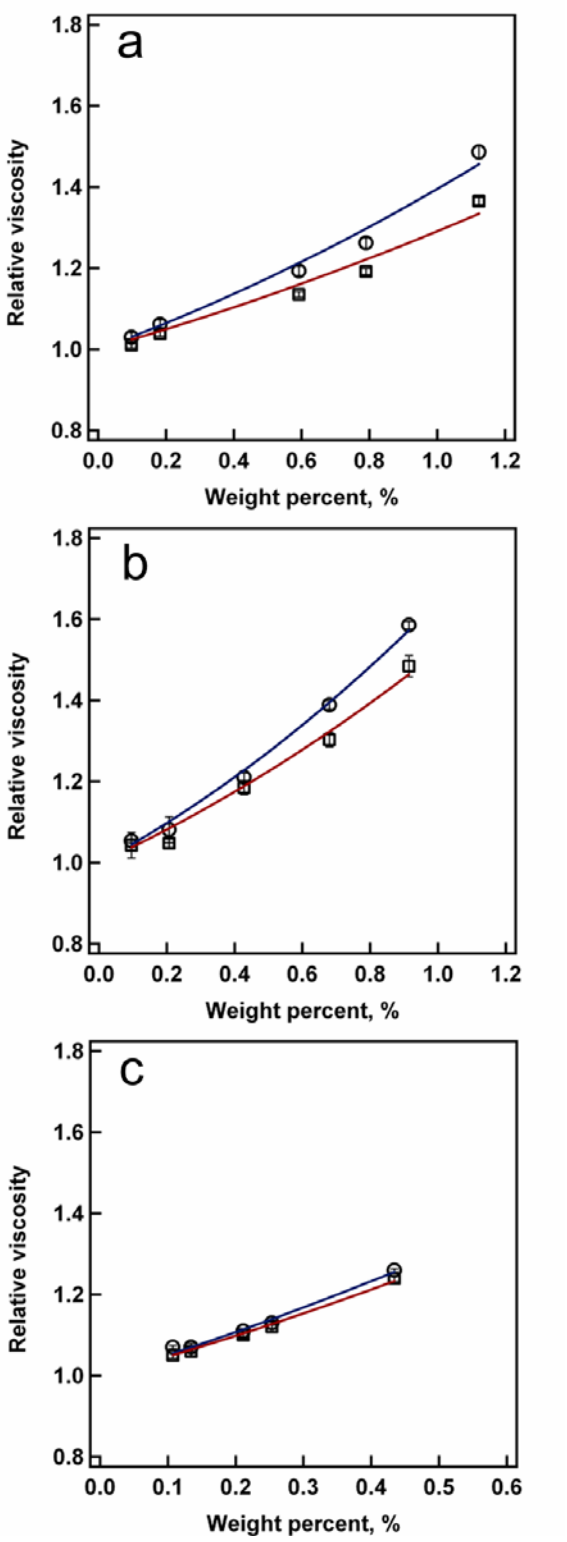

Figure 3.3-2 Viscosity of microgels vs. microgel concentration in weight percent plot at 22 °C (open circle) and 25 °C (open square) at different pHs. Pannel (a) pH 3.0, (b) pH 3.85, and (c) pH 6.5. The error bars represent standard deviation of viscosity measurement at the weight percent. The lines display fitting according to equation 3-4.

Table 3.3-4 The shift factors, *k*, and confidence range at 90 % confidence level, c, of *p*NIPAm-*co*-AAc microgel dispersions of different pH at 22 °C and 25 °C.

	k (±c) at 22 °C	*k* (± c) at 25 °C
pH 3.0	12.3 (± 0.92)	9.5 (± 1.02)
pH 3.85	18.1 (± 0.66)	15.3 (± 1.04)
pH 6.5	19.7 (± 1.02)	18.1 (± 0.66)

Table 3.3-5 Shift factor ratio, volume ratio and shift factor (*k'*) calculated from volume ratio of *p*NIPAm-*co*-AAc microgel dispersions of different pH at 22 °C.

	R_h (nm)	k/k(pH 3.0)	$[R_h/R_h(\text{pH 3.0})]^3$	*k'*
pH 3.0	376.7	1.00	1.00	12.3
pH 3.85	399.3	1.47	1.19	14.6
pH 6.5	447.8	1.59	1.68	20.6

Table 3.3-6 Shift factor ratio, volume ratio and shift factor (*k'*) calculated from volume ratio of *p*NIPAm-*co*-AAc microgel dispersions of different pH at 25 °C.

	R_h (nm)	k/k(pH 3.0)	$[R_h/R_h(\text{pH 3.0})]^3$	*k'*
pH 3.0	345.7	1.00	1.00	9.5
pH 3.85	361.6	1.61	1.14	10.9
pH 6.5	455.5	1.48	2.29	21.8

3.4 Conclusions

In this chapter, the shift factors of *p*NIPAm-*co*-AAc microgel dispersions were determined by performing viscosity measurements as a function of weight percent of microgels. At all pH and temperature, the viscosity increases as weight percent of microgels increases. The shift factors are calculated by fitting the viscosity vs. weight percent according to equation (3-4). At 22 °C, the shift factors of *p*NIPAm-*co*-AAc microgel dispersions of pH 3.0, 3.85, and 6.5 are 12.3, 18.1, and 19.7 respectively. At 25 °C, the shift factors of *p*NIPAm-*co*-AAc microgel dispersions of pH 3.0, 3.85, and 6.5 are 9.5, 15.3, and 18.1 respectively.

References

(1) Rheology of monodisperse latices, I. M. Krieger *J. Colloid Interface Sci.* **1972**, *3*, 111.

(2) Hard sphere colloidal dispersions: Viscosity as a function of shear rate and volume fraction, C. G. Kruif, E. M. F. van Iersel, A. Vrij and W. B. Russel *J. Chem. Phys.* **1985**, *83*, 4717.

(3) Viscoelastic properties of concentrated latexes. Part 2. Theoretical analysis., R. Buscall, J. W. Goodwin, J. Hawkins and R. H. Ottewill *J. Chem. Soc. Faraday Trans.* **1982**, *78*, 2889.

(4) Control of particle size in the formation of polymer latexes, J. W. Goodwin, R. H. Ottewill, H. M. Pelton and D. E. Yates *Br. Polym. J.* **1978**, *10*, 173.

(5) Viscosity and structural relaxation in suspensions of hard-sphere colloids, P. N. Segre, S. P. Meeker, P. N. Pusey and W. C. K. Poon *Phys. Rev. Lett.* **1995**, *75*, 958.

(6) Rheological studies on concentrated polystyrene latex sterically stabilized by poly(ethylene oxide) chains, W. Liang, T. F. Tadros and P. F. Luckham *J. Colloid Interface Sci.* **1992**, *153*, 131.

(7) The viscoelastic properties of polystyrene particles bearing poly(ethylene oxide)-poly(propylene oxide) aba block copolymers, I. T. Kim and P. F. Luckham *Colloids Surf.* **1992**, *68*, 243.

(8) Viscoelastic properties of polyacrylonitrile particles stabilized by a poly(2-vinylpyridine)/poly(tert-butylstyrene) block copolymer, M. A. Ansarifar and P. F. Luckham *Colloid Polym. Sci.* **1989**, *267*, 736.

(9) Equilibrium and shear induced nonequilibrium phase behavior of pmma microgel spheres, S. E. Paulin, B. J. Ackerson and M. S. Wolfe *J. Colloid Interface Sci.* **1996**, *178*, 251.

(10) Temperature sensitive microgel suspensions: Colloidal phase behavior and rheology of soft spheres, H. Senff and W. Richtering *J. Chem. Phys.* **1999**, *111*, 1705.

(11) Rheology of thermoresponsive latex particles including the high-frequency limit, I. Deike, M. Ballauff, N. Willenbacher and A. Weiss *J. Rheol.* **2001**, *45*, 709.

(12) Microgel particles as model colloids: Theory, properties and applications, B. R. Saunders and B. Vincent *Adv. Colloid Interface Sci.* **1999**, *80*, 1.

(13) The rheology of deformable and thermoresponsive microgel particles, O. D. M. Kiminta, P. F. Luckham and S. Lenon *Polymer* **1995**, *36*, 4827.

(14) A new determination of molecular dimensions, A. Einstein *Ann. Phys.* **1906**, *19*, 289.

(15) A new determination of molecular dimensions, A. Einstein *Ann. Phys.* **1911**, *34*, 591.

(16) Shear-induced order in suspensions of hard spheres, B. J. Ackerson and P. N. Pusey *Phys. Rev. Lett.* **1988**, *61*, 1033.

(17) Hydrodynamic and colloidal interactions in concentrated charge-stabilized polymer dispersions, F. M. Horn, W. Richtering, J. Bergenholtz, N. Willenbacher and N. J. Wagner *J. Coll. Inter. Sci.* **2000**, *225*, 166.

(18) Influence of crosslink density on rheological properties of temperature-sensitive microgel suspensions, H. Senff and W. Richtering *Colloid Polym. Sci.* **2000**, *278*, 830.

(19) The effect of Brownian motion on the bulk stress in an suspension of spherical particles, G. K. Batchelor *J. Fluid Mech.* **1977**, *83*, 97.

(20) Normal stresses in colloidal dispersions, J. F. Brady and M. Vicic *J. Rheol.* **1995**, *39*, 545.

(21) Comment on viscosity and structural relaxation in suspensions of hard-sphere colloids, I. M. De Schepper, E. G. D. Cohen and R. Verberg *Phys. Rev. Lett.* **1996**, *77*, 584.

(22) Viscosity and structural relaxation in suspensions of hard-sphere colloids. Reply to comment, P. N. Segre, S. P. Meeker, P. N. Pusey and W. C. K. Poon *Phys. Rev. Lett.* **1996**, *77*, 585.

(23) Experimental studies on the rheology of hard-sphere suspensions near the glass transition, L. Marshall and C. F. Zukoski *J. Phys. Chem.* **1990**, *94*, 1164.

(24) The rheology of a concentrated colloidal suspension of hard spheres, D. A. Jones, B. Leary and D. V. Boger *J. Colloid Interface Sci.* **1991**, *147*, 479.

(25) The rheology of a sterically stabilized suspension at high concentration, D. A. Jones, B. Leary and D. V. Boger *J. Colloid Interface Sci.* **1992**, *150*, 84.

(26) Rheology of a temperature sensitive core-shell latex, H. Senff, W. Richtering, C. Norhausen, A. Weiss and M. Ballauff *Langmuir* **1999**, *15*, 102.

(27) Viscosity transition in aqueous suspensions of hydrogel microspheres, H. H. Hooper, J. Yu, A. P. Sassi and D. S. Soane *J. Appl. Poly. Sci.* **1997**, *63*, 1369.

CHAPTER 4

Effect of Attractive Interaction on the Phase Behavior of pH Responsive Microgel Assemblies

4.1 Introduction

Due to a relatively slow rate of diffusion and a length scale large enough to be seen under an optical microscope, it has been a matter of interest to investigate the phase behavior of colloidal dispersions as a model system for fundamental problems of condensed matter science such as crystal nucleation, phase behavior, and interaction potentials.[1-4] Besides the easy experimental accessibility, recent developments in digital image processing combined with video microscopy[5-9] provide excellent tools for studying colloidal dispersions. To understand phase behavior of such systems, many research groups have investigated effective interactions that govern the phase behavior of colloidal dispersions. The simplest model system is the hard sphere system.[10] Details of hard sphere interaction and hard sphere phase diagram are described in the chapter 1.3.1. More complicated interparticle interactions such as the soft sphere interactions were studied. Latex particles dispersed in a good solvent, star polymers, ionic microgels have been utilized as a model system to study such interactions.[11-15] The effective interaction potential and the phase diagrams of soft spheres are discussed in the chapter 1.3.1 and cited references.[11, 14-18]

Recently, thermoresponsive microgels have gained interest as a new building block to prepare colloidal crystals.[19-25] The microgels are spherical sub-micron sized

water-soluble polymer networks. Below its characteristic lower critical solution temperature (LCST) of ~31 °C, *p*NIPAm exists as a solvated random coil in aqueous media. Some trapped water molecules form ordered clusters called structured water to minimize the energy due to hydrophobic components in the microgel network. However, above the LCST, the chains collapse to a hydrophobic globular state due to the entropically favored release of water from the polymer. Since the water molecules outside of the microgel have much higher freedom, the overall entropy of the collapsed system is higher than in the swollen state. This transition is usually referred to as the volume phase transition (VPT), where the microgel undergoes a transition from a swollen to a de-swollen network. It has been shown that *p*NIPAm microgels form well ordered arrays and they exhibit interesting phase behavior and optical properties due to thermoresponsivity and softness.[21-25] In our previous study, we prepared poly(*N*-isopropylacrylamide-*co*-acrylic acid) (*p*NIPAm-*co*-AAc) microgel crystals and investigated phase behavior of the microgel dispersions. Unusual crystallization at very low effective volume fractions was observed from *p*NIPAm-*co*-AAc microgel dispersions at the pH of ~ 3.8 which is lower than its pK_a.[24, 26] The microgel dispersions showed crystals as low as ϕ_{eff}=0.12 and the center-to-center distance ($d_{c\text{-}c}$) calculated in low ϕ_{eff} crystals was larger than the hydrodynamic radius determined by dynamic light scattering. Our hypothesis said that there is a cooperative attractive interaction between particles. The overall interaction from many particles leads microgels form thermodynamically stable structure i.e. crystal. We further proposed that the origin of this interaction is AAc-AAc and/or AAc-amide hydrogen bonding between the particles.

In this chapter, we will address issues of the phase of pH responsive microgel self-assemblies at different pH to explore the effect of attractive interaction on the phase behavior of pH responsive microgel dispersions. Particular emphasis will be placed on the phase behavior of pH responsive microgel dispersions not only as a function of ϕ_{eff} but also as a function of pH to see how the changes of interactions have affected the phase diagram of microgel dispersions.

4.2 Experimental

Microgel Synthesis and Characterization Responsive microgels, *p*NIPA*m-co-AA*c, were synthesized by surfactant free precipitation polymerization as described previously.[26] The ratio of *N*-isopropylacrylamide(NIPAm) to acrylic acid (AAc) is 90:10 and 2% of cross-linking agent (*N, N*'-methylenebis(acrylamide)) was incorporated in the polymer. The hydrodymic radius and the size distribution of microgels were determined by photon correlation spectroscopy (PCS, Protein Solutions, Inc.). The hydrodynamic radius of the microgels and the volume phase transition of the pH responsive microgels at different pH are shown in Figure 3.2-1 in chapter 3. For pH 3.0 and pH 3.85, 15 mM ionic strength solutions were used to achieve stable pH. Both size and VPT display pH responsivity of *p*NIPAm-*co*-AAc microgel. The hydrodynamic radius of microgel at pH 3.0 and pH 3.85 are 377 nm and 399 nm respectively. At pH 3.0, since the most AAc groups in the microgel are protonated, the microgels have a VPT temperature at around 31 °C which is similar to *p*NIPAm. However, as pH increases, *p*NIPAm-*co*-AAc microgels uptake water molecules due to Coulombic repulsion and osmotic swelling due to counterion influx (Donnan potential) resulting in an increase in the size of the

microgels. The VPT temperature is also shifted to temperatures greater than 31 °C due to Coulombic repulsion in the polymer network.

The freshly made *p*NIPAm-*co*-AAc microgels were freeze-dried overnight; then the freeze-dried microgels were redispersed in buffer solutions of the desired pH. Different pHs were chosen for this study: pH 3.0 (15 mM ionic strength) for fully protonated microgels and pH 3.85 (15 mM ionic strength) for partially deprotonated microgels. Once the microgels were redispersed completely, the microgel dispersions at pH 3.85 were centrifuged at 29 °C at a relative centrifugal force (RCF) of 16,100 g for 1 hour; the microgels redispersed in pH 3.0 buffer solution were centrifuged at a RCF of 13,000 g at 4 °C for 30 minutes to avoid aggregation. The centrifuged microgel assemblies were diluted by adding buffer solution to achieve the desired weight percent for the experiments. The diluted samples were placed on the shaker table over night to completely redisperse the microgels. The microgel dispersions were transferred into rectangular glass tubes (Vitrotube, 0.1 mm × 2.0 mm × 50 mm) for observation under a microscope.

Effective Volume Fraction of Dispersion Determination To determine the effective volume fraction of microgel dispersions at different pH, viscosity experiments were performed.[17] The relative viscosity as a function of weight percent of microgel dispersions was plotted. And the fitting for the relative viscosity vs. weight percent is plotted according to equation (3-4) where the effective volume fraction ϕ_{eff} is substituted by $\phi_{eff} = kc$. Here, k is the shift factor and c is the microgel concentration in weight percent (w/w%). Viscosity measurements at different weight percents were carried out with a cone-plate type rheometer (MCR300, Anton Paar).

The shift factors for pH 3.0 and 3.85 dispersions at 25 °C are 12.3 and 18.1, respectively. The details of the viscosity measurement and fitting will not be covered since they have been discussed in the chapter 3. Once the shift factor is determined, the ϕ_{eff} of microgel dispersion can be determined by multiplying *k* by c.

Microscopy and Particle Tracking Analysis An Olympus IX 70 inverted microscope equipped with a high numerical aperture, oil immersion 100X objective (N.A.=1.30) was used to obtain images of microgel arrays. Images were captured using a black and white CCD camera (PixelFly, Cooke Corporation). For particle analysis, short movies were taken at a speed of 10 frames per second (fps). After the movies were obtained, particle tracking analysis was performed with IDL image analysis (Research Systems, Inc.). IDL uses the trajectories from each sample to calculate the mean square displacement (MSD) for each sample. The trajectories themselves show the phase of each sample so that one can discriminate between glassy and fluid phase. Quantative properties, such as the diffusion of the particles, can be determined by calculating mean square displacement. The mean square displacement (MSD) is an average distance each particle travels. It is defined as

$$MSD(t) = \sum_{i}^{N} \left\langle \Delta r_i(t)^2 \right\rangle = \sum_{i}^{N} \left\langle \left(r_i(t) - r_i(0) \right)^2 \right\rangle \qquad (4\text{-}2)$$

where, $r_i(t)$- $r_i(0)$ is the vector distance traveled by a particle *i* over some time interval of length *t*, and *N* is the number of particles in a system. If the particle encounters no other particles, then the distance it travels would be proportional to the time interval and the

MSD would increase quadratically with *t*. In denser phases, such as the fluid phase, quadratic behavior holds only for a very short time interval beyond which the motion is better described as a random walk. As a result, the MSD increases linearly with time. Finally, as the system becomes solid, particles are confined by their neighbors so that the MSD reaches a plateau over time.

Besides trajectories and MSD vs. time plots, we have determined the radial distribution function, *g(r)*, of microgel dispersions to see their structure and the center-to-center distance ($d_{c\text{-}c}$) between particles. The radial distribution function is defined as follows.

$$\rho(0,r) = \rho \cdot g(r) \qquad (4\text{-}3)$$

where, $\rho=N/V$ is the average density in the fluid of N particles in a container of volume V, $\rho(0,r)$ is the probability that a particle is at a distance r when there is another particle at the origin of coordinates. The absence of long-range order, such as in a fluid or glassy phase, would show very smooth peaks like the solid line in figure 4.2-1, while a well ordered system would have distinctive and sharp peaks like the dotted line in Figure 4.2-1.

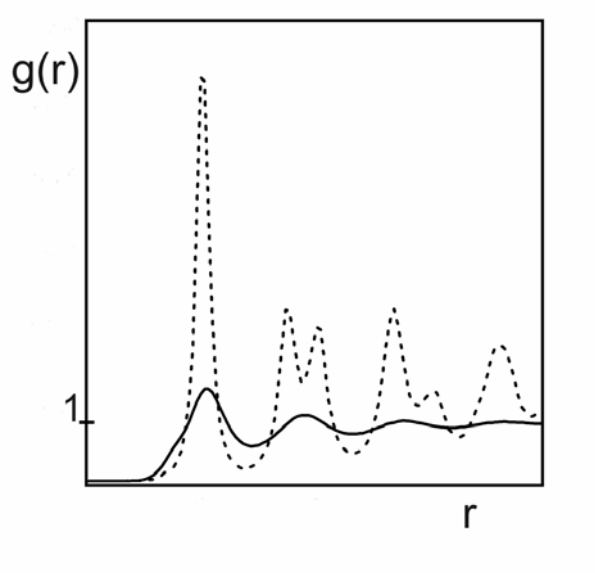

Figure 4.2-1 Radial distribution function of disordered phase (solid line) and ordered phase of hexagonal structure (dotted line).

4.3 Results and Discussion

The effective volume fraction for this study was calculated by multiplying the shift factor and the weight percent of microgels. As mentioned in chapter 3, at pH 3.85, the shift factor determined by viscosity measurements and one calculated from the ratio $[R_h/R_h(\text{pH } 3.0)]^3$ do not agree well. The shift factor measured by viscosity experiments is 18.1 and the shift factor calculated from the ratio is 14.6 at 22 °C. For comparison, both shift factors will be used to determine the effective volume fraction of pH 3.85 microgel dispersions. In all figures, the effective volume fraction calculated from the ratio $[R_h/R_h(\text{pH } 3.0)]^3$ will be presented in parenthesis and denoted as $\phi_{eff,calculated}$.

Figure 4.3-1 shows photographs of different effective volume fractions (ϕ_{eff}) of microgel dispersions at pH 3.85. At the effective volume fraction of 0.65 seen in figure 4.3-1(a), the microgel dispersion looks turbid that could imply a disordered structure.

Very weak color may originate from a couple layers of colloidal crystals on the glass surface rather than from the crystals. As the effective volume fraction of dispersions decreases to 0.60 (figure 4.3-1(b)), the optical properties of the samples change from turbid to iridescent. This change may indicate the phase transition of microgel dispersions from a disordered to a well-ordered structure or crystal. In figure 4.3-1(b)-(d), or ϕ_{eff} range between 0.60-0.45, crystalline phase is observed. At ϕ_{eff} = 0.42, a mixed phase of crystal and disordered is observed. Further decrease of the effective volume fraction leads the microgel dispersion to a disordered phase as shown in figure 4.3-1(f) (ϕ_{eff}= 0.37). The effective volume fractions calculated from the ratio $[R_h/R_h(\text{pH } 3.0)]^3$ have a disordered phase at $\phi_{eff,calculated}$= 0.52, the crystalline phases $\phi_{eff,calculated}$ of between 0.48-0.34 and fluid phase at $\phi_{eff,calculated}$= 0.30. In any case, the melting transition of responsive microgel dispersions occurs at lower effective volume fraction than hard sphere.

To see the pH effect on the phase diagram, microgel dispersions in pH 3.0 buffer solutions are prepared in the same manner as the microgel dispersions at pH 3.85. In figure 4.3-2(a), the sample is turbid implying the disordered phase. Microgel dispersions of pH 3.0 exhibit a change from turbid to irridescent at an effective volume fraction of 0.66 as seen figure 4.3-2(b). The samples are crystalline phase ϕ_{eff} of between 0.66-0.53 as shown in figure 4.3-2(b)-(e). The microgel dispersion is disordered phase again at ϕ_{eff}= 0.49. Microgels dispersed in pH 3.0 buffer solutions have similar melting transition as hard sphere system. More samples (not shown here) represent the melting transition between ϕ_{eff}= 0.51 and 0.49.

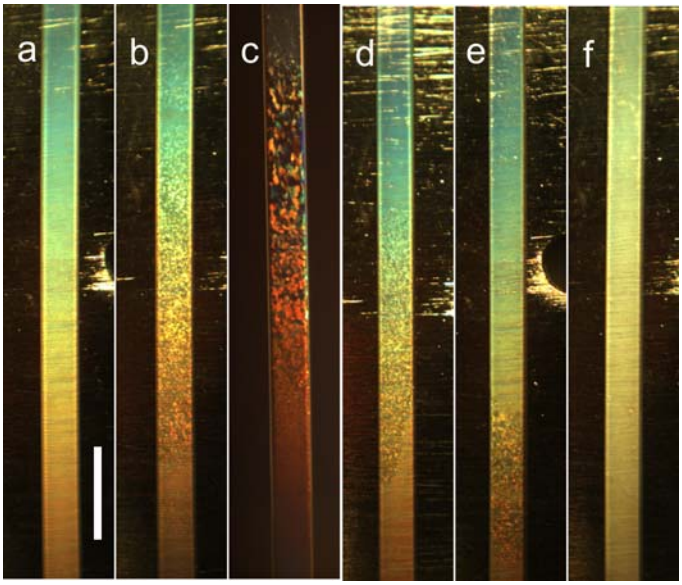

Figure 4.3-1 Photographs of *p*NIPAm-*co*-AAc dispersions in a rectangular glass tube. Photographs were taken from a range of pH 3.85 dispersions. These assemblies were prepared by filling the glass tube by capillary action from heated to right above the LCST of the microgels. The sample was then allowed to cool at room temperature and age for several days. (a) ϕ_{eff}= 0.65 ($\phi_{eff,calculated}$=0.52), (b) ϕ_{eff}= 0.60 ($\phi_{eff,calculated}$=0.48), (c) ϕ_{eff} = 0.48 ($\phi_{eff,calculated}$=0.38), (d) ϕ_{eff} = 0.45 ($\phi_{eff,calculated}$=0.36), (e) ϕ_{eff} = 0.42 ($\phi_{eff,calculated}$=0.34), and (f) ϕ_{eff}= 0.37 ($\phi_{eff,calculated}$=0.30). Scale bar is 5 mm.

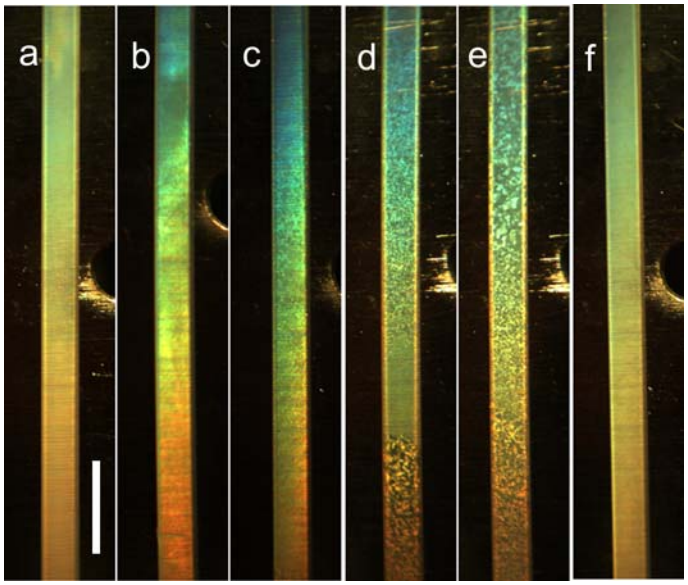

Figure 4.3-2 Photographs of *p*NIPAm-*co*-AAc dispersions in a rectangular glass tube. Photographs were taken from a range of pH 3.0 dispersions. These assemblies were prepared in the same manner was as in Figure 4.3-1. (a) ϕ_{eff}= 0.71, (b) ϕ_{eff}= 0.66, (c) ϕ_{eff} = 0.62, (d) ϕ_{eff} = 0.58, (e) ϕ_{eff} = 0.53, and (f) ϕ_{eff} = 0.49. Scale bar is 5 mm.

The photographic images show an unusually low melting transition at pH 3.85. To see this phase transition of microgel dispersions at the microscopic level, the samples were observed under a microscope. For consistency, the middle of the samples was chosen to take images. Differential interference contrast (DIC) micrograph images of samples are presented in Figure 4.3-3. These are the same samples presented in Figure 4.3-1. As effective volume fraction decreases, *p*NIPAm-*co*-AA microgel dispersions undergo a phase transition from disordered to ordered, and finally to disordered phase.

Richtering has shown a freezing point of $\phi_{eff} \sim 0.59$, for soft, *p*NIPAm microgel dispersions.[17] The results in this study show that the freezing point of comparable *p*NIPAm-*co*-AAc dispersions in pH 3.0 is $\phi_{eff} \sim 0.51$. The similar phase behavior at pH 3.0 as hard sphere system suggests that the interaction between microgels in pH 3.0 buffer solution is mainly repulsive. However, at pH 3.85, microgel dispersions show a stable structure (crystal) at the effective volume fraction as low as 0.42. As observed in some coexistence studies[27-32], this unusual crystalline phase at low effective volume fraction can be explained by weak attractive-type interactions. In our previous study[26], we proposed that the source for the attractive interaction is the hydrogen bonding between AAc-AAc and/or AAc-amide groups. However, our data indicate that partially deprotonated microgel dispersions play a role in the effective interaction between particles. Examination of the chemical structure and morphology of the *p*NIPAm-*co*-AAc microgels suggests that the only sources for the attractive interactions are ion-dipole interactions between deprotonated AAc and AAc and/or amide. According to a literature, the interaction energy between deprotonated AAc and AAc and/or amide were determined as 29.3 kcal/mol and 25.4 kcal/mol, respectively.[33] Since the polymer chains

on the microgel surface are flexible, it would not cost too much energy for polymer chains to rearrange for the interaction. As a result, at pH 3.85, the attractive interactions through ion-dipole interaction give rise to extra stabilization to the microgels.

To understand the phase behavior of microgel dispersions in a quantative manner, we acquired movies and performed particle tracking analysis. The trajectories, shown in figure 4.3-3, confirm the phase of dispersions as seen in the photograph images. The trajectories of dispersions at ϕ_{eff}=0.65 in figure 4.3-3(a) show disordered and confined structure indicating that they are glassy. Here, the particle diffusion is inhibited by their neighbors due to the high energy required to rearrange the particles. At the ϕ_{eff} of 0.60, the mixed phase of crystal and disordered phase is observed. The ϕ_{eff} of microgel dispersions between 0.48 and 0.45 in figure 4.3-3(c) and (d), the samples display ordered phases as seen in the photograph images. Interestingly, particles of lower ϕ_{eff} microgel dispersion have faster diffusion. As ϕ_{eff} decreases to 0.42, the diffusion of particles becomes larger and the particles lose crystalline structure. Some particles look like form short-range ordered structure composed of 4~5 particles, but the sample do not have long-range order. Finally, the microgel dispersion at ϕ_{eff}=0.37 shows disordered structure and a high diffusion that is indicative of the fluid phase.

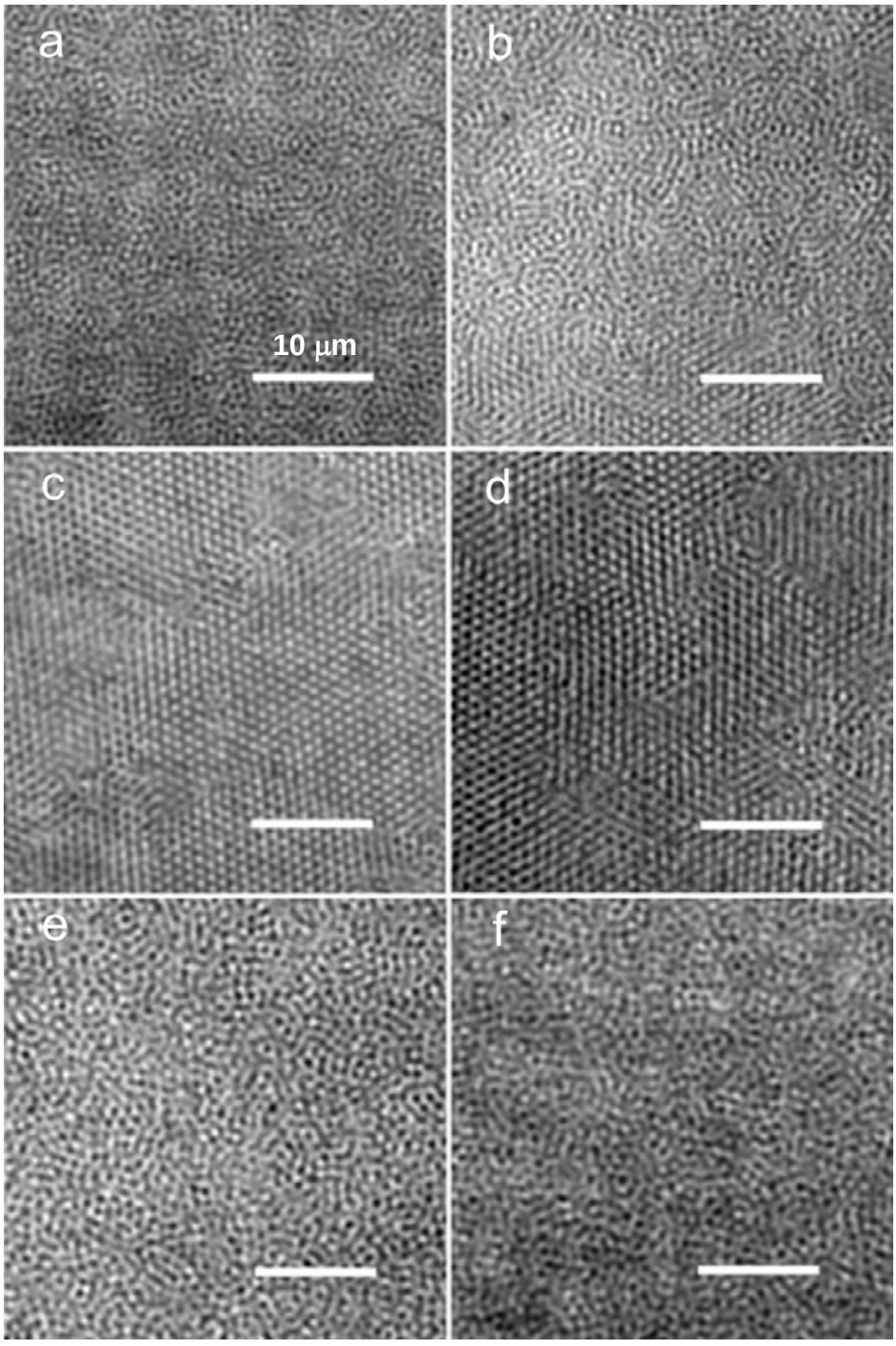

Figure 4.3-3 Differential interference contrast microscopy images of colloidal dispersions assembled from *p*NIPAm-*co*-AAc microgels dispersed in pH 3.85 (15 mM ionic strength) buffer solution. (a) ϕ_{eff}=0.65 ($\phi_{eff,calculated}$=0.52), (b) ϕ_{eff}= 0.60 ($\phi_{eff,calculated}$=0.48), (c) ϕ_{eff} =0.48 ($\phi_{eff,calculated}$=0.38), (d) ϕ_{eff}=0.45 ($\phi_{eff,calculated}$=0.36), (e) ϕ_{eff} =0.42 ($\phi_{eff,calculated}$=0.34), and (f) ϕ_{eff}=0.37 ($\phi_{eff,calculated}$=0.30). Scale bar is 10 μm.

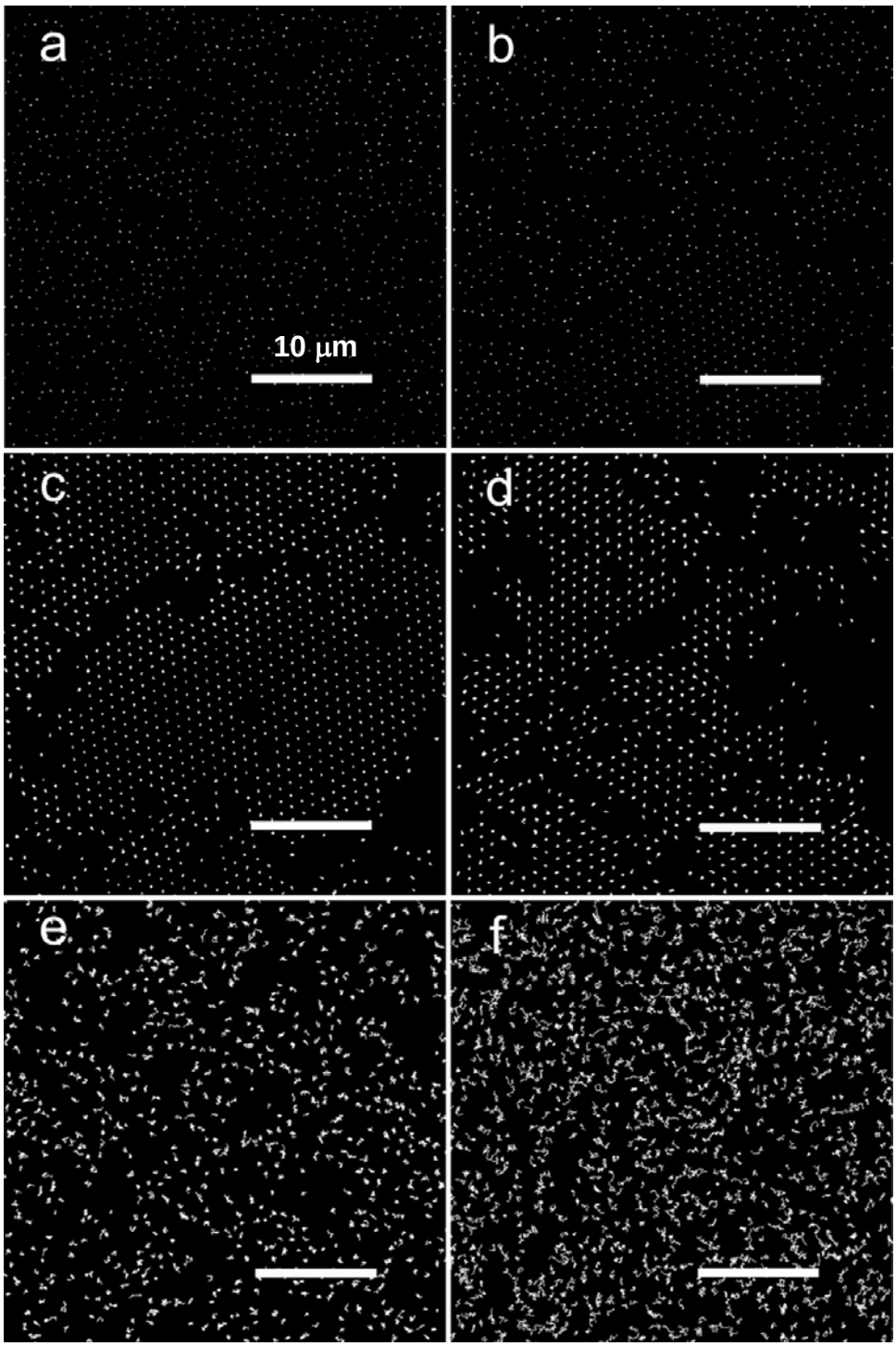

Figure 4.3-4 Particle trajectories of *p*NIPAm-*co*-AAc microgel assemblies (R_h = 399 nm at 22 °C) dispersed in pH 3.85 (μ=15 mM) buffer solution. (a) ϕ_{eff}=0.65 ($\phi_{eff,calculated}$=0.52), (b) ϕ_{eff}= 0.60 ($\phi_{eff,calculated}$=0.48), (c) ϕ_{eff} =0.48 ($\phi_{eff,calculated}$=0.38), (d) ϕ_{eff}=0.45 ($\phi_{eff,calculated}$=0.36), (e) ϕ_{eff} =0.42 ($\phi_{eff,calculated}$=0.34), and (f) ϕ_{eff}=0.37 ($\phi_{eff,calculated}$=0.30). Scale bar is 10 μm.

The particle tracking analysis also gives MSD vs. lag time plots. In the MSD vs. lag time plot seen figure 4.3-5, the diffusion of microgels becomes slower as the effective volume fraction increases. The plot changes from straight line with a slope almost equal to 1 to lines which reach a plateau. This indicates that the diffusion of the system changes from diffusive to non-diffusive behavior. At lower effective volume fraction such as ϕ_{eff}= 0.37, the microgels diffuse freely without confinement by neighboring particles. However, higher particle concentrations leave particles less room to move and more friction to overcome in order to rearrange. As a result, the diffusion at higher particle concentrations is slower than at lower effective volume fractions.

The radial distribution functions, *g(r)*, of microgel dispersions support the phase transitions shown so far. As the effective volume fraction increases, the structure of the samples change from disordered (black line) to ordered (yellow and green lines) and, finally, to disordered structure (purple line). With the help of micrograph images, trajectories and MSD vs. lag time plot, one can see that the disordered structure predicted in *g(r)* of ϕ_{eff}= 0.65 is, in fact, glassy phase. The microgel dispersion at ϕ_{eff} of 0.60 has smooth but distinctive peaks at distance of ~ 2.1 μm and 3.2 μm. These smooth peaks indicate that the dispersion has some ordered structure which has shown in trajectories in Figure 4.3-4(b). Well ordered arrays observed from ϕ_{eff}= 0.55 and 0.42 give rise to sharp and distinctive peaks in the plot. At ϕ_{eff}=0.42, the *g(r)* reveals that the dispersion does not have ordered structure. The dispersion in Figure 4.3-1 (e) has both a disordered and crystalline phase at the same time. Again, since the movie was taken from disordered phase in the sample, *g(r)* show fluid phase. Another disordered structure obtained from the sample at ϕ_{eff}= 0.37 originates from the fluid phase. A closer look at the trajectories

reveals that as the ϕ_{eff} of microgels decreases the first peak shifts toward larger *r*. Since the maximum position of the first peak is highly related to the average d_{c-c} of particles, one can determine the distance from *g(r)* plot. The d_{c-c} at different ϕ_{eff} is presented in table 4.3-1; the d_{c-c} becomes larger as the ϕ_{eff} decreases. This increase of the distance may result from uptaking more water molecules as the samples are diluted with buffer solution. The microgels in the dispersions are highly concentrated so that the particles are close enough to interact with each other. Then, the d_{c-c} would not be larger than hydrodynamic radius. For at all effective volume fractions in this experiment, the d_{c-c} calculated from *g(r)* is larger than hydrodymic diameter, 798 nm, measured by DLS at the same pH and similar temperature. This is mainly due to that the effective volume fraction is much lower than melting point.

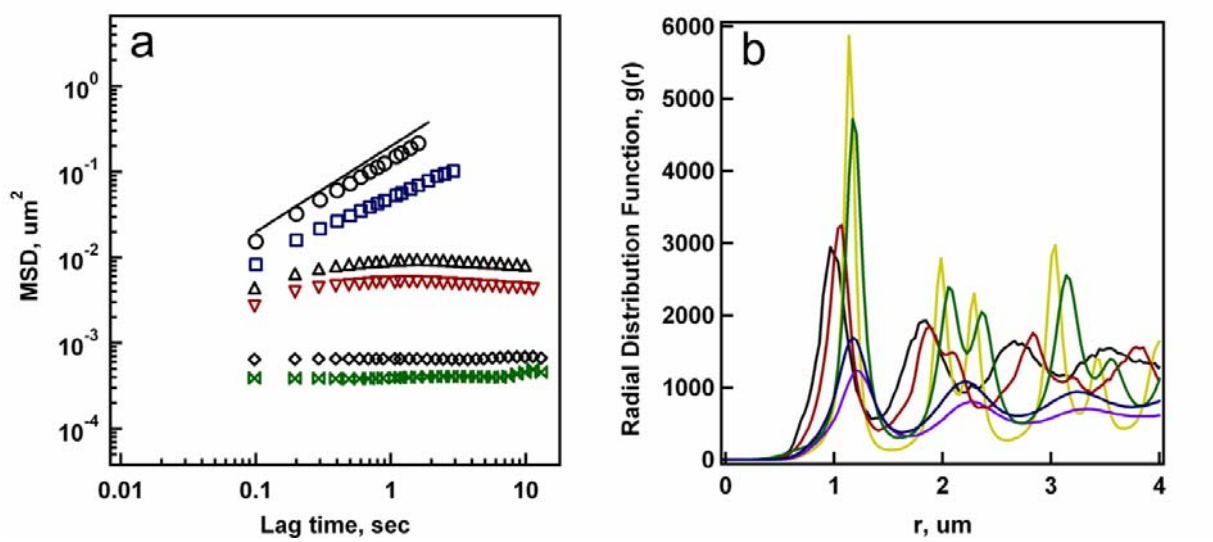

Figure 4.3-5 (a) MSD vs. lag time plots of microgel assemblies dispersed in pH 3.85 (15 mM ionic strength) buffer as effective volume fraction changes. ϕ_{eff}= 0.65 (○, circle), ϕ_{eff}= 0.60 (□, rectangular), ϕ_{eff}= 0.48 (Δ, upper triangle), ϕ_{eff}= 0.45 (∇, inverse triangle), ϕ_{eff}= 0.42 (◊, diamond) and ϕ_{eff}= 0.37 (⋈, bow). The straight line is a trend line. (b) Radial distribution function of the same microgel dispersions as (a). ϕ_{eff}= 0.65 (black), ϕ_{eff}= 0.60 (red), ϕ_{eff}= 0.48 (yellow), ϕ_{eff}= 0.45 (green), ϕ_{eff}= 0.42 (blue) and ϕ_{eff}= 0.37 (purple).

Table 4.3-1 The center-to-center distance (d_{c-c}) distance calculated from *g(r)*.

ϕ_{eff}	0.65	0.60	0.48	0.45	0.42	0.37
d_{c-c} (μm)	0.97	1.07	1.14	1.17	1.17	1.21

Finally, the melting points of the dispersions were measured in order to see if the attractive interaction changes the phase transition behavior of microgel particles in the dispersions. The turbidity change of microgel dispersions upon heating can be used to determine the melting point of microgel dispersions. According to dynamic light scattering experiments, the microgels deswell at 31 °C and the turbidity of microgels increases dramatically due to the increase of reffractive index. Figure 4.3-6 shows the microgel dispersion of pH 3.85 at ϕ_{eff}= 0.57 upon heating. The temperature was increased very slowly to avoid melting due to the thermal convection. This sample is crystalline at room temperature (not shown). As the temperature increases, the sample starts to melt at 59 °C (figure 4.3-6(e)) and loses crystalline phase gradually. As seen in the figure 4.3-6(f), the microgel dispersion does not melt completely even if the sample is heated up to 62 °C. The dispersion at ϕ_{eff}= 0.45 (not shown) starts to lose crystalline phase at 40 °C and melt at 45 °C. Figure 4.3-7 illustrates a microgel dispersion of pH 3.0 at ϕ_{eff}= 0.53 upon heating for comparison. The microgel dispersion of pH 3.0 starts to melt at 26 °C and turns completely opaque at 27 °C.

Significantly higher melting point for crystals observed only in partially protonated conditions clearly implies strong attractive forces between particles under partially protonated conditions. This large difference between crystal melting and the VPT temperature suggests that the attractive interaction is strong enough to overcome the shrinking of polymer chains upon heating. Here, the polymer chains on the microgel surfaces may penetrate each other and orient to the conformation for the attractive interaction.

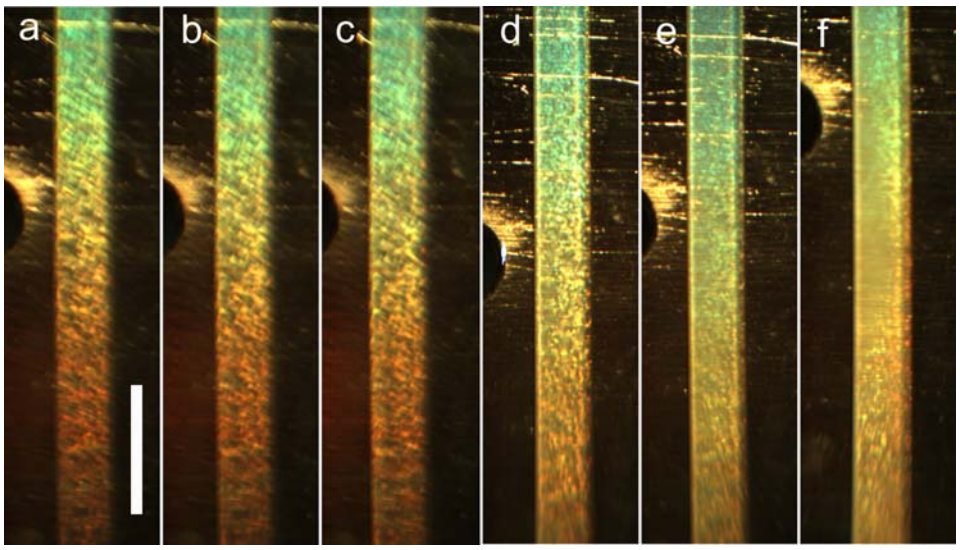

Figure 4.3-6 Photographs of microgel dispersions of ϕ_{eff}= 0.57 in a glass tube at pH 3.85 as the crystal is heated slowly. (a) 29 °C, (b) 36 °C, (c) 40 °C, (d) 56 °C, (e) 59 °C, and (f) 62 °C. Scale bar is 5 mm.

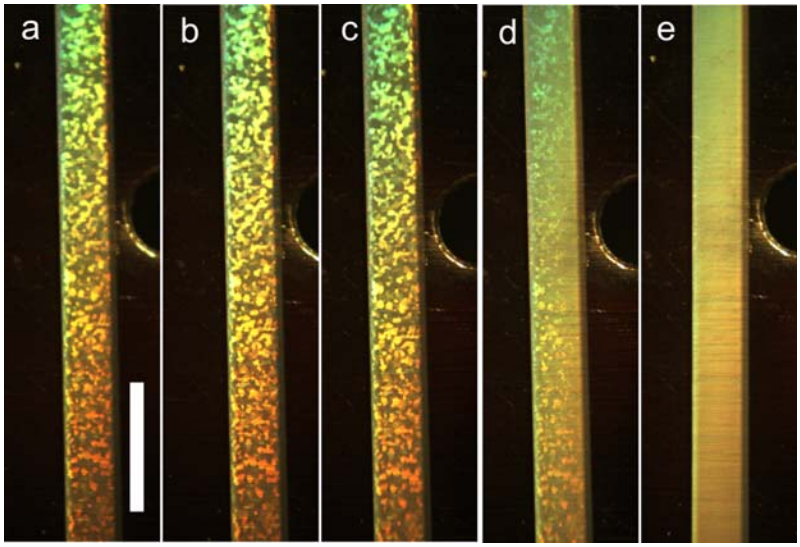

Figure 4.3-7 Photographs of microgel dispersions of ϕ_{eff}= 0.53 in a glass tube at pH 3.0 as the crystal is heated. (a) 20 °C, (b) 23 °C, (c) 25 °C, (d) 26 °C, and (e) 27 °C. Scale bar is 5 mm.

4.4 Conclusions

We presented the phase behavior of pH responsive, *p*NIPAm-*co*-AA*c*, microgels depending on the pH of the dispersions through different approaches. Photographs and micrograph images revealed that pH responsive microgel dispersions undergo phase transition from fluid to the crystal or glassy phase. MSD vs. lag time plot and the radial distribution function confirmed the phase transition of microgel dispersions as effective volume fraction increases. Above all, the unusual crystallization at low effective volume fraction was observed as the pH of the microgel dispersion approaches pK_a of microgels while microgel dispersions at lower pH show a similar phase diagram as hard sphere system. The bulk microgel crystals close to the to pK_a of AAc start to melt at much higher temperature than the LCST of the microgel while the bulk microgel crystals at pH 3.0 melt completely below the LCST of the microgel. The similar phase behavior as hard sphere system and the bulk crystal melting suggest that the interaction between microgels in pH 3.0 buffer solution is mainly repulsive. This melting transition at low effective volume fraction can be explained by an attractive interaction. The attractive interaction is originated from ion-dipole interaction and/or hydrogen bonding. At pH 3.85, ion-dipole interaction between deprotonated AAc and AAc/amide is dominant so that the effective interaction is attractive while the effective interaction at pH 3.0 is repulsive.

References

(1) Microporous materials: Electrochemically grown photonic crystals, P. V. Braun and P. Wiltzius *Nature* **1999**, *402*, 603.

(2) Single-crystal colloidal multilayers of controlled thickness, P. Jiang, J. F. Bertone, K. S. Hwang and V. L. Colvin *Chem. Mat.* **1999**, *11*, 2132.

(3) Thermally switchable periodicities and diffraction from mesoscopically ordered materials, J. M. Weissman, H. B. Sunkara, A. S. Tse and S. A. Asher *Science* **1996**, *274*, 959.

(4) Optical properties of colloidal photonic crystals confined in rectangular microchannels, H. Miguez, S. M. Yang and G. A. Ozin *Langmuir* **2003**, *19*, 3479.

(5) Methods of digital video microscopy for colloidal studies, J. C. Crocker and D. G. Grier *J. Coll. Inter. Sci.* **1996**, *179*, 298.

(6) The microscopic dynamics of freezing in supercooled colloidal fluids, D. G. Grier and C. A. Murray *J. Chem. Phys.* **1994**, *100*, 9088.

(7) Kinetics of crystal growth in charged colloidal suspensions, T. Palberg, M. Wuerth, J. Schwarz and P. Leiderer *Prog. Colloid Polym. Sci.* **1995**, *98*, 6.

(8) Martensitic transition in a confined colloidal suspension, J. A. Weiss, D. W. Oxtoby, D. G. Grier and C. A. Murray *J. Chem. Phys.* **1995**, *103*, 1180.

(9) Video microscopy of colloidal suspensions and colloidal crystals, P. Habdas and E. R. Weeks *Curr. Opinion in Coll. & Inter. Sci.* **2002**, *7*, 196.

(10) Phase behavior of concentrated suspensions of nearly hard colloidal spheres, P. N. Pusey and W. Van Megen *Nature* **1986**, *320*, 340.

(11) Star polymers: From conformations to interactions to phase diagrams, C. N. Likos and H. M. Harreis *Condens. Matter. Phys.* **2002**, *29*, 173.

(12) Phase diagram of star polymer solutions, M. Watzlawek, C. N. Likos and H. Lowen *Phys. Rev. Lett.* **1999**, *82*, 5289.

(13) Star polymers viewed as ultrasoft colloidal particles, C. N. Likos, H. Lowen, M. Watzlawek, B. Abbas, O. Jucknischke, J. Allgaier and D. Richter *Phys. Rev. Lett.* **1998**, *80*, 4450.

(14) Ionic microgels as model systems for colloids with an ultrasoft electrosteric repulsion: Structure and thermodynamics, D. Gottwald, C. N. Likos, G. Kahl and H. Lowen *J. Chem. Phys.* **2005**, *122*, 074903/1.

(15) Equilibrium and shear induced nonequilibrium phase behavior of pmma microgel spheres, S. E. Paulin, B. J. Ackerson and M. S. Wolfe *J. Colloid Interface Sci.* **1996**, *178*, 251.

(16) Thermodynamic properties of the fluid and solid phases for inversed power potentials, W. G. Hoover, S. G. Gray and K. W. Johnson *J. Chem. Phys.* **1971**, *55*, 1128.

(17) Temperature sensitive microgel suspensions: Colloidal phase behavior and rheology of soft spheres, H. Senff and W. Richtering *J. Chem. Phys.* **1999**, *111*, 1705.

(18) Phase transitions in colloidal suspensions and star polymer solutions, H. Lowen, M. Watzlawek, C. N. Likos, M. Schmidt, A. Jusufi and A. R. Denton *J. Phys.: Condens. Matter* **2000**, *12*, A465.

(19) Pnipam-co-polystyrene core-shell microgels: Structure, swelling behavior, and crystallization, T. Hellweg, C. D. Dewhurst, W. Eimer and K. Kratz *Langmuir* **2004**, *20*, 4330.

(20) Colloidal crystals made of poly(n-iospropylacrylamide) microgel particles, T. Hellweg, C. D. Dewhurst, E. Bruckner, K. Kratz and W. Eimer *Colloid Polym. Sci.* **2000**, *278*, 972.

(21) Optical properties of n-isopropylacrylamide microgel spheres in water, J. Gao and Z. Hu *Langmuir* **2002**, *18*, 1360.

(22) Crystallization kinetics of thermosensitive colloids probed by transmission spectroscopy, S. Tang, Z. Hu, Z. Cheng and J. Wu *Langmuir* **2004**, *20*, 8858.

(23) Phase behavior of thermally responsive microgel colloids, J. Wu, B. Zhou and Z. Hu *Phys. Rev. Lett.* **2003**, *90*, 048304/1.

(24) Color-tunable colloidal crystals from soft hydrogel nanoparticles, J. D. Debord, S. Eustis, S. B. Debord, M. T. Lofye and L. A. Lyon *Adv. Mater.* **2002**, *14*, 658.

(25) Thermoresponsive photonic crystals, J. D. Debord and L. A. Lyon *J. Phys. Chem. B* **2000**, *104*, 6327.

(26) Influence of particle volume fraction on packing in responsive hydrogel colloidal crystals, S. B. Debord and L. A. Lyon *J. Phys. Chem. B* **2003**, *107*, 2927.

(27) Visible evidence for interparticle attraction in polymer latex dispersions, N. Ise, T. Okubo, K. Ito, S. Dosho and I. Sogami *Langmuir* **1985**, *1*, 176.

(28) How homogeneous are "homogeneous dispersions"? Counterion-mediated attraction between like-charged species, N. Ise, T. Konishi and B. V. R. Tata *Langmuir* **1999**, *15*, 4176.

(29) Like-charge attractions in metastable colloidal crystallites, A. E. Larsen and D. G. Grier *Nature* **1997**, *385*, 230.

(30) Colloids: A surprisingly attractive couple, D. G. Grier *Nature* **1998**, *393*, 621.

(31) Pair interaction of charged colloidal spheres near a charged wall, S. H. Behrens and D. G. Grier *Phys. Rev. E* **2001**, *64*, 050401/1.

(32) When like charges attract: Interactions and dynamics in charge-stabilized colloidal suspensions, D. G. Grier *J. Phys.: Condens. Matter* **2000**, *12*, A85.

(33) Ionic hydrogen bond and ion solvation. 6. Interaction energies of the acetate ion with organic molecules. Comparison of CH_3COO^- with Cl^-, CN^-, and SH^-, M. Meot-Ner *J. Am. Chem. Soc.* **1988**, *110*, 3854.

CHAPTER 5

Phase Evolution of pH Responsive Microgel Dispersions

5.1 Introduction

Colloidal assemblies have been a subject of study for both their potential applications such as photonic crystals,[1] optical materials[2, 3] and for fundamental studies of phase transitions in condensed matter.[4-8] The nucleation and growth of colloidal crystals has been intensively studied to understand fundamental properties such as freezing or melting transitions.[9-13] Hard sphere like colloidal particles such as silica, polystyrene (PS) and polymethylmethacrylate (PMMA) particle suspensions have been widely used as model systems to investigate the nucleation and growth of crystals.[14-17] Models based on classical nucleation theory have been employed to analyze nucleation kinetics.[18-20] In the case of dispersions of particles with long-range Coulombic interactions, the crystal size is found to increase linearly with time,[21] whereas, for particles with short-range, hard-sphere interactions, the size of the crystals increases by the square root with time.[22] These and other studies have enhanced the understanding of crystallization kinetics.[19, 20, 23] However, since steady state nucleation rate is generally assumed in these works, comparisons between experimental results and model calculations have shown discrepancies that cannot be attributed to approximations of theory or uncertainties in experiments.[22, 24] Classical nucleation theory predicts the increase of nucleation rate[20, 22] as the volume fraction increases while the experimental results show the colloidal nucleation rate increases as the volume fraction increases and then the rate decreases above a certain volume fraction.[13, 18] Model calculations by the Zukoski group suggest

that the nucleation rate, crystal growth velocity and induction time are affected by the decrease in the background monomer volume fraction as crystallization progresses.[25] Also, it is observed that above the melting point volume fraction, crystal growth appears to be suppressed by high nucleation rate.[13, 26]

Recently, responsive microgels have gained interest as a new building block for colloidal self-assemblies. When the building block is thermoresponsive material, the phase of the microgel dispersions is determined not only by the effective volume fraction of a dispersion but also by the temperature.[27] Thermoresponsivity affects on the optical properties[28] and results in interesting melting transitions.[14] Finally, the Bragg peaks of such assemblies can be easily tuned by changing the water content in the microgel assemblies.[29]

In the previous chapter, we have shown that pH responsive microgel, *p*NIPAm-*co*-AAc), dispersions exhibited crystals at unusually low effective volume fractions as the microgel dispersions approach pK_a of the AAc. The microgel dispersions at pH 3.85 form a well ordered structure as low as ϕ_{eff}=0.42, while the same microgels redispersed in pH 3.0 buffer show the ordered-to-disordered transition at ϕ_{eff}=0.51. Short-range, cooperative weak attractive forces between particles were proposed to explain the melting transition at low effective volume fraction of dispersions at the pH close to pK_a. The origins of the attractive force between particles are the ion-dipole interaction and/or the hydrogen bonding. The bulk crystal melting transition dependency on the pH supported our hypothesis. At pH 3.85, the crystal of ϕ_{eff} =0.57 started to lose crystallinity at 59 °C that is much higher than LCST of microgel, while the microgel crystal of ϕ_{eff}=0.53 at pH 3.0 completely melt at 27 °C. This huge increase of crystal stability shown by the pH 3.85

sample data can be attributed to the attractive interaction between microgel particles. One can imagine that different energetics due to the attractive interaction would also affect the dynamics of samples. In this chapter, our goal is to explore the dynamics of pH responsive microgel dispersions over time to understand how energetics governs the dynamics of pH responsive microgel dispersions. Different pH values are chosen for this study: pH 3.0 (15 mM ionic strength) for fully protonated microgels and pH 3.85 (15 mM ionic strength) for partially deprotonated microgels. Fully protonated microgels have few sources for the attractive interaction while partially protonated microgels have sources for both hydrogen bonding and ion-dipole interaction. First, phase evolutions of samples at different pHs are studied. We observe the microgel dispersions of a variety of effective volume fractions at different pHs. Second, microscope images and trajectories are presented to investigate the phase evolution at the microscopic level. Third, mean square displacement (MSD) data are presented for quantative analysis. Two different spots are chosen to see spatially heterogeneous nature of the samples. Also, MSD data calculated from pH 3.0 dispersions are presented for comparison. Fourth, the radial distribution function shows the structural change of evolving samples. Then, we will discuss the phase and particle diffusion dependency on the position during crystal growth. For this experiment, several spots in a sample are chosen during crystallization processes. Finally, the melting transition of bulk samples is discussed. In chapter 4, the pH dependency on the bulk crystal melting was presented. In this study, we also investigate the bulk sample melting dependency on the phase of dispersions.

5.2 Experimental

Materials and Particle Synthesis. See chapter 2 for details.

Crystal Assembly. The purified microgels were freeze-dried and redispersed in buffer solution of desired pH and ionic strength. Once the microgels were redispersed completely, the dispersions at pH 3.85 was centrifuged at 29 °C at a relative centrifugal force (RCF) of 16,100 g for 1 hour; the microgels redispersed in pH 3.0 buffer solution were centrifuged at a RCF of 13,000 g at 4 °C for 30 minutes to avoid aggregation. After centrifugation, the supernatant water was removed to isolate the particle pellet. Diluted crystal samples were prepared by adding the same buffer solutions as above to the pellet in the centrifuge tube while maintaining the ionic strength of samples at 15 mM. After dilution, the samples were place on the shaker table over night to redisperse the microgels completely. The crystals were transferred into Vitrotube borosilicate rectangular capillaries (0.1 mm × 2.0 mm × 50 mm) by capillary action to observe the microgels under a microscope.

Microscopy. Differential interference contrast (DIC) images were taken with an Olympus IX-70 inverted microscope using standard DIC optics. An Olympus 100× oil immersion objective (UplanFl 1.30 NA) was utilized to obtain images. Micrograph images and movies were taken at 1/10s interval using black and white CCD camera (Cooke Corp.). At this magnification and camera type, the 1280 × 1024 pixel field of view corresponds to a visible area of ~78.5 μm × 63 μm. To avoid any perturbations associated with interactions mediated by the glass surface, the movies were taken at the depth of ~30 μm from the wall of the sample holder. The 15-second movies were taken on the day the microgel particles are transferred to the glass tube (day 0), the next day (day 1) and so on to investigate the evolution of microgel assemblies over time. For all

samples, movies were taken from two different spots to observe kinetics at different areas. The two spots were 25 mm and 12.5 mm from the end of the tube.

Effective Volume Fraction Calculation. The details are described in the chapter 3. The shift factors of pH 3.0 and 3.85 used in this experiment are 12.3 and 18.1, respectively. The effective volume fraction for this study was calculated by multiplying the shift factor and the weight percent of microgels. As mentioned in chapter 3, at pH 3.85, the shift factor determined by viscosity measurements and one calculated from the ratio $[R_h/R_h(\text{pH } 3.0)]^3$ do not agree well. The shift factor measured by viscosity experiments is 18.1 and the shift factor calculated from the ratio is 14.6 at 22 °C. For comparison, both shift factors will be used to determine the effective volume fraction of pH 3.85 microgel dispersions. In all figures, the effective volume fraction calculated from the ratio $[R_h/R_h(\text{pH } 3.0)]^3$ will be presented in parenthesis and the effective volume fraction will be denoted as $\phi_{eff,calculated}$.

Particle Tracking Analysis. The details of particle tracking analysis and MSD calculations are described in chapter 4.2. Besides trajectories and MSD vs. time plots, the radial distribution function, g(r), was calculated to analyze the structure of particles in a system. Since the radial distribution function represents the probability of finding particles at a distance r, g(r) allows calculating the average center-to-center distance ($d_{c\text{-}c}$) between particles in the dispersion.

5.3 Results and Discussion

Figure 5.3-1 and 5.3-2 show the time evolution of microgel dispersions at different pH values. The photographs were taken from the same sample over time for

each figure *to observe the change of phases.* In figure 5.3-1, the microgels are dispersed in pH 3.85 buffer and the sample has an ϕ_{eff}=0.48 ($\phi_{eff,calculated}$ =0.38). At day 0, the sample is turbid implying a disordered structure. Interestingly, at day 1 and 2, the crystals form from the ends of the sample and grow toward the middle of the sample over time. The interface between the disordered and ordered phase is clearly seen. By day 3, the dispersion crystallizes completely and after day 3 the sample does not change dramatically. Other effective volume fraction samples, ϕ_{eff}=0.57 ($\phi_{eff,calculated}$ =0.46) and ϕ_{eff} =0.45 ($\phi_{eff,calculated}$ =0.36), show similar crystallization process. Higher volume fraction dispersion (ϕ_{eff}=0.65, $\phi_{eff,calculated}$=0.52, not shown) does not change its phase but the sample changes from turbid to clear over time. At ϕ_{eff} =0.42 ($\phi_{eff,calculated}$=0.34, not shown), the crystals grow from the ends of the sample and only part of the sample remains as a crystalline phase and does not evolve after day 1. The dispersions at ϕ_{eff} =0.37 ($\phi_{eff,calculated}$ =0.30, not shown) is disordered phase at day 0 and the phase does not change over time. This sample changes from turbid to clear as seen at ϕ_{eff}=0.65 ($\phi_{eff,calculated}$ =0.52). Figure 5.3-2 represents the *p*NIPAm-*co*-AAc microgels redispersed in pH 3.0 buffer and the sample has an ϕ_{eff}=0.53. Figure 5.3-2(a) shows that freshly made sample is turbid i.e. the sample has a disordered structure. In 1 day (figure 5.3-2(b)), the crystals grow from the ends of the sample, but the interface is not as clear as in figure 5.3-1. At day 2, the sample is homogeneously crystalline and after 3 days the sample does not change significantly. For pH 3.0 microgel dispersions, ϕ_{eff} =0.66, ϕ_{eff} =0.62 and ϕ_{eff} =0.58 (not shown) show similar crystallization as figure 5.3-2. The dispersions of ϕ_{eff} =0.80 and ϕ_{eff} =0.47 (not shown) have a disordered phase and do not change their phase over time.

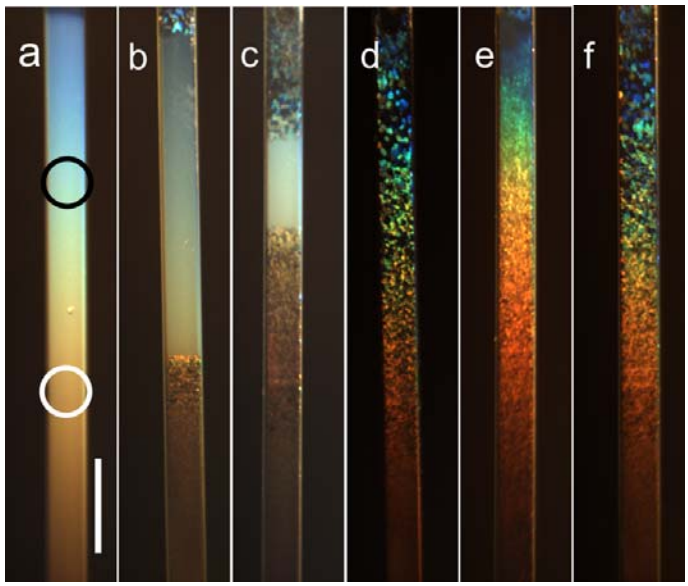

Figure 5.3-1 Photographs of *p*NIPAm-*co*-AAc dispersions in a rectangular glass tube upon aging. These photographs were taken from ϕ_{eff} = 0.48 ($\phi_{eff,calculated}$ =0.38) microgel dispersion at pH 3.85. These assemblies were prepared by filling the tube by depletion force from heated to right above the LCST of the microgels. The sample was then allowed to cool at room temperature and age at room temperature (22 °C). DIC images and movies are taken from two different spots; one at 25 mm from the endend and another at 12.5 mm from the endend. Black circle and white circle indicate 25 mm and 12.5 mm from the endend respectively. (a) day 0, (b) day 1, (c) day 2, (d) day 3, (e) day 4, and (f) day 7. The scale bar is 5 mm.

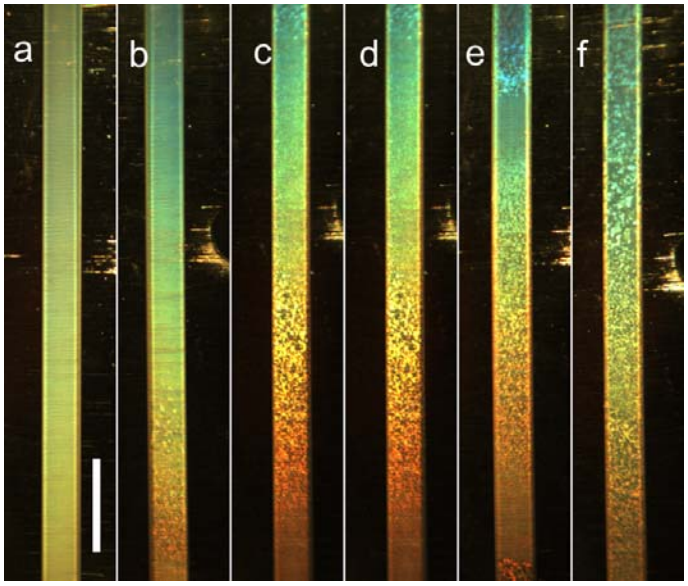

Figure 5.3-2 Photographs of *p*NIPAm-*co*-AAc dispersions in rectangular glass tubes over time. These photographs were taken from $\phi_{eff} = 0.53$ microgel dispersion at pH 3.0. These assemblies were prepared in the same manner as pH 3.85 samples. (a) day 0, (b) day 1, (c) day 2, (d) day 3, (e) day 4, and (f) day 7. The scale bar is 5 mm.

The phase evolution observed from figure 5.3-1 suggests that microgels in pH 3.85 dispersions form nuclei at the ends of sample and the crystals grow toward the middle (fluid phase). Even though the ends of samples are sealed with epoxy glue, there is some air contact with the dispersions. Microgels at the three-phase interfaces can form nuclei via the depletion force. The microgels near by the nuclei collide with nuclei and they adsorb on the nuclei resulting in crystals. Once the crystals form, microgels crystallize in the same manner as crystal growth from the nuclei at the ends. If the effective interaction is purely repulsive, the microgels still collide due to thermal motion but they would redisperse due to low particle density. The attractive interaction is weak so that multiple particles should be involved to form an ordered structure. We proposed that the source of the attractive interactions are dipole interaction and/or hydrogen bonding in the previous chapter.

To study the phase transitions of microgel dispersions at the microscopic level, the sample shown in figure 5.3-1 was observed on an optical microscope. Figure 5.3-3 shows DIC images and trajectories obtained at 25 mm from the end (black circle in figure 5.3-1), 0, 2, 3 and 4 days after the sample preparation. DIC images in column (i) show that the dispersion changes the phase dramatically from a disordered to an ordered phase at day 2 (figure 5.3-3(c)). The trajectories present much more interesting results. At 0 day and 1 day (not shown here), the trajectories show that the microgel dispersion has a disordered phase with high diffusion, i.e. a fluid phase. Two days after the sample preparation, the sample still has a disordered phase. However, the diffusion of particles drops dramatically as seen in figure 5.3-3(b). A closer look reveals that the motion of some particles is restricted like particles in a solid phase. At this state, short-range orders

are not observed yet. At day 3, particles form well-ordered arrays and have slower diffusion than the previous day. After day 3, there is no change of the phase and particle motion becomes more restricted. DIC images and the trajectories confirm the phase transition from a fluid phase to crystalline phase seen photographs. Also, the trajectories imply that the dynamics of the phase transition is slow.

DIC images and the trajectories show that the microgel particle diffusion becomes slower before the microgel particles crystallize. The photographs in figure 5.3-1 show that crystals nucleation occurs at the ends of samples. Micrograph images and DIC suggest that microgel particles decrease particle diffusion, become restricted and finally form a long-range ordered phase.

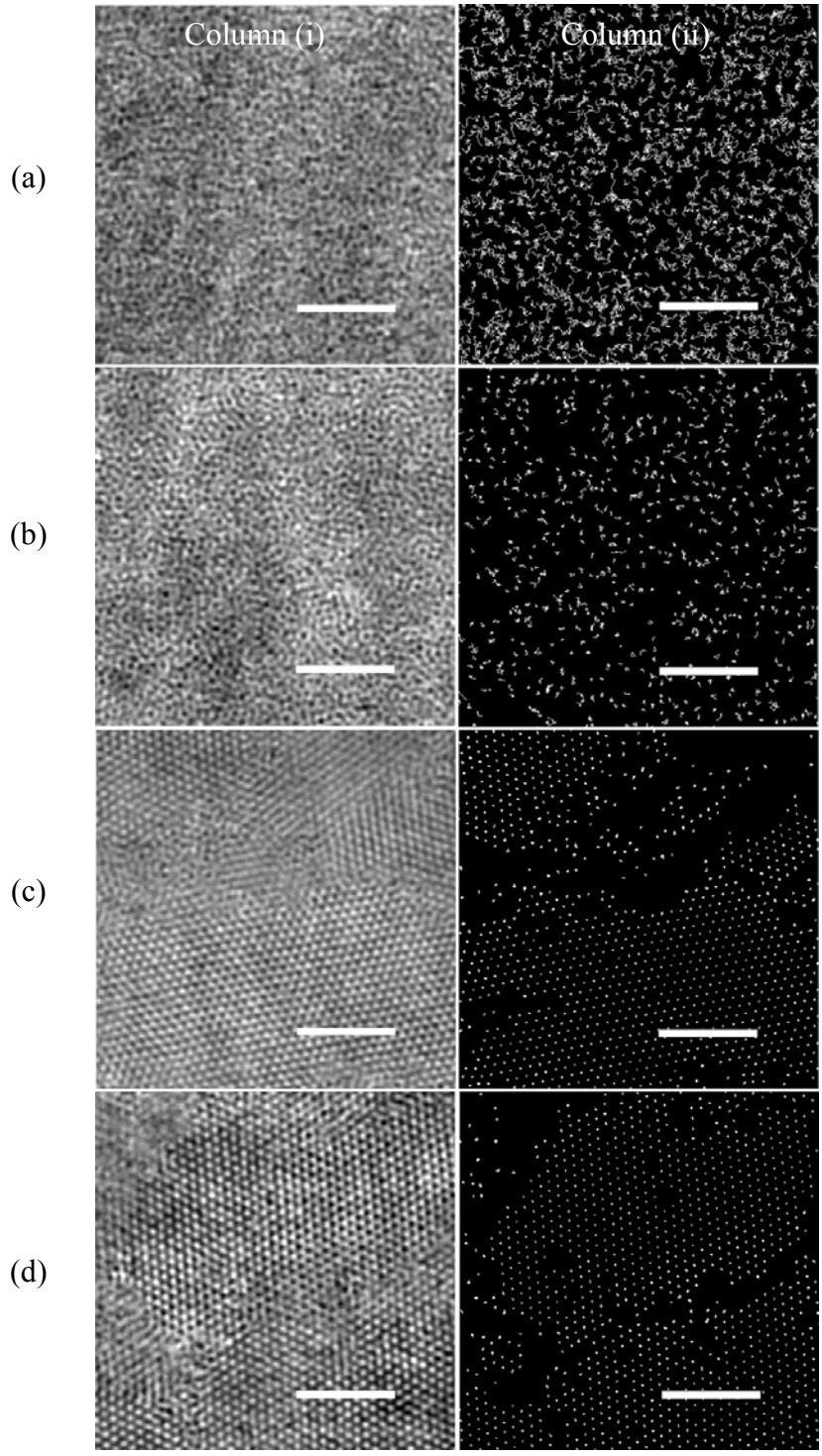

Figure 5.3-3 Column (i) DIC micrograph images of *p*NIPAm-*co*-AAc microgel dispersion over time. The microgels are dispersed in pH 3.85 buffer and this sample has ϕ_{eff}=0.48 ($\phi_{eff,calculated}$=0.38). Column (ii) the trajectories of microgel dispersion obtained by performing the particle tracking analysis. Panel (a) day 0, (b) day 2, (c) day 3, and (d) day 4. Scale bar is 10 μm.

Once the trajectories of samples are obtained, the mean-squared displacement (MSD) is calculated for a quantative analysis. Movies were taken from two different spots, at 25 mm (black circle in figure 5.3-1) and 12.5 mm (white circle in figure 5.3-1) from the ends, to see the dynamics of microgel particles depending on the position. Figure 5.3-4 shows the MSD vs. lag time plots of microgels at pH 3.85 at 25 mm from the sample end. For most samples, the diffusion of particles decreases dramatically over time. The DIC images (not shown) of microgel dispersion at ϕ_{eff}=0.65 ($\phi_{eff,calculated}$=0.52) show a disordered structure and the phase of the sample did not change over time. MSD data in figure 5.3-4(a) implies that this sample changes the phase from a fluid to a glassy phase at day 2. At the effective volume fraction range between 0.57 ~ 0.45 ($\phi_{eff,calculated}$ =0.46~36, figure 5.3-4(b)~(d)), the graphs show slow crystallization. At day 0, the plots of all three samples have straight lines with a slope of ~ 1. This indicates the diffusion of particles in these samples is Brownian, i.e. the particles are thermally active and move in random walk fashion. At the ϕ_{eff} of 0.57 ($\phi_{eff,calculated}$ =0.46), the microgel dispersion forms an ordered structure at day 2. For ϕ_{eff}=0.48 ($\phi_{eff,calculated}$=0.38, figure 5.3-4(c)), the particle diffusion shows liquid-like behavior up to day 2 even though the diffusion of particles is much slower than the previous day. At day 3, the diffusion of particles becomes much slower than day 2, and the structure of the sample changes from a disordered to an ordered structure. Figure 5.3-4(d) shows that the microgel self-assembly at ϕ_{eff}=0.45 ($\phi_{eff,calculated}$ =0.36) displays a phase transition from a disordered to ordered structure at day 4. In figure 5.3-4(e) and (f), microgel dispersions of effective volume fraction 0.42 and 0.37 ($\phi_{eff,calculated}$ =0.34 and 0.30) do not form crystals after aging but the diffusion of particles decreases order of magnitude after day 2.

Figure 5.3-5 shows the MSD vs. lag time plots of microgel dispersions of pH 3.85 at 12.5 mm. The diffusion of particles also drops dramatically as seen figure 5.3-4 during aging. However, figures 5.3-5(b)~(d) show that the transition occurs 24 hours after the sample preparation. A more interesting result is observed in figure 5.3-5(e) where the ϕ_{eff} is 0.42 ($\phi_{eff,calculated}$=0.34). The microgel dispersion is fluid-like at day 0 and the diffusion decreases on day 1. Unlike other MSD plots, this sample does not change its phase nor decreases diffusion dramatically over time. It seems that this sample forms a mixed phase microscopically at day 1 and the crystals do not grow more at this effective volume fraction. As a result, the diffusion of particles after day 1 is dependent on the phase. At the ϕ_{eff} of 0.37 ($\phi_{eff,calculated}$=0.30), the diffusion changes but the phase of the dispersions remains as a disordered phase.

The next two figures present the MSD vs. lag time plots for microgels dispersed in pH 3.0 buffer solutions. Microgel dispersions with ϕ_{eff}=0.80 and ϕ_{eff}=0.47 do not show dramatic changes in particle diffusion over time. DIC images (not shown) and MSD data show that the microgel dispersions with ϕ_{eff} =0.80 is in a glassy phase and the microgel with ϕ_{eff} =0.47 is in a fluid phase. The MSD plots in figure 5.3-6 and 5.3-7 show that the dispersions with ϕ_{eff} =0.66~0.51 decrease the diffusion ~ 2 order of magnitude over time. The microgel dispersions here show further decrease of diffusion even after samples form a well-ordered structure while the pH 3.85 dispersions did not evolve more once they form crystals. Compared to the results observed the pH 3.85 dispersions (e.g. figures 5.3-4 and 5.3-5), microgels dispersed in pH 3.0 buffer do not show large differences in behavior between 25 mm and 12.5mm.

As a model system for purely repulsive interaction, *p*NIPAm (2% BIS) microgels are redispersed in the water and the phase evolution are studied. Figure 5.3-8 shows the MDS data obtained from *p*NIPAm microgel dispersions where there is no attractive interaction due to ion-dipole interaction. These samples are spatially heterogeneous and evolve their diffusion much less significantly than *p*NIPAm-*co*-AAc microgels shown earlier.

MSD data indicated that microgel dispersions at the presence of attractive interaction sources showed slow crystallization processes. Also, particle diffusion decreases as the microgels are closer to crystalline phase. And the data show that the crystallization and the diffusion of two different spots are different. These data agree well the crystal nucleation and growth proposed earlier. Microgels at the ends of samples can form nuclei via depletion force at three-phase interface of water, air, and glass and crystals grow toward the bulk fluid by templating the existing crystals. In the presence of an attractive force, once nuclei form, microgels in the fluid phase collide with nuclei and many of them become crystals rather than dissolving into the fluid phase again. Next, we investigate the structural changes by investigating the radial distribution function over time.

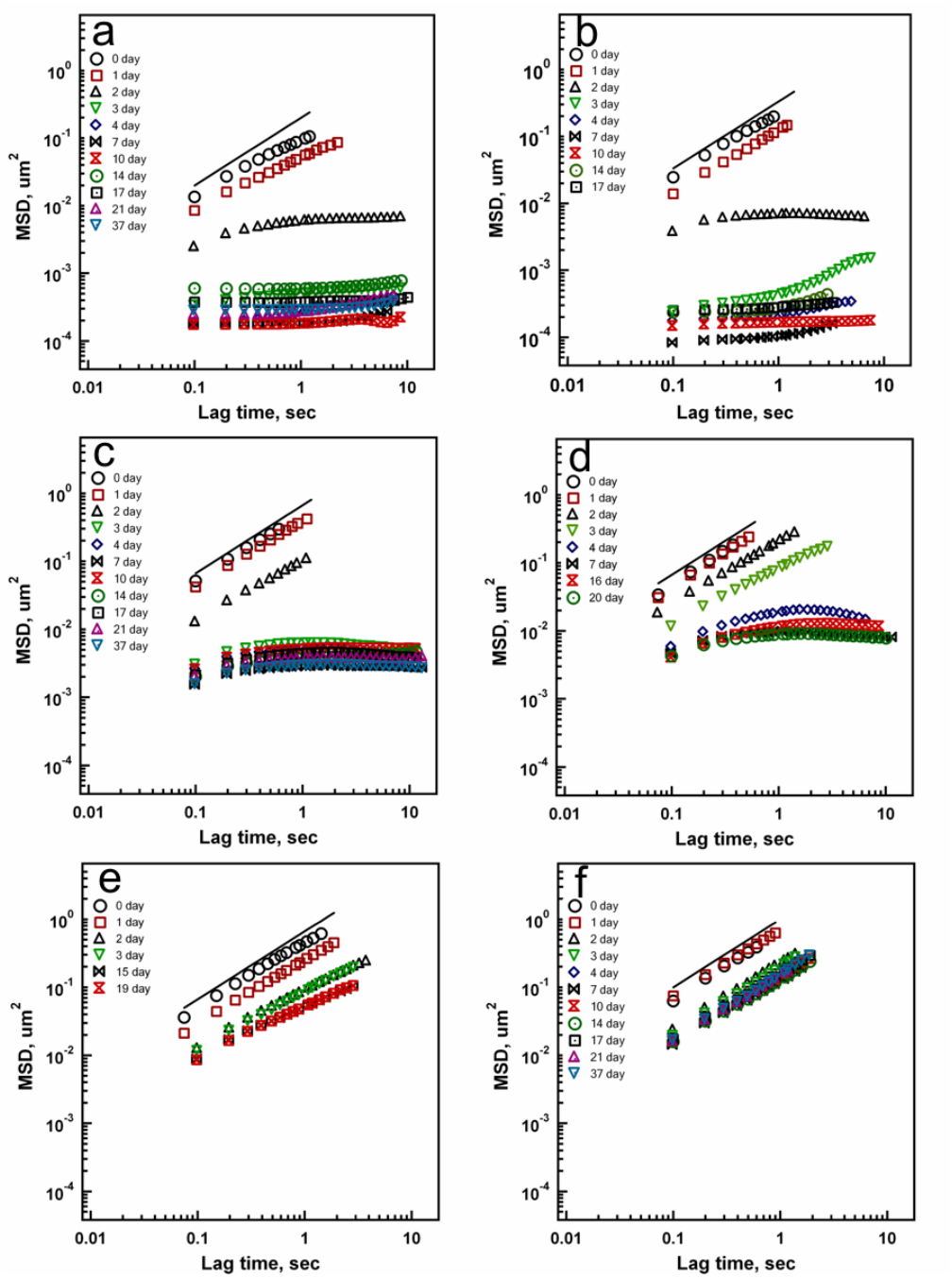

Figure 5.3-4 The MSD evolution of *p*NIPAm-*co*-AAc microgel dispersions upon aging. The microgels are dispersed in pH 3.85 buffer solution. The movies were recorded at 25 mm from the ends. (a) ϕ_{eff} =0.65 ($\phi_{eff,calculated}$ =0.52), (b) ϕ_{eff} =0.57 ($\phi_{eff,calculated}$ =0.46), (c) ϕ_{eff} =0.48 ($\phi_{eff,calculated}$ =0.38), (d) ϕ_{eff} =0.45 ($\phi_{eff,calculated}$ =0.36), (e) ϕ_{eff} =0.42 ($\phi_{eff,calculated}$ =0.34), and (f) ϕ_{eff} =0.37 ($\phi_{eff\ calculated}$=0.30). The trend lines have slope 1 and indicate free Brownian diffusion. The $\phi_{eff,calculated}$ in parenthesis are the effective volume fraction determined by calculated shift factor and the weight percent of dispersions. The details on the calculated shift factors are discussed in the chapter 3.

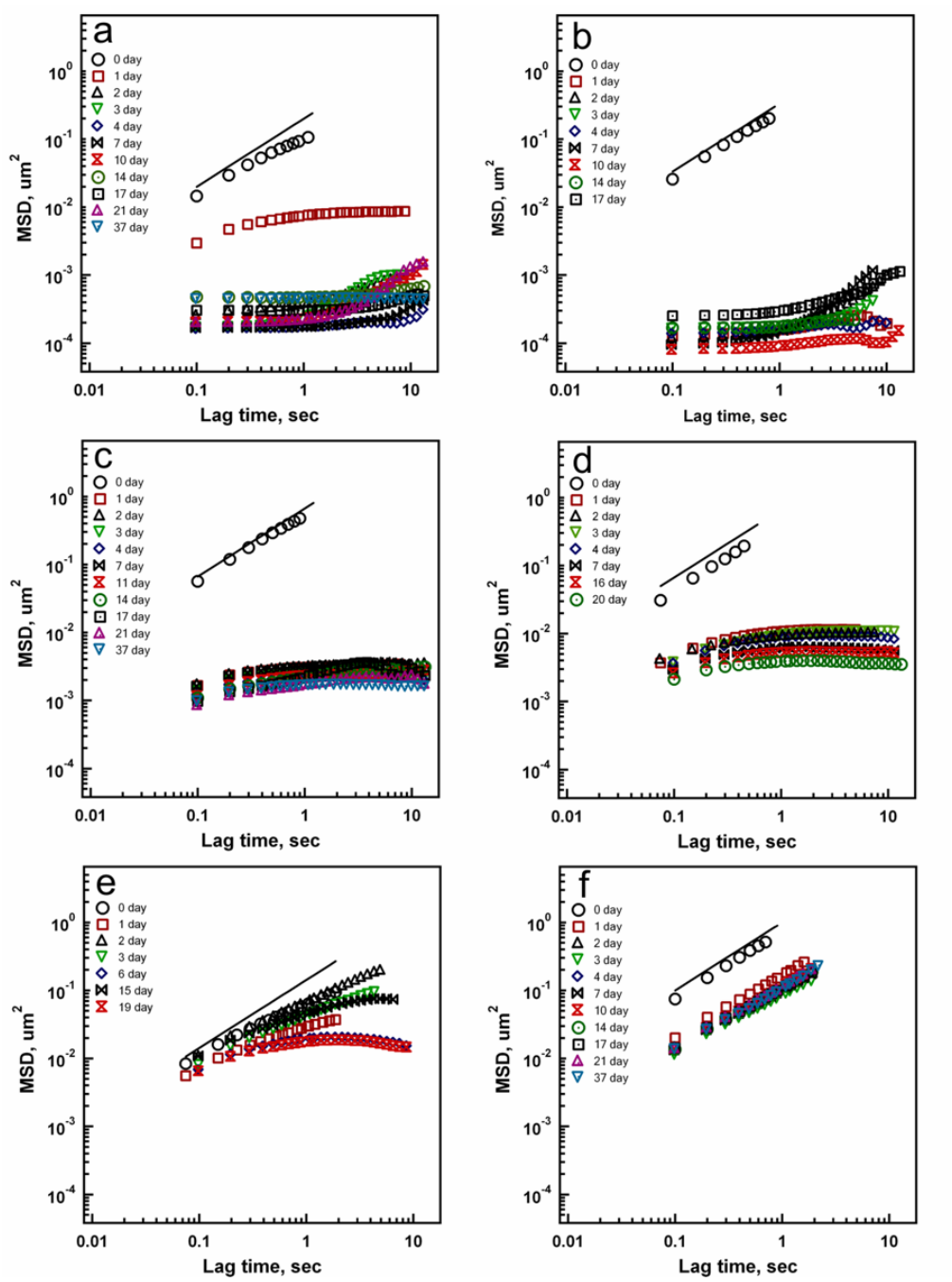

Figure 5.3-5. The MSD evolution of *p*NIPAm-*co*-AAc microgel dispersions upon aging. The microgels are redispersed in pH 3.85 buffer solution. The movies were recorded at 12.5 mm from the end. (a) ϕ_{eff} =0.65 ($\phi_{eff,calculated}$ =0.52), (b) ϕ_{eff} =0.57 ($\phi_{eff,calculated}$ =0.46), (c) ϕ_{eff} =0.48 ($\phi_{eff,calculated}$ =0.38), (d) ϕ_{eff}=0.45 ($\phi_{eff,calculated}$ =0.36), (e) ϕ_{eff} =0.42 ($\phi_{eff,calculated}$ =0.34), and (f) ϕ_{eff} =0.37 ($\phi_{eff\ calculated}$=0.30). The trend lines have slope 1.

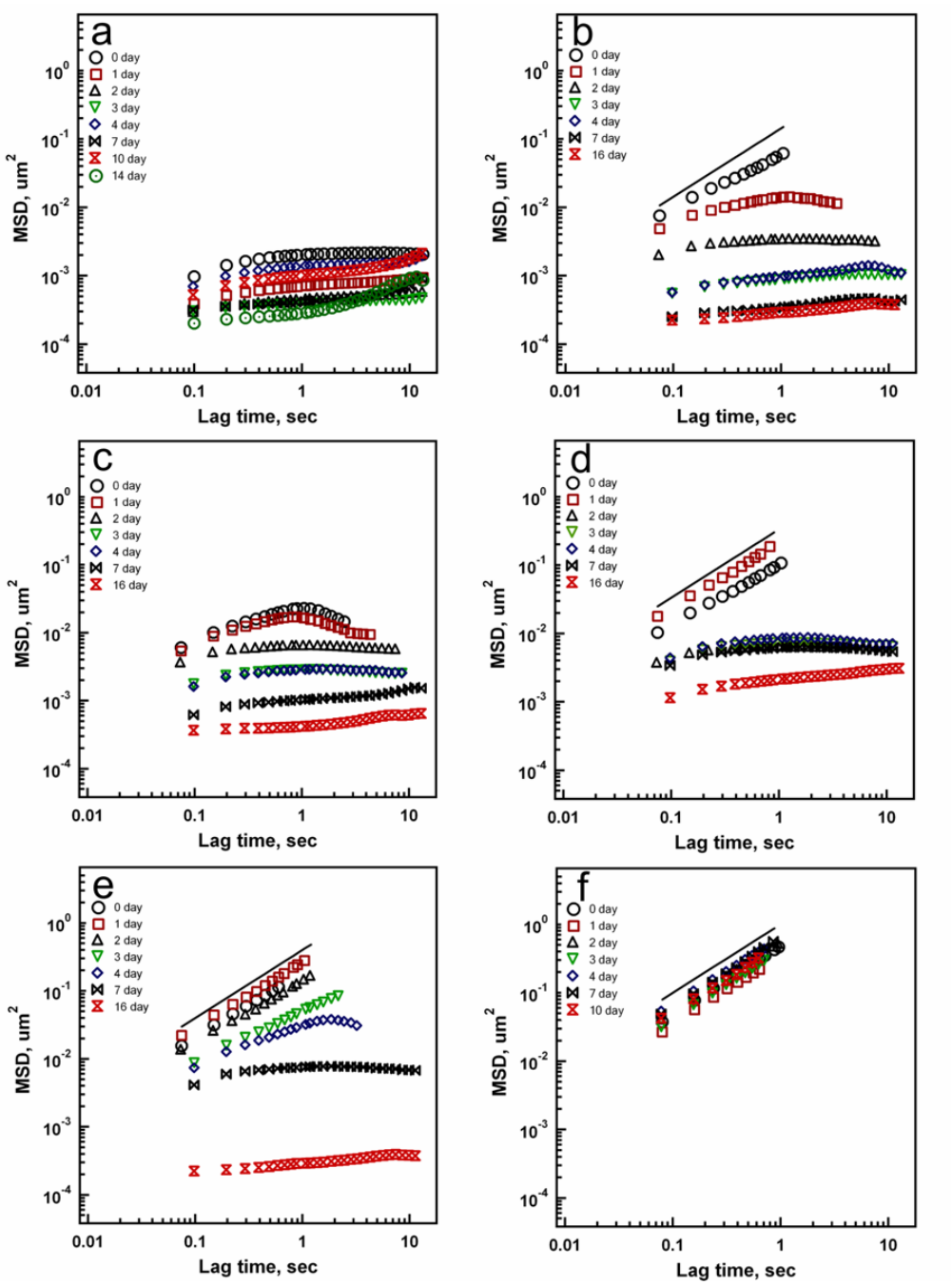

Figure 5.3-6 The MSD evolution of *p*NIPAm-*co*-AAc microgel dispersions upon aging. The microgels are redispersed in pH 3.0 buffer solution. The movies were recorded at 25 mm from the ends. (a) ϕ_{eff}=0.80, (b) ϕ_{eff}=0.66, (c) ϕ_{eff} =0.62, (d) ϕ_{eff} =0.58, (e) ϕ_{eff}=0.51, and (f) ϕ_{eff} =0.47. The trend lines have slope 1.

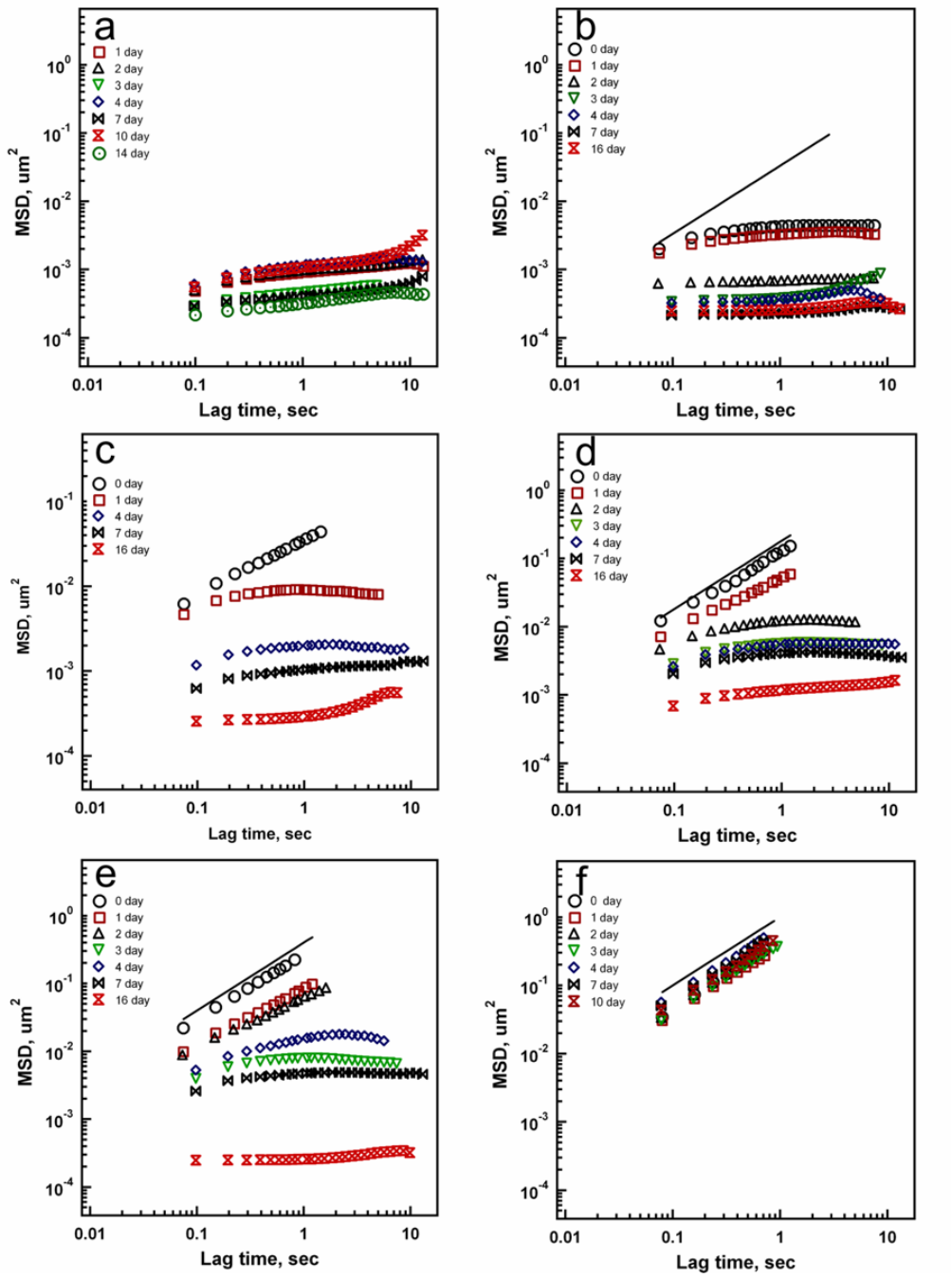

Figure 5.3-7 The MSD evolution of *p*NIPAm-*co*-AAc microgel dispersions upon aging. The microgels are redispersed in pH 3.0 buffer solution. The movies were recorded at 12.5 mm from the end. (a) ϕ_{eff}=0.80, (b) ϕ_{eff}=0.66, (c) ϕ_{eff} =0.62, (d) ϕ_{eff} =0.58, (e) ϕ_{eff}=0.51, and (f) ϕ_{eff} =0.47. The trend lines have slope 1.

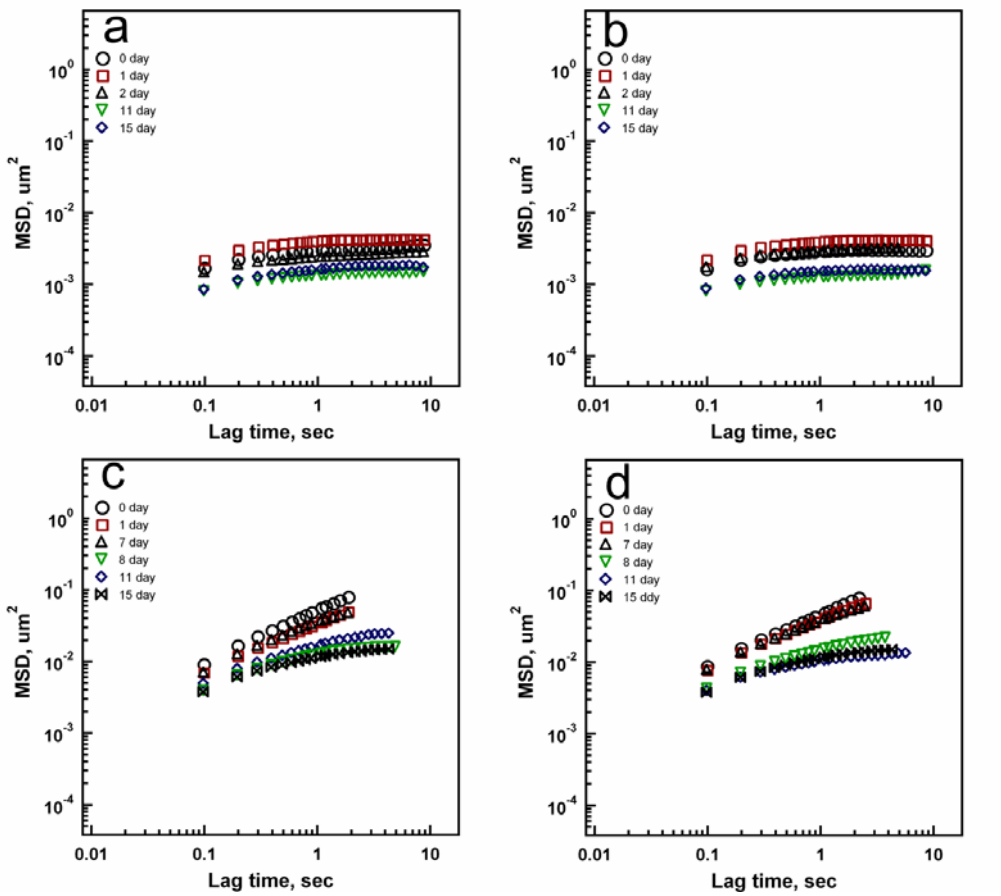

Figure 5.3-8 The MSD evolution of *p*NIPAm microgel dispersions upon aging. The microgels are redispersed in water. (a) ϕ_{eff} =0.67, 25 mm from the end, (b) ϕ_{eff} =0.67, 12.5 mm from the end, (c) ϕ_{eff}=0.55, 25 mm from the end, and (d) ϕ_{eff}=0.55, 12.5 mm from the end.

Figure 5.3-9 presents the radial distribution function, g(r), vs. distance plot of the pH 3.85 dispersion at ϕ_{eff}=0.48 ($\phi_{eff,calculated}$=0.38). The results for g(r) support the results presented in trajectories and MSD plots. The microgel assemblies show peak intensity growth and decreases in peak width over time. Higher order peaks appear after day 2 showing that the sample becomes organized. The first peak in the g(r) vs. distance plot can give d_{c-c} in microgel dispersion. An interesting observation is that the first peak position does not change over time indicating that the d_{c-c} remains constant. This result indicates the particle density of each aging stage is constant even though the phase of the sample changes from a fluid to a crystal. The distance is 1.14 μm which is larger than the diameter determined by PCS (~ 0.8 μm).

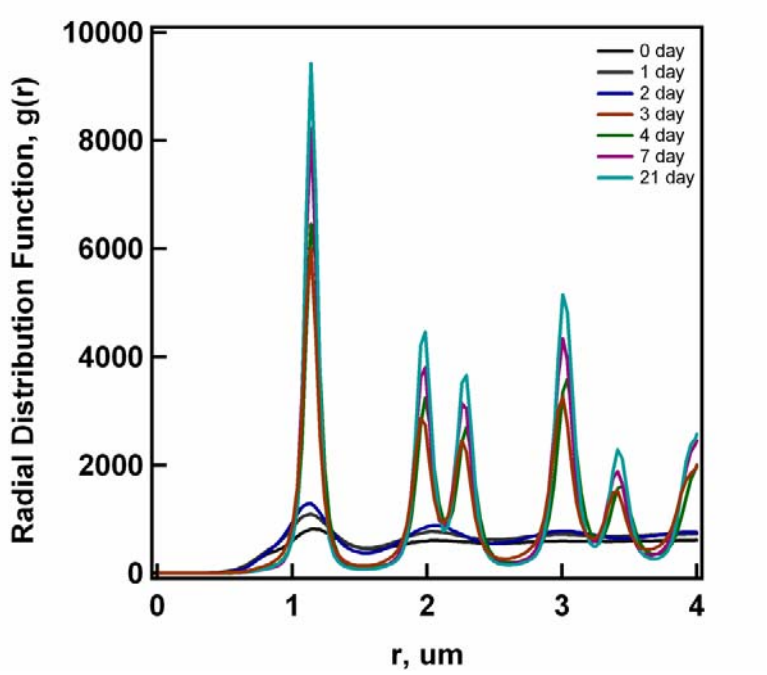

Figure 5.3-9 Radial distribution of microgel assemblies over time. ϕ_{eff} = 0.48 ($\phi_{eff,calculated}$ =0.38), at pH=3.85. 0 day (black), 1 day (gray), 2 day (blue), 3 day (red), 4 day (green), 7 day (purple) and 21 day (sky blue).

During crystal growth, microgel dispersions exhibit three different phases; a bulk crystal, a bulk fluid, and a interface between fluid and crystal (see figure 5.3-1(b) and (c)). Here, we will explore the particle diffusion along the sample and look closely the diffusion of microgels at the interfaces. For this experiment, the movies were recorded at every 2 mm for example, 25 mm from the end, 23 mm, 21 mm etc. At the interfaces, movies were taken from three different structures, a disordered, a mixed and an ordered phase, to compare the motion of particles at these phases to bulk fluid or bulk crystals. Also, a couple of movies were taken from a disordered phase at the interface for 5 minutes intervals to observe the crystal growth.

Figure 5.3-10 shows the three different structures observed at the interface at day 0. In figure 5.3-10(a), the majority of the microgel particles form a disordered structure and some particles have a short-range order. The diffusion of particles here is slower than the diffusion of particle in the bulk fluid (figure 5.3-3(a)). Figure 5.3-10(b) has the mixed phase of an ordered and a disordered structure. In the mixed phase, the particles in the ordered phase have slower diffusion than ones in a disordered phase. In figure 5.3-10(c), the sample is mainly composed of an ordered structure. Compared to the diffusion of particles in the bulk crystals shown in figure 5.3-3(c), the particles in figure 5.3-10(c) have a smaller crystal size and faster diffusion. These results reveal the gradient of diffusion along the sample. In figure 5.3-11, the radial distribution function for a 0 day old dispersion also support the results seen the trajectories. Microgels in the bulk fluid (25 mm) do not show structure, while bulk crystals (7 mm) have an ordered structure. The structures of interface are intermediate between bulk fluid and bulk crystals.

Figure 5.3-12 shows the crystal growth of microgels at the interface. Here, the trajectories in figure 5.3-12(a) are obtained from a disordered phase near from the interface. Compared to bulk fluid phase (see figure 5.3-3(a)), microgels in this disordered phase has slower diffusion. Some particles are diffusive but the motion of many particles is prohibited by neighbor particles. Some restricted particles even form short-range ordered structures which consist of several microgel particles. In 5 minutes, the next movie was recorded at the same spot as (a). In figure 5.3-12(b), several tiny crystals composed of 30~50 microgels appear on the left side of the image. Another 5 minutes later, seen in figure 5.3-12(c), the crystals shown figure (b) become larger and more new crystals appear.

The MSD vs. lag time plot calculated from different spots at different aging stage is presented in figure 5.3-13. At day 0, microgel particles between from 25 mm to 11mm have a fluid phase and the interface exists between 11 mm and 9 mm. The microgels form a well-ordered phase between 9 mm and the end. The disordered phase at the interface has slower diffusion than bulk fluid phase and the diffusion of the ordered phase at the interface is faster than bulk crystals as mentioned earlier. After day 1, figure 5.3-13(b), the crystals grow more so that the interface moves toward the middle. Now, the interface exhibits between 19 mm and 17 mm. As seen above, the diffusion of particles at the interface is between bulk fluid and bulk crystals. At day 2 (figure 5.3-13(c)), the crystals grow more and the interface moves further. The diffusion of bulk fluid not only decreases but also the slope of the MSD plot deviates from a straight line of slope 1. These changes indicate that particles in the bulk fluid at day 2 start to be restricted.

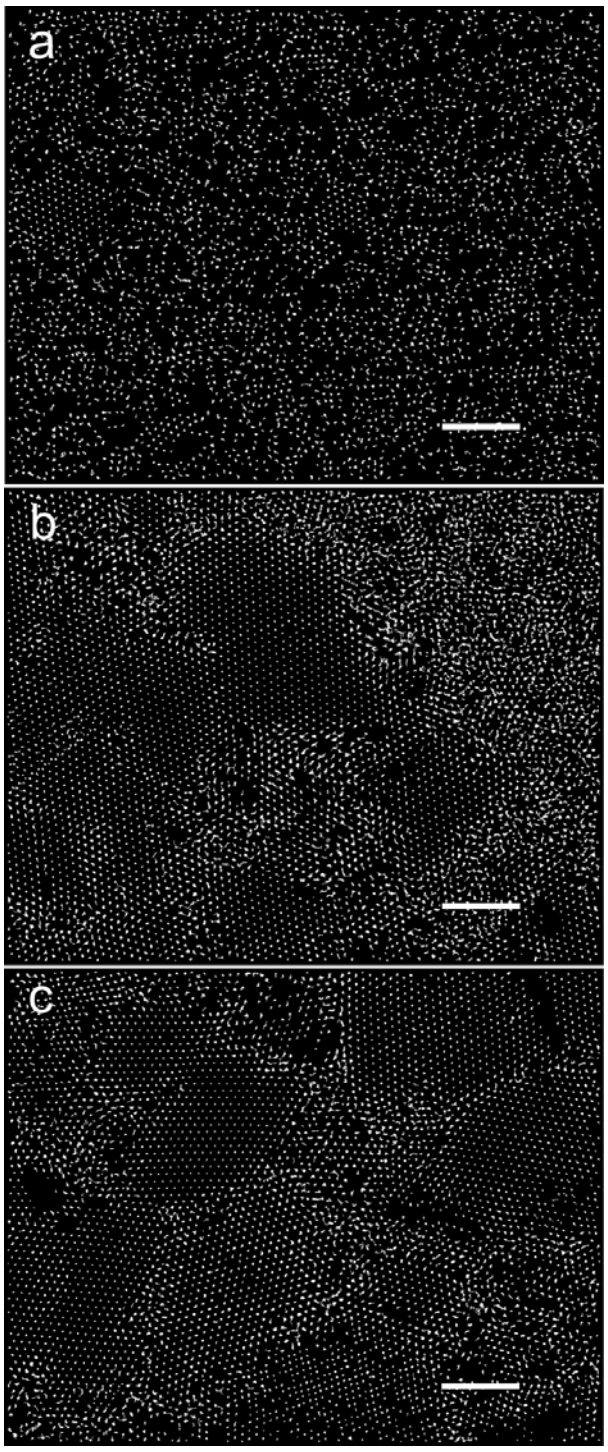

Figure 5.3-10 Particle trajectories of *p*NIPAm-*co*-AAc microgels (R_h=399 nm at 22 °C) dispersed in pH 3.85 (15 mM ionic strength) buffer solution at day 0. This dispersion has ϕ_{eff}=0.48 ($\phi_{eff,calculated}$=0.38). The movies were recorded at the interface of crystal and fluid phases. At day 0, this interface exists between 11 and 9 mm from the end. (a) Disordered phase, (b) mixed phase of a disordered and an ordered phase, and (c) ordered phase. Scale bar is 10 μm.

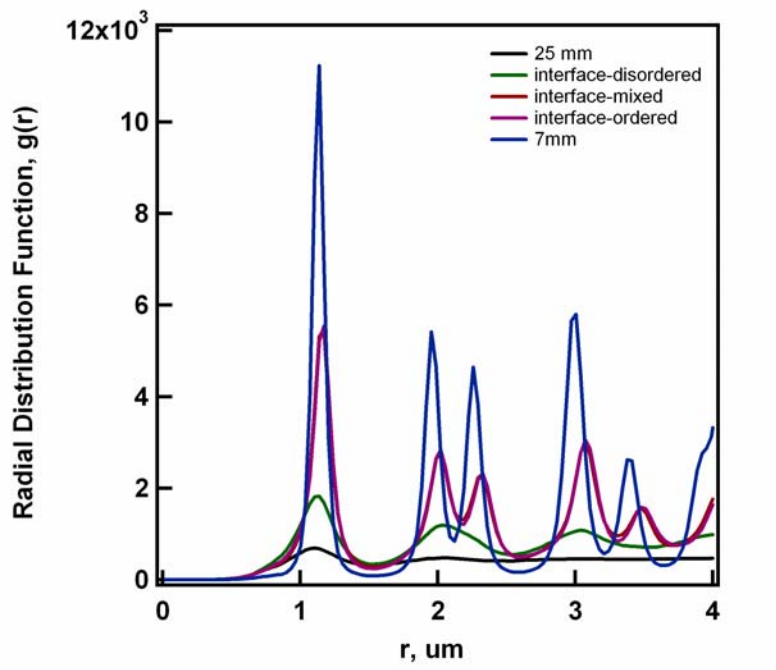

Figure 5.3-11 Radial distribution function of 0 day old sample at different positions. Responsive microgel, *p*NIPAm-*co*-AAc, are redispersed in pH 3.85 buffer and this sample has ϕ_{eff} =0.48 ($\phi_{eff,calculated}$=0.38). The interface exists between 11 mm and 9 mm from the end.

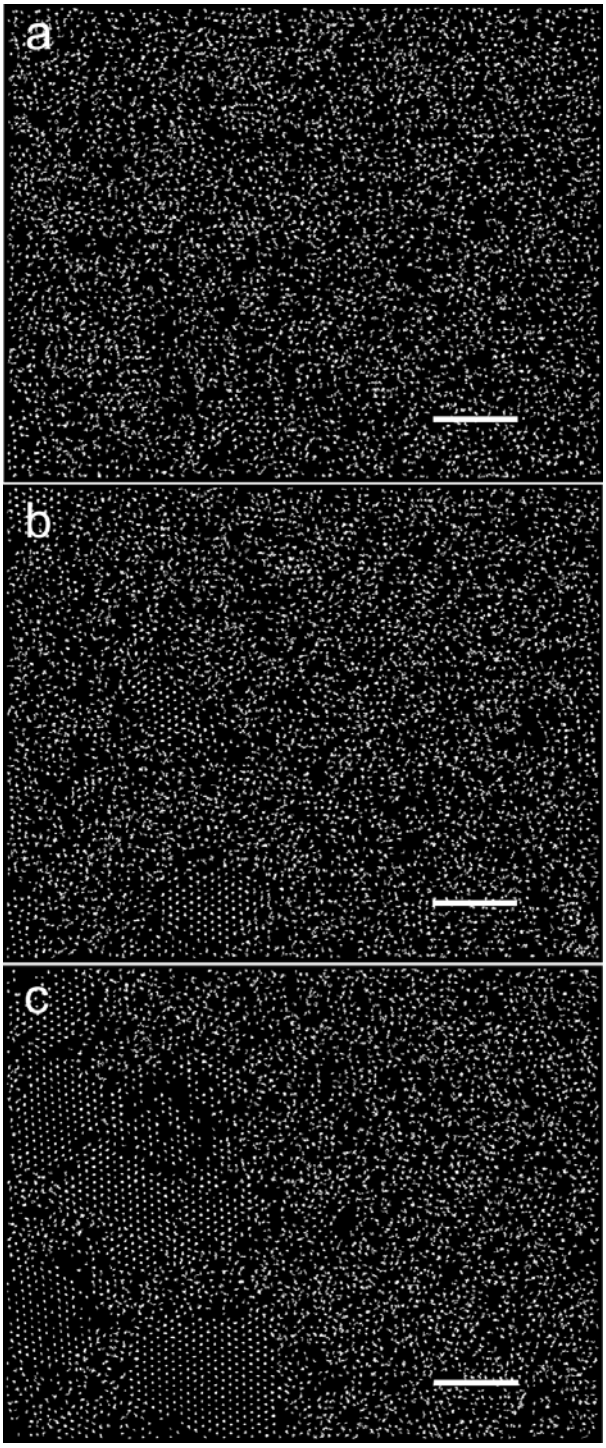

Figure 5.3-12 Crystal growth of *p*NIPAm-*co*-AAc microgels (R_h = 399 nm at 22 °C) at the interface of crystal and fluid. The microgels are redispersed in pH 3.85 (15 mM ionic strength) buffer solution. This dispersion has ϕ_{eff} =0.48 ($\phi_{eff,calculated}$=0.38). These trajectories are obtained at the interface at day 1. (a) 0 minute, (b) 5 minutes after (a), and (c) 10 minutes after (a). Scale bar is 10 μm.

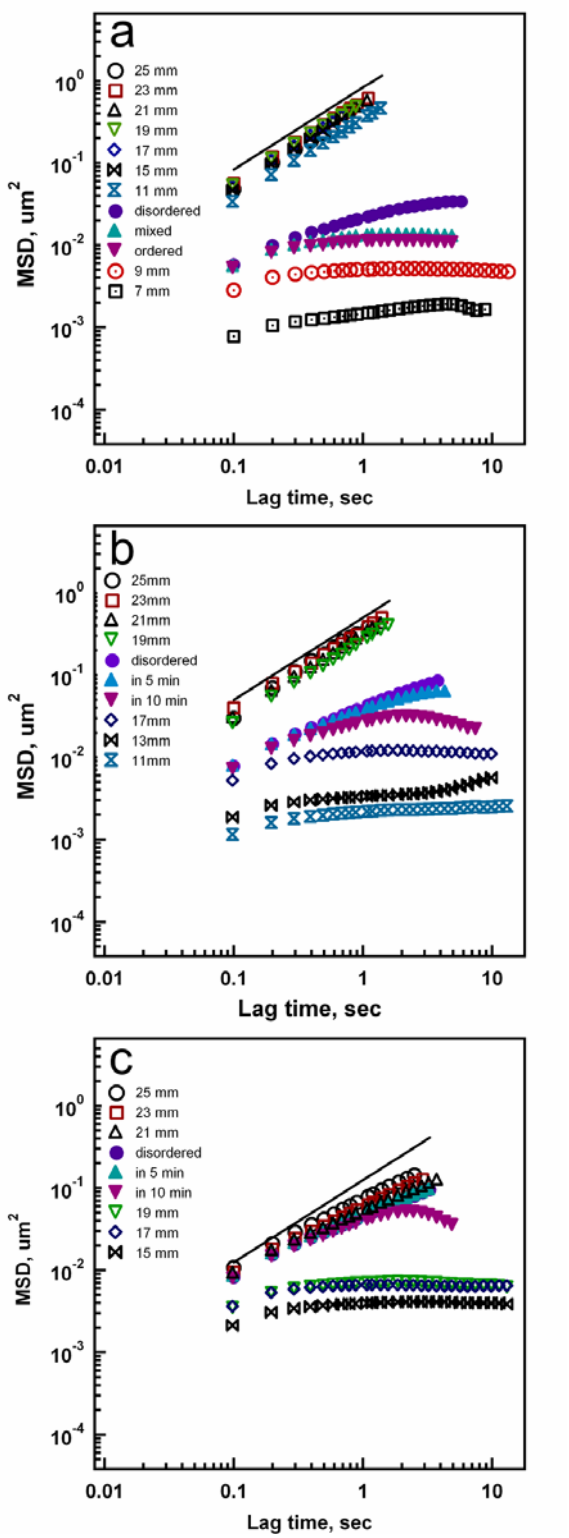

Figure 5.3-13 The MSD vs, lag time plot calculated from different positions over time. The microgels have ϕ_{eff} =0.48 and are redispersed in pH 3.85 buffer solution. (a) 0 day, (b) 1 day, and (c) 2 day. The straight lines are trend lines with a slope of 1.

The results shown so far suggest that in the presence of attractive forces the crystal nucleation occurs at the ends of the samples and crystals grow slowly. Colloidal particles dispersed in a medium undergo constant Brownian motion due to their random collisions with the solvent molecules and have thermal (kinetic) energies of the order of k_BT. In traditional nucleation and growth theory, the ordering of any system is basically due to competition between the interaction energy U_0 and thermal energy k_BT.

Crystal nuclei are created by random particle collisions with the help of the depletion force and they develop by templating the existing crystals. As seen in figure 5.3-10, the interface has three different phases; a disordered, a mixed and a ordered phase. In terms of the diffusion, there is a difference between the disordered phase at the interface and at the bulk fluid. Also, there is a difference between particle diffusion in the bulk crystals and the diffusion in the crystals at the interface. The results are shown in figure 5.3-13(a) and this suggests that there is a diffusion gradient along the sample. The MSD data shown in the figure support the crystals growth hypothesis that we proposed earlier. Once the microgels form nuclei at the ends of the samples via depletion force, the nuclei grow and form crystals. These crystals grow by collision of microgels in a disordered phase onto the crystals. Since the attractive interaction is weak, the number of particles in the crystals should be much larger than 2 so that the microgels can crystallize via multiple weak attractive interactions. Without attractive interactions, microgels collide with crystals and redissolve into the disordered phase.

The AAc mediated stabilization could change the bulk melting transition that occurs upon heating. Here, the attractive interaction hinders the deswelling behavior of the microgel in crystals when the system is heated. Figure 5.3-14 ~16 show the melting

transition of *p*NIPAm-*co*-AAc microgel dispersions at ϕ_{eff} = 0.57 ($\phi_{eff,calculated}$ =0.46) and pH 3.85. Figure 5.3-14, 15 and 16 represent 0 day, 1 day and 9 day old sample respectively. At day 0 (figure 5.3-14), the sample has a disordered phase at room temperature. As the sample is heated, the microgel dispersion turns completely opaque at 31 °C, which is the volume phase transition temperature of microgels. In 1 day, the microgel dispersion shows crystalline phase forming at the end of the sample and a disordered phase in the middle as in figure 5.3-15. As 1 day old sample is heated, the disordered part of the sample turns opaque at 33 °C while the crystalline phase is intact up to 55 °C. The crystalline phase starts to melt at 55 °C and the sample still does not turn completely opaque at 62°C. The well-aged sample in figure 5.3-16 shows that the crystals start to melt at 59 °C. Here, the polymer chains on the microgel surfaces may rearrange to have the conformation for the attractive interactions. Once the microgels stabilize and reach at the minimum of potential energy, the interaction between microgels is strong enough to overcome the deswelling upon heating.

The pH dependence of the melting transition of the microgel crystals is also studied. Figure 5.3-17 show the microgel crystals at ϕ_{eff} =0.53 which is 7 day old. The crystal starts to become turbid at 26 °C and turns completely opaque at 27 °C. At pH 3.0, where most AAc groups are protonated and the attractive interaction is much weaker than pH 3.85. The results show that the attractive interaction due to the hydrogen bonding may not be strong enough to overcome the microgel deswelling upon heating.

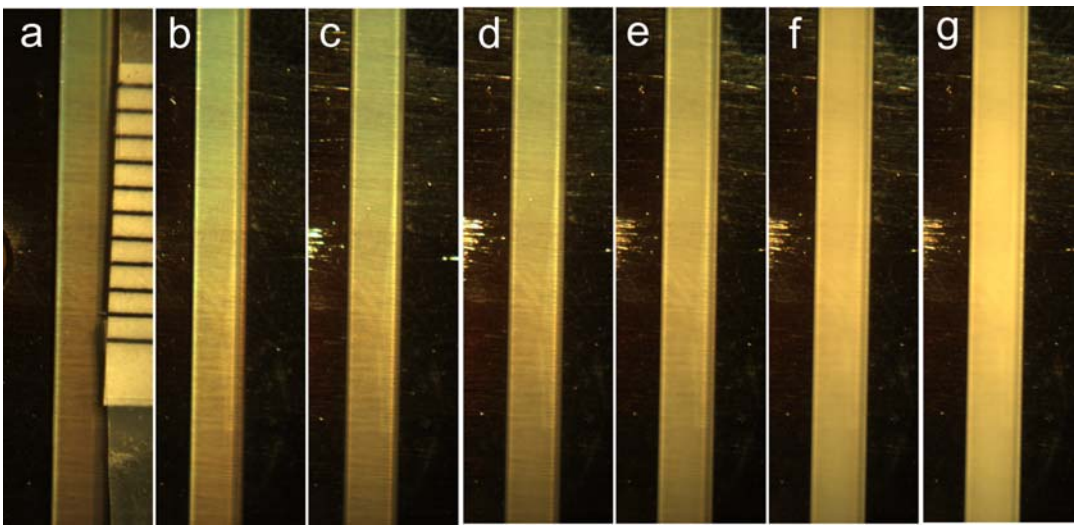

Figure 5.3-14 Melting transition of microgel dispersions of ϕ_{eff}= 0.57 ($\phi_{eff,calculated}$ =0.46) in a glass tube at pH 3.85 as the sample is heated slowly. These photos are taken at day 0 and the sample is disordered. (a) 25 °C, (b) 27 °C, (c) 29 °C, (d) 30 °C, (e) 31 °C, (f) 32°C, and (g) 33 °C.

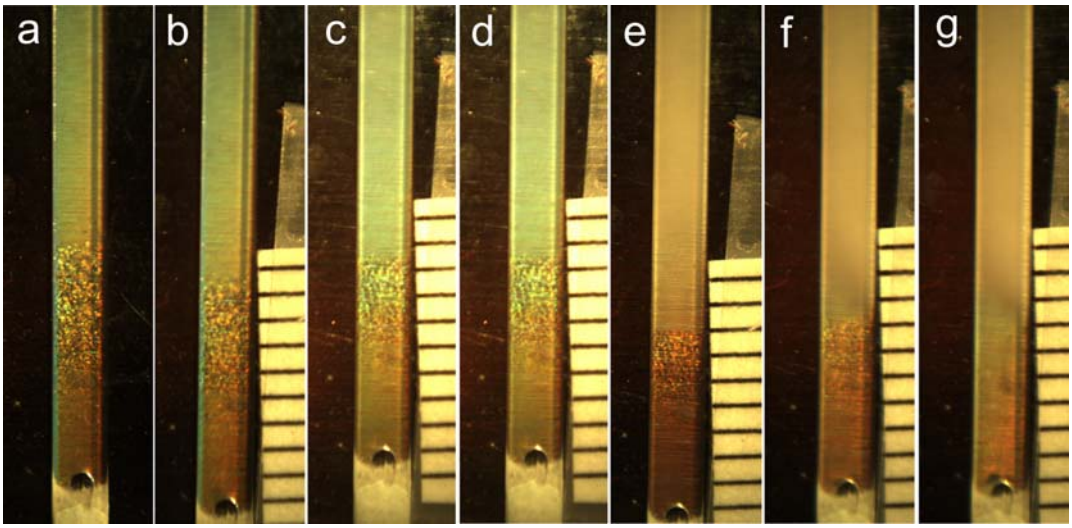

Figure 5.3-15 Melting transition of microgel dispersions of ϕ_{eff}= 0.57 ($\phi_{eff,calculated}$ =0.46) in a glass tube at pH 3.85 as the sample is heated slowly. This sample is 1 day old and has a mixed phase. (a) 25 °C, (b) 27 °C, (c) 29 °C, (d) 31 °C, (e) 35 °C, (f) 55°C, and (g) 62 °C.

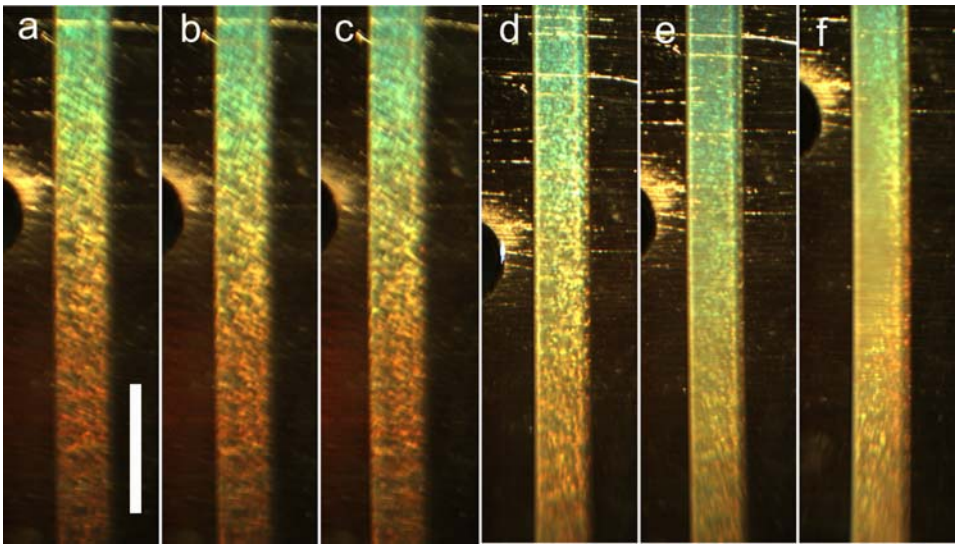

Figure 5.3-16 Photographs of microgel dispersions of ϕ_{eff}= 0.57 ($\phi_{eff,calculated}$ =0.46) in a glass tube at pH 3.85 as the sample is heated slowly. This sample is 9 day old and crystallization is completed. (a) 29 °C, (b) 36 °C, (c) 40 °C, (d) 56 °C, (e) 59 °C, and (f) 62 °C. Scale bar is 5 mm.

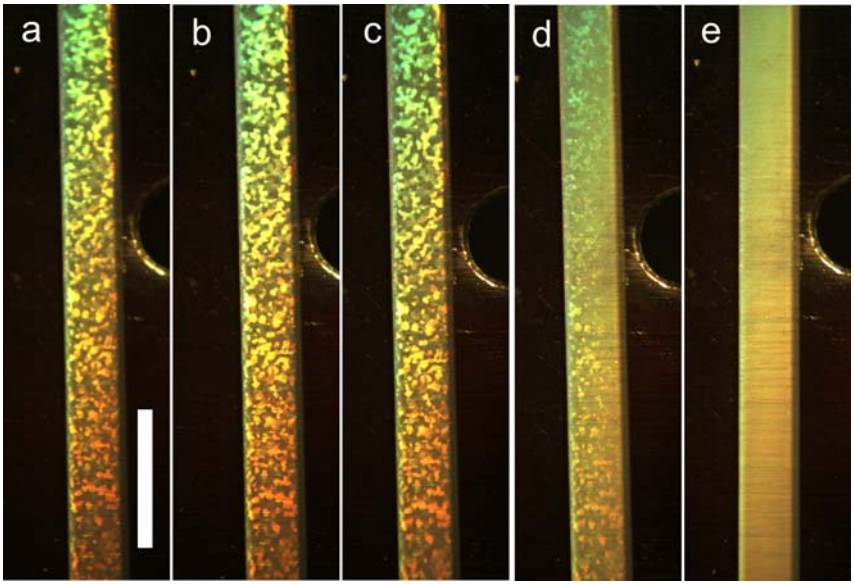

Figure 5.3-17 The melting transition of *p*NIPAm-*co*-AAc crystal dispersed in pH 3.0 buffer. The effective volume fraction of this crystal is 0.53 and this is 7 days old. (a) 20 °C, (b) 23 °C, (c) 25 °C, (d) 26 °C, and (e) 27 °C. The scale bar is 5 mm.

5.4 Conclusions

In this chapter, we investigated the phase evolution of pH responsive microgel dispersions. At pH 3.0, dispersions range of ϕ_{eff}=0.66~0.51 show crystals. The crystals grow from the ends but the interface during crystallization is not that clear. However, at pH 3.85, crystals are observed from the dispersions of ϕ_{eff}=0.57~0.42 ($\phi_{eff,calculated}$ =0.46~0.34). Photographs, DIC images, MSD data, and radial distribution functions show that the samples have an interesting nucleation and crystal growth. These results suggest that the nucleation occurs at the ends of sample and microgels form crystals by templating the existing crystals. The nuclei form at the three phases of the air, the glass surface and the dispersion by depletion force. The microgels in a disordered phase adsorb on the existing crystals via attractive interaction. At the lower effective volume fraction below the hard sphere melting, particles cannot form crystals without any attraction interactions. The melting point of bulk samples strongly depends the phase and pH of the dispersions. The surprisingly high melting point of pH 3.85 crystals suggests that the attractive interaction between particles stabilize particles and the interaction between particles is strong enough to overcome the deswelling upon heating. In summary, by introducing a weak attractive force to the soft repulsion, we were able to observe a complex phase behavior. Also, this weak attractive interaction resulted in slow crystal growth and phase evolution during crystal growth.

References

(1) Optical properties of colloidal photonic crystals confined in rectangular microchannels, H. Miguez, S. M. Yang and G. A. Ozin *Langmuir* **2003**, *19*, 3479.

(2) Photoresponsive azobenzene photonic crystals, M. Kamenjicki, I. K. Lednev and S. A. Asher *J. Phys. Chem. B* **2004**, *108*, 12637.

(3) Thermally switchable periodicities and diffraction from mesoscopically ordered materials, J. M. Weissman, H. B. Sunkara, A. S. Tse and S. A. Asher *Science* **1996**, *274*, 959.

(4) Nature of an electric-field-induced colloidal martensitic transition, A. Yethiraj, A. Wouterse, B. Groh and A. van Blaaderen *Phys. Rev. Lett.* **2004**, *92*, 058301/1.

(5) Ionic colloidal crystals of oppositely charged particles, M. E. Leunissen, C. G. Christova, A.-P. Hynninen, C. P. Royall, A. I. Campbell, A. Imhof, M. Dijkstra, R. van Roij and A. van Blaaderen *Nature* **2005**, *437*, 235.

(6) Diffraction of light by ordered suspensions, P. A. Hiltner and I. M. Krieger *J. Phys. Chem.* **1969**, *73*, 2386.

(7) Phase behaviour of concentrated suspensions of nearly hard colloidal spheres, P. N. Pusey and W. van Megen *Nature* **1986**, *320*, 340.

(8) Colloidal crystals, P. Pieranski *Contemp. Phys.* **1983**, *24*, 25.

(9) The effect of polydispersity on the crystallization of hard spherical colloids, P. N. Pusey *J. Phys. (Les Ulis, Fr.)* **1987**, *48*, 709.

(10) A time resolved static light scattering study on nucleation and crystallization in a colloidal system, J. K. G. Dhont, C. Smits and H. N. W. Lekkerkerker *J. Colloid Interface Sci.* **1992**, *152*, 386.

(11) Dynamics of crystallization in hard-sphere suspensions, Y. He, B. J. Ackerson, W. van Megen, S. M. Underwood and K. Schaetzel *Phys. Rev. E: Stat. Phys., Plasmas, Fluids, Relat. Interdiscip. Top.* **1996**, *54*, 5286.

(12) K. Schatzel *Ordering and phase transitions in charged colloids*, 1996.

(13) Crystallization kinetics of suspensions of hard colloidal spheres, J. L. Harland and W. van Megen *Phys. Rev. E* **1997**, *55*, 3054.

(14) Premelting at defects within bulk colloidal crystals, A. M. Alsayed, M. F. Islam, J. Zhang, P. J. Collings and A. G. Yodh *Science* **2005**, *309*, 1207.

(15) Recent advances in the kinetic and dynamic properties of colloidal crystals, T. Okubo *Curr. Top. Colloid Interface Sci.* **1997**, *1*, 169.

(16) Effect of particle size distribution on crystallization and the glass transition of hard sphere colloids, S. I. Henderson, T. C. Mortensen, S. M. Underwood and W. Van Megen *Physica a* **1996**, *233*, 102.

(17) Three-dimensional direct imaging of structural relaxation near the colloidal glass transition, E. R. Weeks, J. C. Crocker, A. C. Levitt, A. Schofield and D. A. Weitz *Science* **2000**, *287*, 627.

(18) Crystallization kinetics of repulsive colloidal spheres, T. Palberg *J. Phys.-Condens. Matter* **1999**, *11*, R323.

(19) Enhancement of protein crystal nucleation by critical density fluctuations, P. R. ten Wolde and D. Frenkel *Science* **1997**, *277*, 1975.

(20) Classical growth of hard-sphere colloidal crystals, B. J. Ackerson and K. Schaetzel *Phys. Rev. E* **1995**, *52*, 6448.

(21) Nucleation and growth of colloidal crystals, D. J. W. Aastuen, N. A. Clark, L. K. Cotter and B. J. Ackerson *Phys. Rev. Lett.* **1986**, *57*, 1733.

(22) Density fluctuations during crystallization of colloids, K. Schaetzel and B. J. Ackerson *Phys. Rev. E* **1993**, *48*, 3766.

(23) Homogeneous nucleation : Theory adn experiment, D. W. Oxtoby *J. Phys.: Condens. Matter* **1992**, *4*, 7627.

(24) Comparison of experimental estimates and model predictions of protein crystal nucleation rates, N. M. Dixit, A. M. Kulkarni and C. F. Zukoski *Colloids and Surf., A* **2001**, *190*, 47.

(25) Nucleation rates and induction times during colloidal crystallization. Links between models and experiments, N. M. Dixit and C. F. Zukoski *Phys. Rev. E* **2002**, *66*, 051602/1.

(26) Observation of accelerated nucleation in dense colloidal fluids of hard sphere particles, J. L. Harland, S. I. Henderson, S. M. Underwood and W. van Megen *Phys. Rev. Lett.* **1995**, *75*, 3572.

(27) Phase behavior of thermally responsive microgel colloids, J. Wu, B. Zhou and Z. Hu *Phys. Rev. Lett.* **2003**, *90*, 048304/1.

(28) Thermoresponsive photonic crystals, J. D. Debord and L. A. Lyon *J. Phys. Chem. B* **2000**, *104*, 6327.

(29) Color-tunable colloidal crystals from soft hydrogel nanoparticles, J. D. Debord, S. Eustis, S. B. Debord, M. T. Lofye and L. A. Lyon *Adv. Mater.* **2002**, *14*, 658.

CHAPTER 6

Phase Behavior of Charged pH Responsive Colloidal Dispersions

6.1 Introduction

Numerous theoretical and experimental studies on the phase behavior of colloidal dispersions have been performed for both practical applications[1-9] and fundamental studies.[10-19] The simplest colloids are solid, spherical particles, such as, polystyrene, polymethylmethacrylate (PMMA) or silica spheres. These are hard and impenetrable spheres so that the main interaction between particles is a steric repulsion. The phase of such dispersions is mainly determined by the volume fraction of a system.[10] Due to this simple interaction potential, the phase behavior[10] and the kinetics of crystallization[20-24] of such dispersions have been extensively investigated. Soft spheres can provide more complex interaction potentials and richer phase behaviors. Neutral star polymers have been widely utilized to calculate the soft sphere interactions since they display tunable softness in their conformations and associated effective potentials.[25-30] Closely related to neutral star polymers are networks composed by polyelectrolyte chains. Lowen and coworkers and Denton have focused on polyelectrolyte stars and ionic microgels as a model system to study ultra soft interactions.[31-37] The theoretical calculations predicted that the interaction potential of polyelectrolyte stars[33, 38] and ionic microgels[32, 39] is dependent on the density as neutral star polymers. When the center-to-center distance is longer than particle diameter, the interaction force between particles is found to be Coulombic repulsion. However, when center-to-center distance between particles is

shorter than the particle diameter, the interaction is ultra-soft repulsive due to the interpenetration of polymer chains. This chain penetration is explained by the entropic contribution of the trapped counterions.[35, 36, 39] Theory combined with a general algorithm presented the ultra-soft interaction potential results into an unusual phase diagram including reentrance melting transition and more open crystalline structures such as body-centered-cubic (*bcc*), body-centered-orthogonal (*bco*), and hexagonal structure.[32, 39]

Our group prepared uniform spherical poly(*N*-isopropylacrylamide-*co*-acrylic acid) (*p*NIPAm-*co*-AAc) microgels and has shown that the microgels have pH responsivity. At pH below pK_a of AAc (such as at pH=3.0), AAc groups in the microgel are protonated and the microgels exhibit a similar volume phase transition to *p*NIPAm homopolymer microgels as seen figure 3.2-1 in chapter 3. As the pH of microgel dispersions increase, AAc molecules begin to be deprotonated. The deprotonation continues as pH of microgel dispersion exceeds pK_a of AAc. This deprotonation results in charges in the polymer chains and the microgels swell by uptaking more water molecules inside the microgels due to the electrostatic interaction of charged polymer chains and the osmotic pressure from counterions inside the microgels. For the charged microgels, the volume phase transition temperature is shifted toward higher temperature due to the Coulombic repulsion between charged polymer chains. Figure 6.1-1 represents typical volume phase transition curves obtained from *p*NIPAm-*co*-AAc microgels dispersed in different pH buffer solutions. The hydrodynamic radii are dependent on the pH of the dispersions as mentioned earlier. The figure also shows that the volume phase transition is shifted toward higher temperature as the pH of dispersion increases.

In the previous chapters, we investigated the phase behavior and the phase evolution of pH responsive, *p*NIPAm-*co*-AAc, microgels dispersions at different pH values. At pH 3.0, microgel dispersions display an order-to-disorder transition at ϕ_{eff}=0.51. This phase transition is similar to hard sphere phase transition.[10] As the pH of dispersion approaches the pK_a of AAc (eg. pH=3.85), an order-to-disorder transition occurs at ϕ_{eff}=0.42 that is lower than the phase transition of hard spheres. At pH=3.85, the microgel dispersions show very slow crystallization and the crystals grew exclusively from the ends of the samples. The melting point of bulk crystals upon heating also is dependent on the pH. The microgel crystals close to the to pK_a of AAc start to melt at much higher temperature than the LCST of the microgel while the microgel crystals at pH 3.0 melt completely below the LCST of the microgel. The similar phase behavior as hard sphere system and the bulk crystal melting suggest that the interaction between microgels in pH 3.0 buffer solution is mainly repulsive. The hydrogen bonding from AAc-AAc and/or AAc-amide may contribute to the effective interaction between particles but the results imply that this interaction is not dominant at this pH. However, at pH 3.85, microgel dispersions show a stable structure (crystal) at the effective volume fraction as low as 0.42. As observed in some coexistence studies,[40-45] this unusual crystalline phase at low effective volume fraction can be explained by weak short-range attractive interactions. In our previous study,[46] we proposed that the source for the attractive interaction is the hydrogen bonding between AAc-AAc and/or AAc-amide groups. The results shown in the chapter 4 and 5 indicate that partially deprotonated microgel dispersions play a role in the effective interaction between particles. Examination of the chemical structure and morphology of the *p*NIPAm-*co*-AAc

microgels suggests that the only sources for the attractive interactions are an ion-dipole interaction and/or hydrogen bonding. The interaction energy between deprotonated AAc and AAc and/or amide were determined as 29.3 kcal/mol and 25.4 kcal/mol, respectively.[47] A theoretical calculation predicted that the AAc-AAc and/or AAc-amide hydrogen bonding to be 2~15 kcal/mol.[48] These results support that as the pH of dispersion approaches the pK_a, the ion-dipole interactions become dominant and the interactions are strong enough for microgels to form an ordered structure at lower effective volume fraction than hard sphere melting point.

In this chapter, we investigate the phase behavior of microgel dispersions at higher pH than pK_a of AAc where most AAc groups are deprotonated. Particular emphasis will be placed on the concentration effect on phase behavior and the dynamics of charged microgel dispersions. To study phase behavior of microgel dispersions, DIC micrograph images and particle trajectories will be obtained. The radial distribution function also will be used to determine the structure of microgel dispersions. Mean square displacement (MSD) data will be calculated to determine the evolution of dispersions.

6.2 Experimental

Microgel Synthesis and Characterization Chapter 2.2 covers details of this issue. The microgel solution was filtered and purified by centrifugation and redistribution at least three times to get rid of unreacted monomers and soluble oligomers. The purified *p*NIPAm-*co*-AAc microgel dispersion was freeze-dried over night then the freeze-dried microgels were redispersed in buffer solutions of desired pH. Buffer solution of pH 6.5

(ionic strength=100 mM) was used for the experiments and relative high concentration was chosen for stable pH. Once the microgels are redispersed completely, the redispersed sample was centrifuged at 29 °C at a relative centrifugal force (RCF) 16,100 g for 1 hour. The centrifuged microgel assemblies were diluted by adding buffer solution to achieve desired weight percent for the further experiments. The diluted samples were placed on the shaker table overnight to redisperse the microgels completely. The microgel dispersions were transferred into rectangular glass tubes (Vitrotube, 0.1 mm × 2.0 mm × 50 mm) for observation under a microscope.

Effective Volume Fraction Determination The details of the shift factor determination are described in the chapter 3. The shift factor for pH 6.5 dispersions is 19.6 at 22 °C. Once the shift factor is determined, the ϕ_{eff} of a microgel dispersion can be calculated by multiplying *k* by c.

Microscopy and Particle Tracking Analysis Details for particle tracking analysis are explained in the chapter 4 and 5.

6.3 Results and Discussion

Figure 6.3-1 shows DIC images obtained from microgel dispersions over a range of effective volume fractions. The images were taken 25 mm from the end of samples. The dispersions of effective volume fraction 0.66 and 0.59 exhibit an ordered structure and the dispersion at ϕ_{eff} = 0.56 shows a mixed phase. The crystal-to-fluid transition occurs at ϕ_{eff} =0.52 and microgel dispersions are disordered below ϕ_{eff} =0.50. It is not surprising that these dispersions have a similar crystal-to-fluid transition to hard spheres, since these dispersions do not have attractive interactions. The effective interaction

between ionic microgels at low ionic strength condition is known to be mainly repulsive due to the Coulombic interaction when the center-to-center distance is larger than size of particles.[32, 39] When the center-to-center is shorter than the radius of the particles, ionic microgels repel very softly.[32, 39] Since our microgels are dispersed in high ionic strength solution (100 mM), the Debye screening layer is thin (< ~3 nm). As a result, the electrostatic repulsion would not contribute significantly to the effective interaction. Also, this thin Debye screening layer would not contribute the effective volume fraction, so that the melting transition in this pH occurs similar effective volume fraction as a hard sphere system.

The trajectories corresponding to the DIC images in figure 6.3-1 are presented in figure 6.3-2. The trajectories confirm that microgel dispersions have a crystalline phase at ϕ_{eff}=0.66 and 0.59, a mixed phase at ϕ_{eff}=0.56, and a fluid phase ϕ_{eff}=0.52 ~ 0.45 as shown in micrograph images. The trajectories show the diffusion of particles qualatatively. Figure 6.3-2(a)~(c) clearly represent that as the effective volume fraction decreases, the microgel diffusion increases.

Figure 6.3-3 represents the radial distribution functions, *g(r)*, of microgel dispersions. Radial distribution function of a well-ordered structure has distinctive and sharp peaks while a disordered phase shows very smooth peaks. As the effective volume fraction decreases, the structure of the samples change from an ordered (green and blue lines) to a mixed phase (purple line) and, finally, to a disordered structure (red, black and sky blue lines). Due to a disordered phase, ϕ_{eff}=0.45 show no distinctive peaks. As the effective volume fraction of ϕ_{eff}=0.50 and 0.52, peak height grows but still distinctive peaks are not seen. The microgel dispersion at ϕ_{eff} of 0.56 has smooth but distinctive

peaks at distance of ~ 1.9 μm and 2.2 μm. These smooth peaks indicate that the dispersion has some ordered structure which has shown in trajectories in figure 6.3-2(c). Well ordered arrays observed from ϕ_{eff}=0.66 and 0.59 give rise to sharp and distinctive peaks in the plot. The radial distributions of microgel dispersions support the phase transitions observed from micrograph images and trajectories. The table 6.3-1 represents the center-to-center distances (d_{c-c}) calculated from the first peak of radial distribution function. The data show that as the effective volume decreases, d_{c-c} increases. The d_{c-c} calculated from ordered structures (ϕ_{eff}=0.66 and 0.59) is larger than the diameter (0.9 μm) determined by PCS.

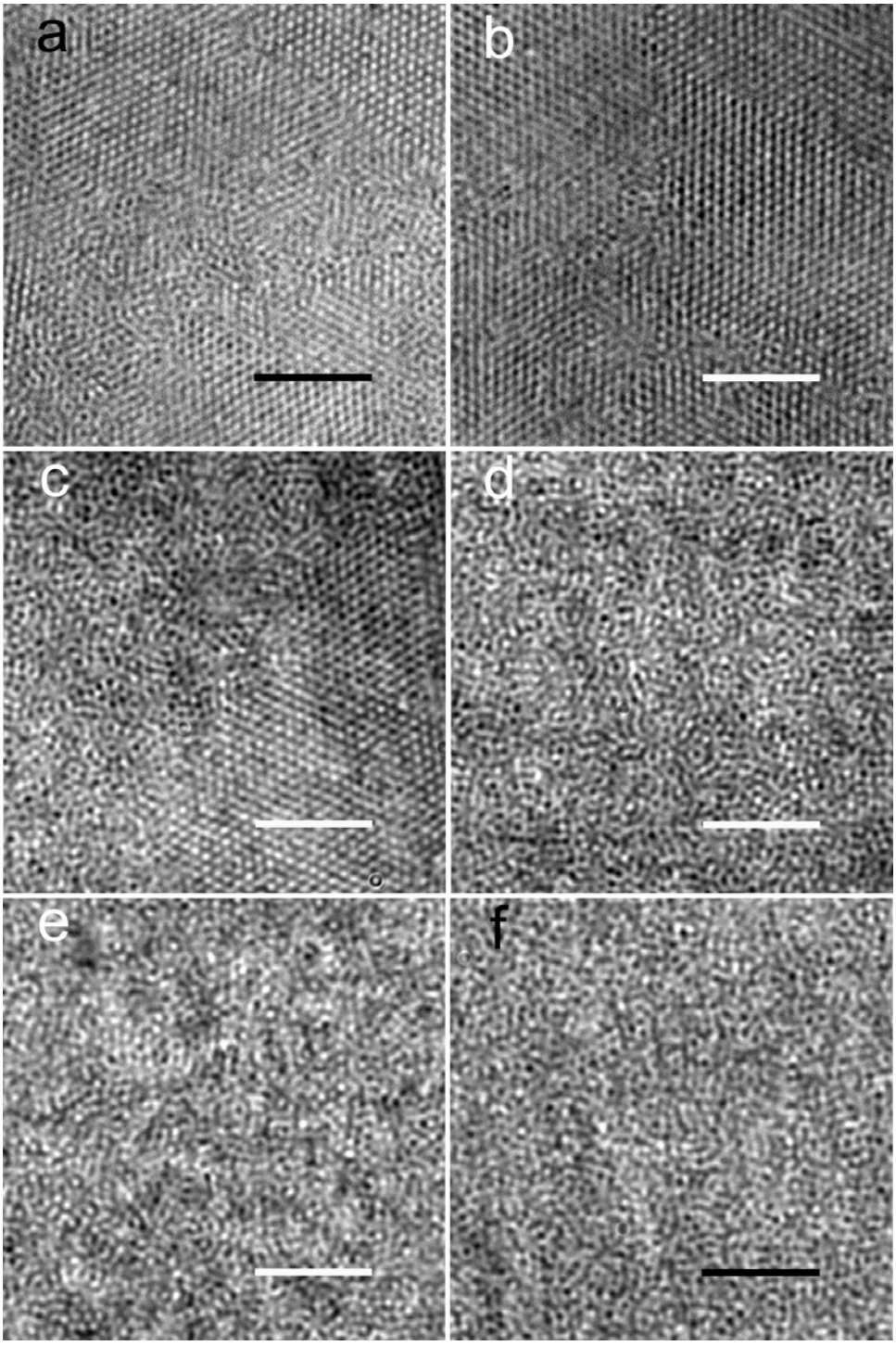

Equation 6.3.1 DIC micrograph images of *p*NIPAm-*co*-AAc microgels (R_h = 450 nm at 22 °C) dispersed in pH 6.5 buffer solution. The movies were recorded at 25 mm from the ends. (a) ϕ_{eff}=0.66, (b) ϕ_{eff} =0.59, (c) ϕ_{eff} =0.56, (d) ϕ_{eff}=0.52, (e) ϕ_{eff}=0.50, and (f) ϕ_{eff}=0.45. Scale bar is 10 μm.

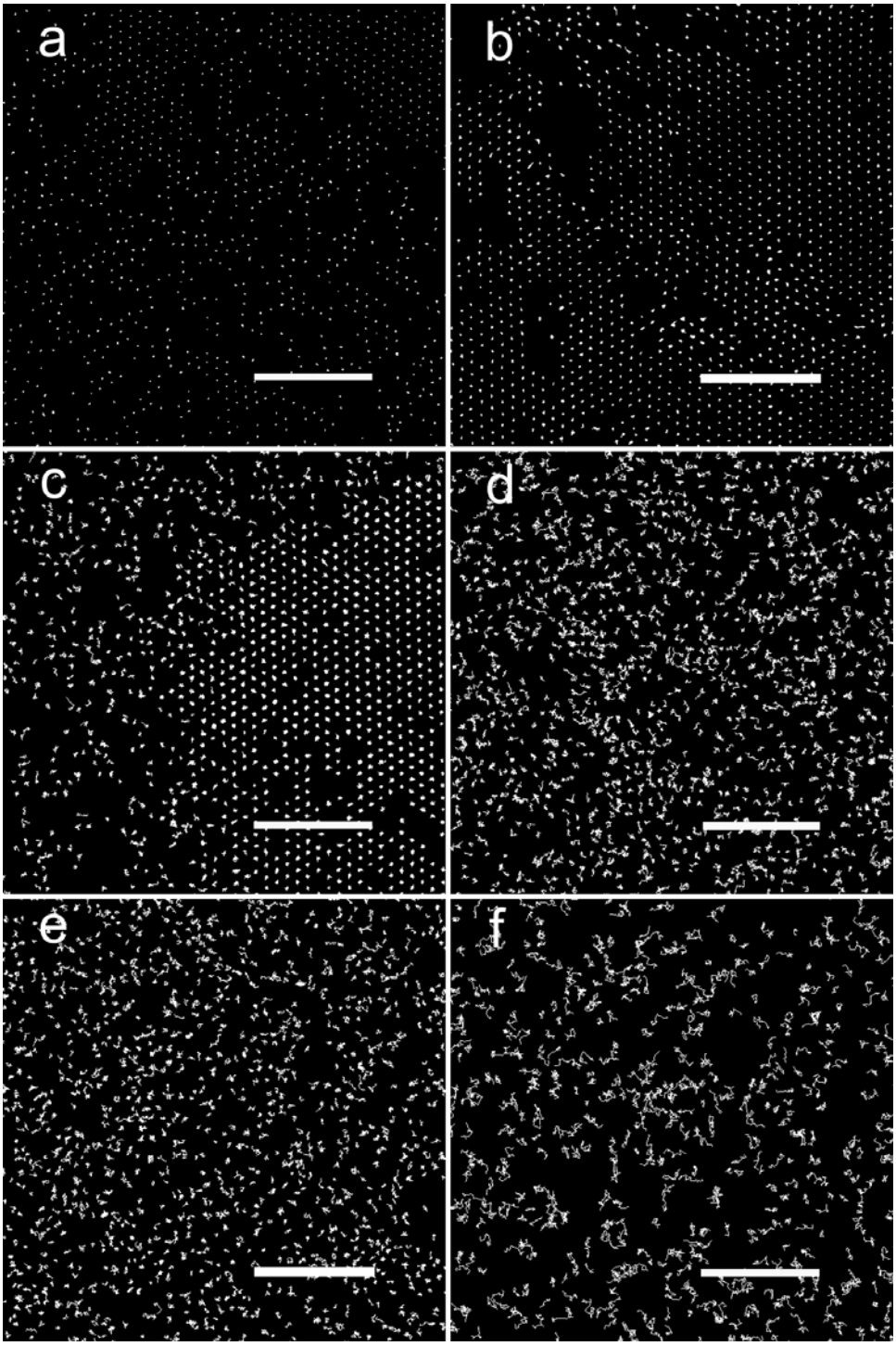

Equation 6.3.2 Particle trajectories of *p*NIPAm-*co*-AAc microgels (R_h = 450 nm at 22 °C) dispersed in pH 6.5 buffer solution. The movies were recorded at 25 mm from the ends. (a) ϕ_{eff}=0.66, (b) ϕ_{eff} =0.59, (c) ϕ_{eff} =0.56, (d) ϕ_{eff}=0.52, (e) ϕ_{eff}=0.50, and (f) ϕ_{eff}=0.45. Scale bar is 10 μm.

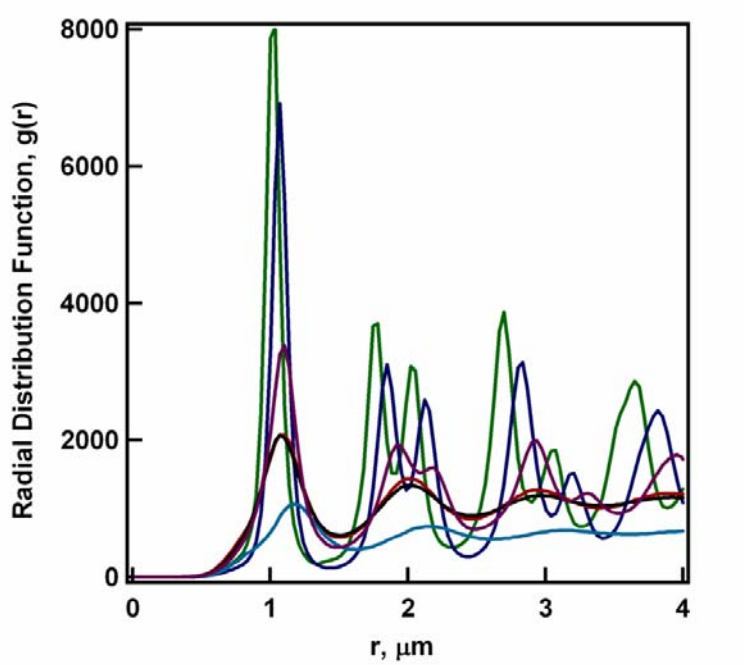

Equation 6.3.3 The radial distribution function of the responsive microgel dispersions. The g(r) was calculated 25 mm from the ends. ϕ_{eff}=0.66 (green), ϕ_{eff}=0.59 (blue), ϕ_{eff}=0.56 (purple), ϕ_{eff}=0.52 (red), ϕ_{eff}=0.50 (black) and ϕ_{eff}=0.45 (sky blue).

Table 6.3-1 The center-to-center distance ($d_{c\text{-}c}$) calculated from *g(r)*

ϕ_{eff}	0.66	0.59	0.56	0.52	0.50	0.45
$d_{c\text{-}c}$ (μm)	1.04	1.07	1.10	1.10	1.07	1.17

The evolution of microgel dispersions can be obtained in the MSD data. Figure 6.3-3 shows the MSD vs. lag time plots of microgel dispersions of pH 6.5 at 25 mm from the ends. Unlike MSD evolution seen from pH 3.0 and 3.85 samples, *p*NIPAm-*co*-AAc microgels dispersed in pH 6.5 buffer solution do not show a significant decrease of diffusion. Instead, the diffusion constant of microgels increases over time. For some effective volume fractions seen in figure 6.4-3(c) and (d), the diffusion increases significantly. The increase of diffusion constant can be explained by the conformation changes of polymer chains on the microgel surfaces. At day 0, the charged polymer chains stretch due to the electrostatic repulsion between chains. These stretched polymer chains on the microgel surface would create the friction between particles during particle movements. This friction hinders microgel particles from moving freely. Over time, the stretched chains form coils to gain entropy. As a result, the friction between particles decreases and the diffusion of particles increases.

Figure 6.3-4 shows the MSD vs. lag time plots of microgels dispersed in pH 6.5 buffer solution at 12.5 mm from the ends of samples. The MSD data obtained from the two different spots show similar dynamics implying that the samples are spatially homogeneous. Due to the repulsive nature of interaction, one can imagine that the nucleation and crystal growth of charged microgels would be similar fashion as the nucleation and crystal growth of hard spheres.

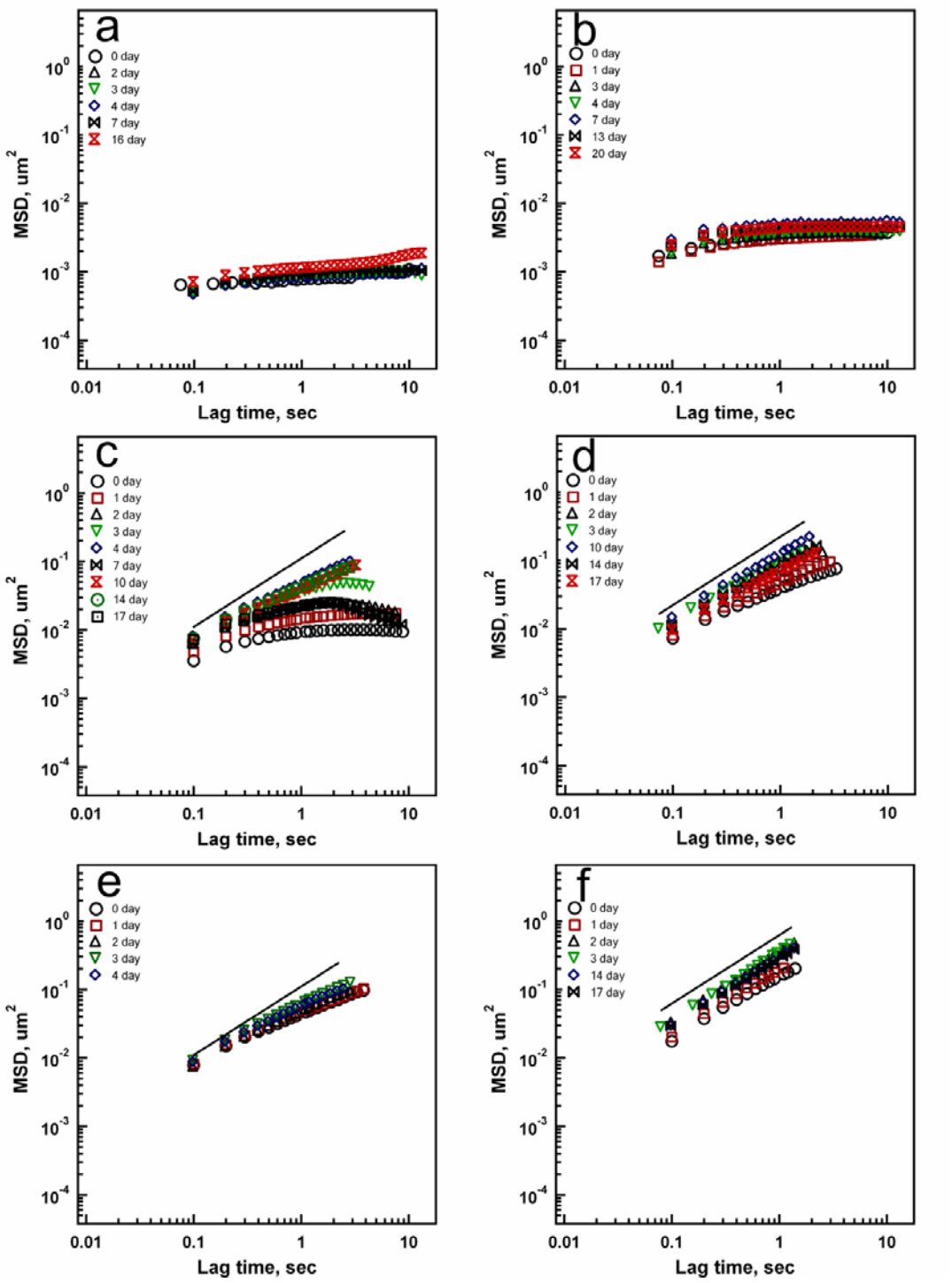

Equation 6.3.4 The MSD evolution of microgel dispersions upon aging. The microgels are dispersed in pH 6.5 buffer solution. The movies were recorded at 25 mm from the end. (a) ϕ_{eff}=0.66, (b) ϕ_{eff} =0.59, (c) ϕ_{eff} =0.56, (d) ϕ_{eff}=0.52, (e) ϕ_{eff}=0.50, and (f) ϕ_{eff}=0.45. The trend lines have slope 1 and indicate free Brownian diffusion.

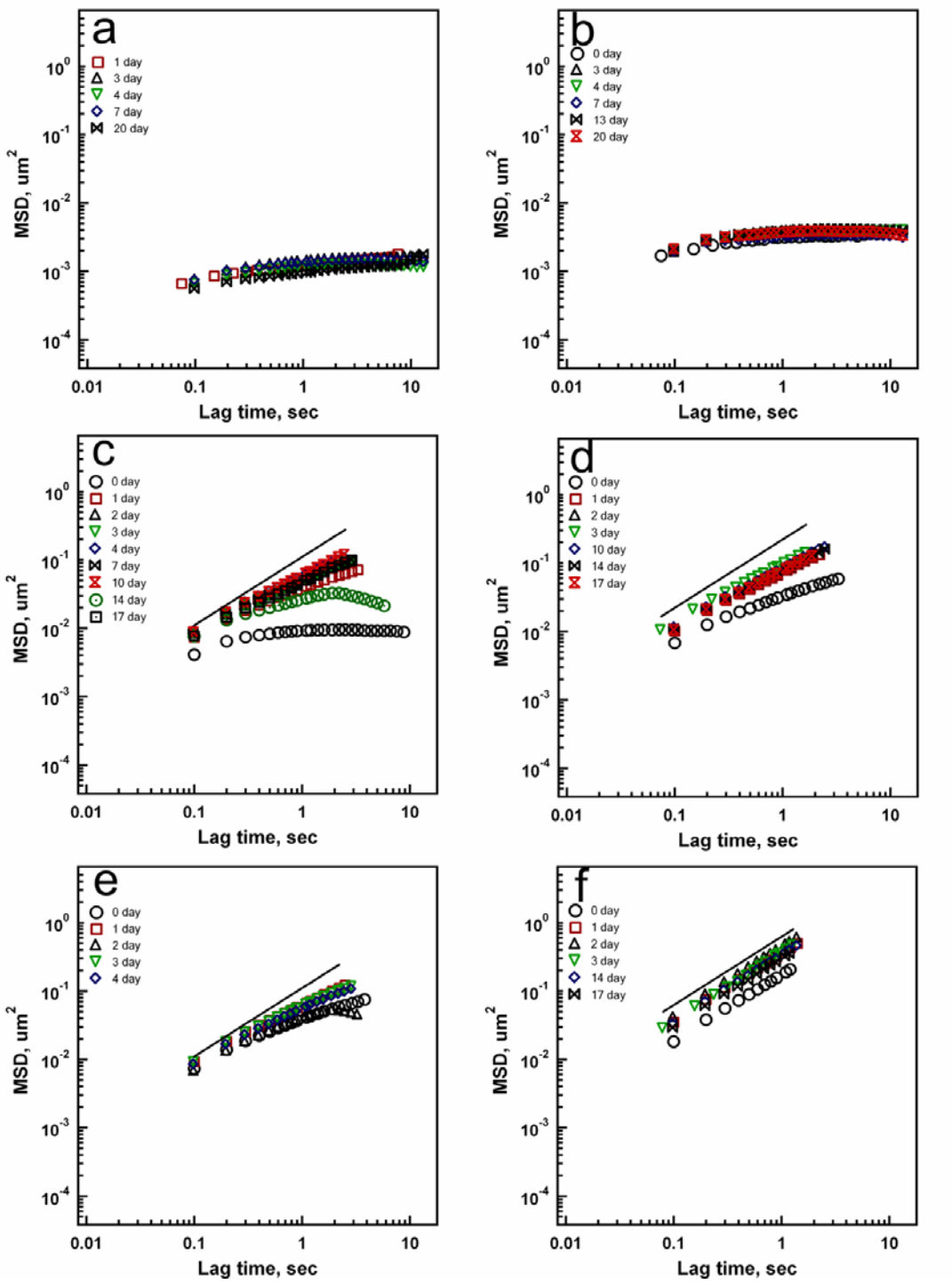

Equation 6.3.5 The MSD evolution of microgel dispersions upon aging. The microgels are dispersed in pH 6.5 buffer solution. The movies were recorded at 12.5 mm from the end. (a) ϕ_{eff}=0.66, (b) ϕ_{eff} =0.59, (c) ϕ_{eff} =0.56, (d) ϕ_{eff}=0.52, (e) ϕ_{eff}=0.50, and (f) ϕ_{eff}=0.45. The trend lines have slope 1 and indicate free Brownian diffusion.

6.4 Conclusions

In this chapter, the phase behavior and the dynamics of charged microgel dispersions have been described. Since the *p*NIPAm-*co*-AAc microgel is pH responsive, the charged microgel dispersions are easily obtained by simply redispersing the microgels in the pH =6.5 buffer solution. PCS data showed that microgels in pH 6.5 buffer is larger and have higher volume phase transition temperature implying the microgels are highly charged.

DIC images show that the order-to-disorder transition is observed at ϕ_{eff}=0.52. This phase transition is similar to hard sphere systems. Here, the main interaction between microgel particles would be the repulsion. The trajectories show that the diffusion of particles increases as the effective volume fraction of microgel dispersions. The radial distribution function, *g(r)* confirms the phase transition seen in micrograph images and trajectories. MSD data revealed that the microgels dispersed in pH 6.5 buffer do not show a dramatic phase evolution or decreases of diffusion constant as seen in pH 3.0 and pH 3.85 dispersions. Instead, the diffusion of charged microgels increases over time for some samples. We hypothesize that the stretched polymer chains form coils to gain entropy over time. This change reduces the friction between particles and increases the particle diffusion.

References

(1) Photonic crystal carbohydrate sensors: Low ionic strength sugar sensing, S. A. Asher, V. L. Alexeev, A. V. Goponenko, A. C. Sharma, I. K. Lednev, C. S. Wilcox and D. N. Finegold *J. Am. Chem. Soc.* **2003**, *125*, 3322.

(2) Photonic crystal optrode sensor for detection of pb2+ in high ionic strength environments, C. E. Reese and S. A. Asher *Anal. Chem.* **2003**, *75*, 3915.

(3) Polymerized colloidal crystal hydrogel films as intelligent chemical sensing materials, J. H. Holtz and S. A. Asher *Nature* **1997**, *389*, 829.

(4) Optical properties of planar colloidal crystals: Dynamical diffraction and the scalar wave approximation, D. M. Mittleman, J. F. Bertone, P. Jiang, K. S. Hwang and V. L. Colvin *J. Chem. Phys.* **1999**, *111*, 345.

(5) Preparation of photonic crystals made of air spheres in titania, J. Wijnhoven and W. L. Vos *Science* **1998**, *281*, 802.

(6) Photonic band structure: The face-centered-cubic case, E. Yablonovitch and T. J. Gmitter *Phys. Rev. Lett.* **1989**, *63*, 1950.

(7) Large-scale synthesis of a silicon photonic crystal with a complete three-dimensional bandgap near 1.5 micrometres, A. Blanco, E. Chomski, S. Grabtchak, M. Ibisate, S. John, S. W. Leonard, C. Lopez, F. Meseguer, H. Miguez, J. P. Mondia, G. A. Ozin, O. Toader and H. M. van Driel *Nature* **2000**, *405*, 437.

(8) Inhibited light propagation and broadband reflection in photonic air-sphere crystals, M. S. Thijssen, R. Sprik, J. Wijnhoven, M. Megens, T. Narayanan, A. Lagendijk and W. L. Vos *Phys. Rev. Lett.* **1999**, *83*, 2730.

(9) Band spectroscopy of colloidal photonic crystal films, H. Miguez, V. Kitaev and G. A. Ozin *Appl. Phys. Lett.* **2004**, *84*, 1239.

(10) Phase behaviour of concentrated suspensions of nearly hard colloidal spheres, P. N. Pusey and W. van Megen *Nature* **1986**, *320*, 340.

(11) Structure of crystals of hard colloidal spheres, P. N. Pusey, W. Van Megen, P. Bartlett, B. J. Ackerson, J. G. Rarity and S. M. Underwood *Phys. Rev. Lett.* **1989**, *63*, 2753.

(12) Observation of a glass transition in suspensions of spherical colloidal particles, P. N. Pusey and W. Van Megen *Phys. Rev. Lett.* **1987**, *59*, 2083.

(13) Melting transition and communal entropy for hard spheres, W. G. Hoover and F. H. Ree *J. Chem. Phys.* **1968**, *49*, 3609.

(14) Phase behavior of small attractive colloidal particles, D. Rosenbaum, P. C. Zamora and C. F. Zukoski *Phys. Rev. Lett.* **1996**, *76*, 150.

(15) The glass paradigm for colloidal glasses, gels, and other arrested states driven by attractive interactions., K. A. Dawson *Curr. Opin. Colloid Interface Sci.* **2002**, *7*, 218.

(16) Real-space structure of colloidal hard-sphere glasses, A. Vanblaaderen and P. Wiltzius *Science* **1995**, *270*, 1177.

(17) Subdiffusion and the cage effect studied near the colloidal glass transition, E. R. Weeks and D. A. Weitz *Chem. Phys.* **2002**, *284*, 361.

(18) Properties of cage rearrangements observed near the colloidal glass transition, E. R. Weeks and D. A. Weitz *Phys. Rev. Lett.* **2002**, *89*, 095704/1.

(19) Direct visualization of ageing in colloidal glasses, R. E. Courtland and E. R. Weeks *J. Phys.: Condens. Matter* **2003**, *15*, S359.

(20) Classical growth of hard-sphere colloidal crystals, B. J. Ackerson and K. Schaetzel *Phys. Rev. E* **1995**, *52*, 6448.

(21) Crystallization kinetics of repulsive colloidal spheres, T. Palberg *J. Phys.: Condens. Matter* **1999**, *11*, R323.

(22) Colloidal hard-sphere crystallization kinetics in microgravity and normal gravity, Z. Cheng, J. Zhu, W. B. Russel, W. V. Meyer and P. M. Chaikin *Appl. Opt.* **2001**, *40*, 4146.

(23) Kinetic study on the colloidal crystallization of silica spheres in the highly diluted and exhaustively deionized suspensions as studied by light-scattering and reflection spectroscopy, T. Okubo, S. Okada and A. Tsuchida *J. Colloid Interface Sci.* **1997**, *189*, 337.

(24) Crystallization kinetics of suspensions of hard colloidal spheres, J. L. Harland and W. van Megen *Phys. Rev. E* **1997**, *55*, 3054.

(25) Effective interactions in soft condensed matter physics, C. N. Likos *Phys. Rep.* **2001**, *348*, 267.

(26) Star polymers viewed as ultrasoft colloidal particles, C. N. Likos, H. Lowen, M. Watzlawek, B. Abbas, O. Jucknischke, J. Allgaier and D. Richter *Phys. Rev. Lett.* **1998**, *80*, 4450.

(27) Ordering phenomena of star polymer solutions approaching the .Theta. State, C. N. Likos, H. Lowen, A. Poppe, L. Willner, J. Roovers, B. Cubitt and D. Richter *Phys. Rev. E: Stat. Phys., Plasmas, Fluids, Relat. Interdiscip. Top.* **1998**, *58*, 6299.

(28) Star polymers: From conformations to interactions to phase diagrams, C. N. Likos and H. M. Harreis *Condens. Matter. Phys.* **2002**, *29*, 173.

(29) Phase diagram of star polymer solutions, M. Watzlawek, C. N. Likos and H. Lowen *Phys. Rev. Lett.* **1999**, *82*, 5289.

(30) Partial structure factors in star polymer/colloid mixtures, J. Stellbrink, J. Allgaier, D. Richter, A. Moussaid, A. B. Schofield, W. C. K. Poon, P. N. Pusey, P. Lindner, J. Dzubiella, C. N. Likos and H. Lowen *Appl. Phys. A* **2002**, *74*, S355.

(31) Counterion penetration and effective eletrostatic interactions in solutions of polyelectrolyte stars and microgels, A. R. Denton *Phys. Rev. E* **2003**, *67*, 011804/1.

(32) Ionic microgels as model systems for colloids with an ultrasoft electrosteric repulsion: Structure and thermodynamics, D. Gottwald, C. N. Likos, G. Kahl and H. Lowen *J. Chem. Phys.* **2005**, *122*, 074903/1.

(33) Structure and phase behavior of polyelectrolyte star solutions, N. Hoffmann, C. N. Likos and H. Lowen *J. Chem. Phys.* **2004**, *121*, 7009.

(34) Exotic fluids and crystals of soft polymeric colloids, C. N. Likos, N. Hoffmann, H. Lowen and A. A. Louis *J. Phys.: Condens. Matter* **2002**, *14*, 7681.

(35) Conformations and interactions of star-branched polyelectrolytes, A. Jusufi, C. N. Likos and H. Lowen *Phys. Rev. Lett.* **2002**, *88*, 018301.

(36) Counterion-induced entropic interactions in solutions of strongly stretched, osmotic polyelectrolyte stars, A. Jusufi, C. N. Likos and H. Lowen *J. Chem. Phys.* **2002**, *116*, 11011.

(37) Charged colloids, polyelectrolytes and biomolecules viewed as strongly coupled coulomb systems, H. Lowen, E. Allahyarov, C. N. Likos, R. Blaak, J. Dzubiella, A. Jusufi, N. Hoffmann and H. M. Harreis *J. Phys. A: Math. Gen.* **2003**, *36*, 5827.

(38) Interactions and phase behavior of polyelectrolyte star solutions, C. N. Likos, N. Hoffmann, A. Jusufi and H. Lowen *J. Phys.: Condens. Matter* **2003**, *15*, S233.

(39) Phase behavior of ionic microgels, D. Gottwald, C. N. Likos, G. Kahl and H. Lowen *Phys. Rev. Lett.* **2004**, *92*, 680103/1.

(40) Visible evidence for interparticle attraction in polymer latex dispersions, N. Ise, T. Okubo, K. Ito, S. Dosho and I. Sogami *Langmuir* **1985**, *1*, 176.

(41) How homogeneous are "homogeneous dispersions"? Counterion-mediated attraction between like-charged species, N. Ise, T. Konishi and B. V. R. Tata *Langmuir* **1999**, *15*, 4176.

(42) Like-charge attractions in metastable colloidal crystallites, A. E. Larsen and D. G. Grier *Nature* **1997**, *385*, 230.

(43) Colloids: A surprisingly attractive couple, D. G. Grier *Nature* **1998**, *393*, 621.

(44) Pair interaction of charged colloidal spheres near a charged wall, S. H. Behrens and D. G. Grier *Phys. Rev. E* **2001**, *64*, 050401/1.

(45) When like charges attract: Interactions and dynamics in charge-stabilized colloidal suspensions, D. G. Grier *J. Phys.: Condens. Matter* **2000**, *12*, A85.

(46) Influence of particle volume fraction on packing in responsive hydrogel colloidal crystals, S. B. Debord and L. A. Lyon *J. Phys. Chem. B* **2003**, *107*, 2927.

(47) Ionic hydrogen bond and ion solvation. 6. Interaction energies of the acetate ion with organic molecules. Comparison of ch_3coo^- with cl^-, cn^-, and sh^-, M. Meot-Ner *J. Am. Chem. Soc.* **1988**, *110*, 3854.

(48) A simple functional representation of angular-dependent hydrogen-bonded systems. 1. Amide, carboxylic acid, and amide-carboxylic acid pairs, K. T. No, O. Y. Kwon and S. Y. Kim *J. Phys. Chem.* **1995**, *99*, 3478

Appendix A

Microgel Mixture Dispersions

A. 1 Introduction

In this chapter, microgel mixture crystals prepared from microgels of different LCSTs and/or size will be discussed. Here, one microgel was added as a minor component (dopant) to another microgel dispersion. The original motivation of this experiment was to explore the melting behavior of doped microgel crystals in which the dopant had a lower LCST. It was hypothized that microgels with a lower LCST in a mixture would deswell first upon heating and would cause point defects, which may change the melting behavior of doped microgel crystals. Random copolymers of tert-butyl acrylamide (TBA), NIPAm, AAc and BIS (*p*NIPAm-*co*-AAc-*co*-TBA : known from now on as TBA microgel) have shown tunable LCST depending on the amount of TBA.[1] In this chapter, TBA microgels with LCSTs lower than 31 °C are doped into *p*NIPAm microgel dispersion so that TBA microgels shrink prior to *p*NIPAm microgels during heating to induce defects in the two-component crystal. Turbidity measurements by UV-VIS revealed that TBA doped *p*NIPAm microgel crystals do not show significantly different turbidity change as a function of temperature in comparison to *p*NIPAm crystals. To see how doped crystals behave during melting at the microscopic level, two-component crystals were observed under an optical microscope while the temperature of the sample was controlled using an objective heater as well as a temperature stage. After heating and cooling the TBA microgel doped *p*NIPAm crystals,

interesting particle distributions were observed. Larger TBA microgels rose to the top of the sample while smaller *p*NIPAm microgels sank to the bottom. In this chapter, this particle redistribution after the heating and cooling process and observation from other doped microgel systems will be discussed.

A. 2 Experimental

Particle Synthesis and Characterization. The TBA microgels were synthesized based on Debord's paper.[1] NIPAm (93-X mol%), AAc (5 mol%), BIS (2 mol%) and 0.01 g of SDS were dissolved in 50 mL of water and the resulting solution was filtered through #2 Whatman paper filter to remove particulate matter. Tert-butylacrylamide (TBA, X mol %) was dissolved in 1 mL of ethanol before addition to the monomer solution, resulting in a total monomer concentration of 0.75 g/L (65 mM). The reaction mixture was heated to 55-60 °C under a stream of nitrogen over the course of 1 hour. Following the addition of APS (0.03 g), the polymerization was carried out at 55-60 °C for 3 h under a nitrogen atmosphere. In these studies, only 3 mol% TBA (X=3) was used. PNIPAm microgels composed of different amounts of cross-linker, and *p*NIPAm-*co*-AAc microgels were prepared in the same manner as papers published by our group.[2, 3] The 3 mol% TBA microgels (from now on TBA microgels) were purified by dialysis (Spectra/Por 7 dialysis membrane, MWCO 10,000, VWR) with daily changes of water for four days. PNIPAm and *p*NIPAM-*co*-AAc microgels were cleaned by centrifugation and redispersion. The size and thermoresponsive behavior of the *p*NIPAm and TBA microgels were confirmed by photon correlation spectroscopy (PCS, Protein Solutions Inc.) prior to their use in crystal preparation. The hydrodynamic radii (R_h) at pH 3.5 in 1

mM HCl solution at 25 °C of *p*NIPAm and TBA microgels are ~313 nm and ~506 nm, respectively. Figure A.2-1 shows the volume phase transition diagram for *p*NIPAm and TBA microgels. The LCSTs of *p*NIPAm and TBA microgels are ~31 °C and ~29 °C, respectively. As seen in figure A.2-1, the size of TBA microgels is larger than *p*NIPAm microgels at all temperatures.

For some microgels, 0.01 mol % of 4-Aminofluorescein (AFA) was incorporated for observation under a fluorescence microscope. It has been shown that co-polymerizing 0.01 % AFA does not change volume phase transition behavior of microgels significantly.

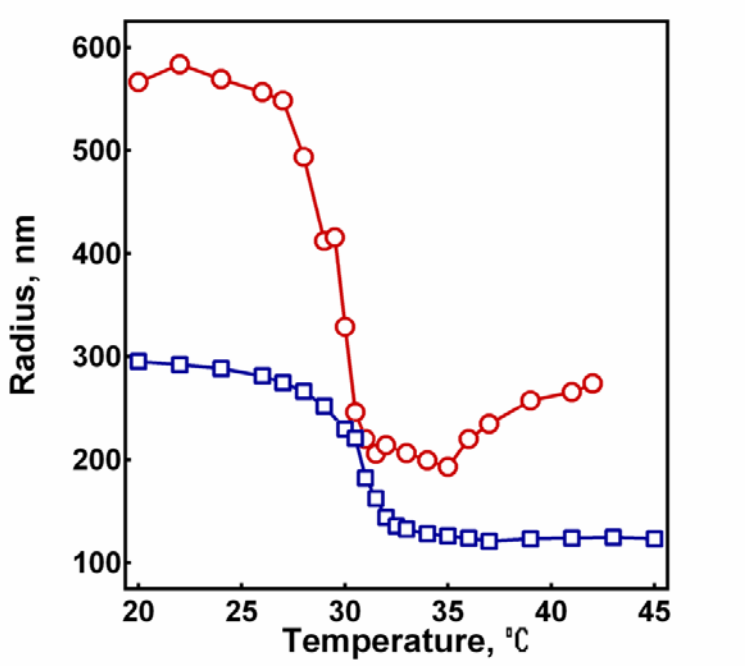

Figure A.2-1 Volume phase transition diagram of 3 mol % TBA (○, open circle) and *p*NIPAm (□, open square) microgels in 1 mM HCl solution. The pH of the sample is 3.5.

Different density microgels are prepared by using different amount of cross-linking agent to prepare mixed colloidal dispersions. 2%, 5% and 7% BIS was incorporated and the microgels were synthesized by surfactant free precipitation polymerization as described in chapter 2. Surfactant free precipitation polymerization, in general, provides larger microgels. The R_h of 2%, 5% and 7% BIS incorporated *p*NIPAm at 24 °C in 1 mM HCl, pH 3.5 solution are 316 nm, 296 nm and 215 nm, respectively. Volume phase transition diagrams of 2%, 5% and 7% BIS incorporated *p*NIPAm are presented in figure A.2-2.

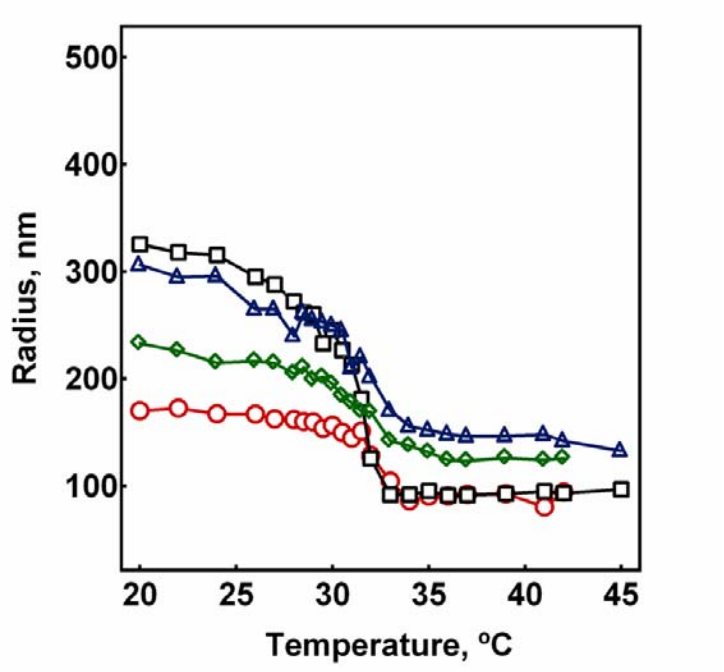

Figure A.2-2 Volume phase transition diagram of *p*NIPAm incorperated with (a) 2% BIS (○, open circle), (b) 2% BIS (□, open square), (c) 5% BIS (Δ, open upper triangle), and (d) 7% BIS (◊, open diamond). All microgels are dispersed in 1 mM HCl solution. The pH of the dispersions is fixed 3.5.

Also, smaller 2% BIS microgels were synthesized by precipitation polymerization using a surfactant. Here, sodium dodecyl sulfate (SDS) was utilized during polymerization process to stabilize the particles resulting in smaller particles than surfactant free precipitation polymerization. The R_h at 24 °C in pH ~ 3.5, 1mM HCl solution is 167 nm and the volume phase transition diagram is presented in figure A.2-2. Green fluorescence labeled polystyrene (PS) latex particles, 0.51 μm and 1.0 μm, were purchased from Duke Scientific Corp.

When two-component crystals were prepared, each set of microgels was centrifuged separately and then mixed. The two-component crystals were transferred into a 100 μm vitrotube as described in the experimental section of chapter 2. The two-component crystals in the vitrotube were placed on the microscope and both the temperature stage and the objective heater were used to control the temperature of the sample. To see the melting behavior, the two-component crystals were heated until the sample became completely fluid. When the microgels were heated, the temperature was raised very slowly to avoid melting induced by thermal convection. The micrograph images were taken at least 20 minutes after the sample reached the desired temperature so that the phase observed is an equilibrium state. Once the microgel mixture melts completely, the temperature stage and the objective heater were cooled slowly.

Microscopy and Temperature controlling. Differential interference contrast (DIC) images were taken with an Olympus IX-70 inverted microscope using standard DIC optics. An Olympus 100× oil immersion objective (UplanFl 1.30 NA) was utilized to acquire images. Micrograph images were taken using black and white CCD camera (The Cooke Co.). The temperature of samples was controlled using a microscope objective

heater (Bioptechs) and a Peltier temperature stage (Physitemp). To avoid thermal convection, the temperature was increased very slowly during heating. Laser scanning confocal microscopy was performed on a Leica instrument using the 488 nm excitation line from an Ar^+ laser.

A. 3 Results and Discussion

Our approach for investigating the melting behavior of mixture crystals is to see the samples under a microscope after mixing two different microgels. Figure A.3-1 shows DIC images taken from TBA doped *p*NIPAm at 23 °C. As seen in figure A.3-1, *p*NIPAm microgels form ordered structure around TBA microgels resulting in a nice mixture crystal. It is amazing that much larger TBA microgels form ordered structures with *p*NIPAm microgels. One might hypothesize that TBA microgels are so soft that they can deform easily. To confirm that the brighter particles on DIC images are TBA particles, AFA incorporated TBA microgels (AFA-TBA microgels) were synthesized, and AFA-TBA microgels doped *p*NIPAm microgel crystals were observed under fluorescence microscope and confocal laser scanning microscope (CLSM). Fluorescence microscope images (not shown here) reveal that TBA microgels are sitting among *p*NIPAm microgels separately and homogeneously. When the TBA doped crystals were heated, *p*NIPAm microgels became fluid at ~ 31 °C and the brightness of TBA microgels started getting darker ~ 33 °C. At 35 °C, the microgel mixture completely and homogeneously becomes fluid as seen Figure A.3-2. It is interesting that TBA microgels in the *p*NIPAm crystal change its optical properties at temperature higher than the LCST (~ 29 °C) measured by dynamic light scattering shown in figure A.3-2.

After the doped crystal melts, the temperature stage is cut off, and cools immediately while the temperature of objective heater decreases slowly, resulting in thermal gradient in z-direction. Figure A.3-3 shows the DIC images of the TBA doped *p*NIPAm microgel crystal after heating and cooling. Interestingly, TBA microgels rise to the top while *p*NIPAm microgels sink to the bottom. The opposite thermal gradient is applied, but the result is the same as shown in figure A.3-3.

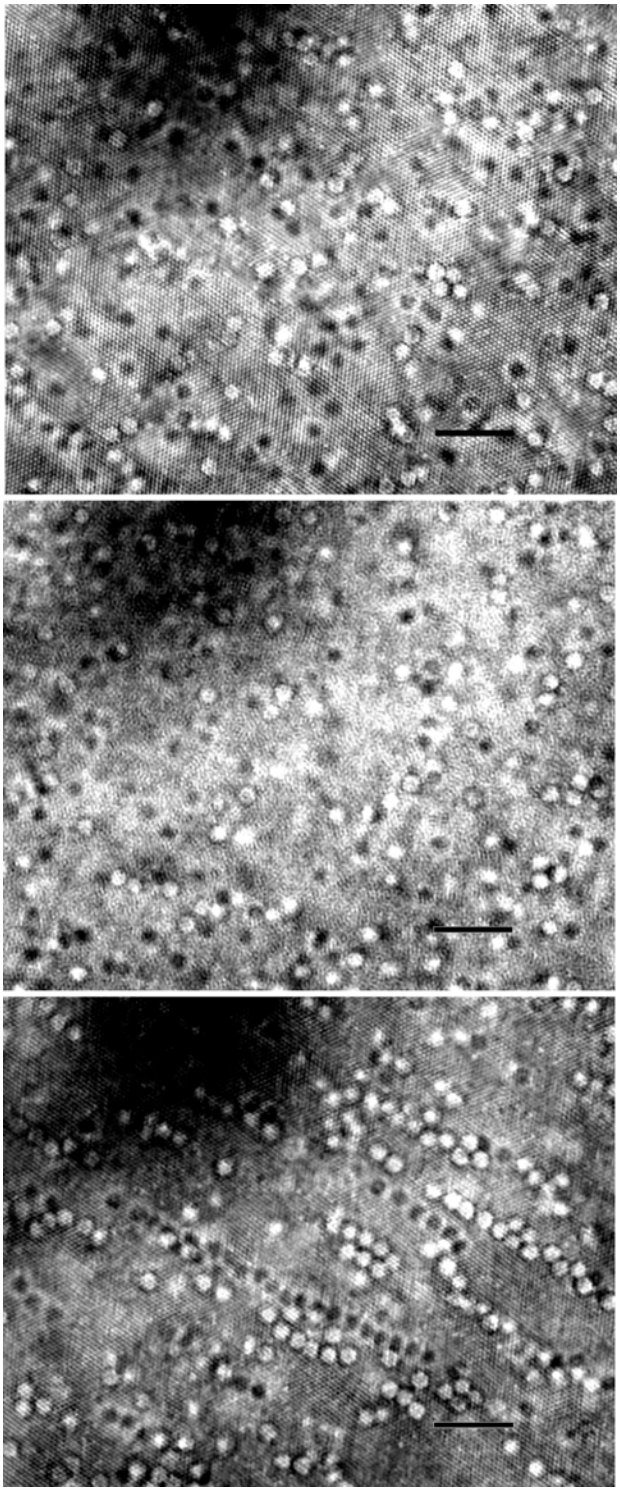

Figure A.3-1 Micrograph image of TBA-*p*NIPAm mixture sample at 23 °C. (a), (b) and (c) are taken from bottom, middle and top of the sample, respectively. Scale bar =10 μm.

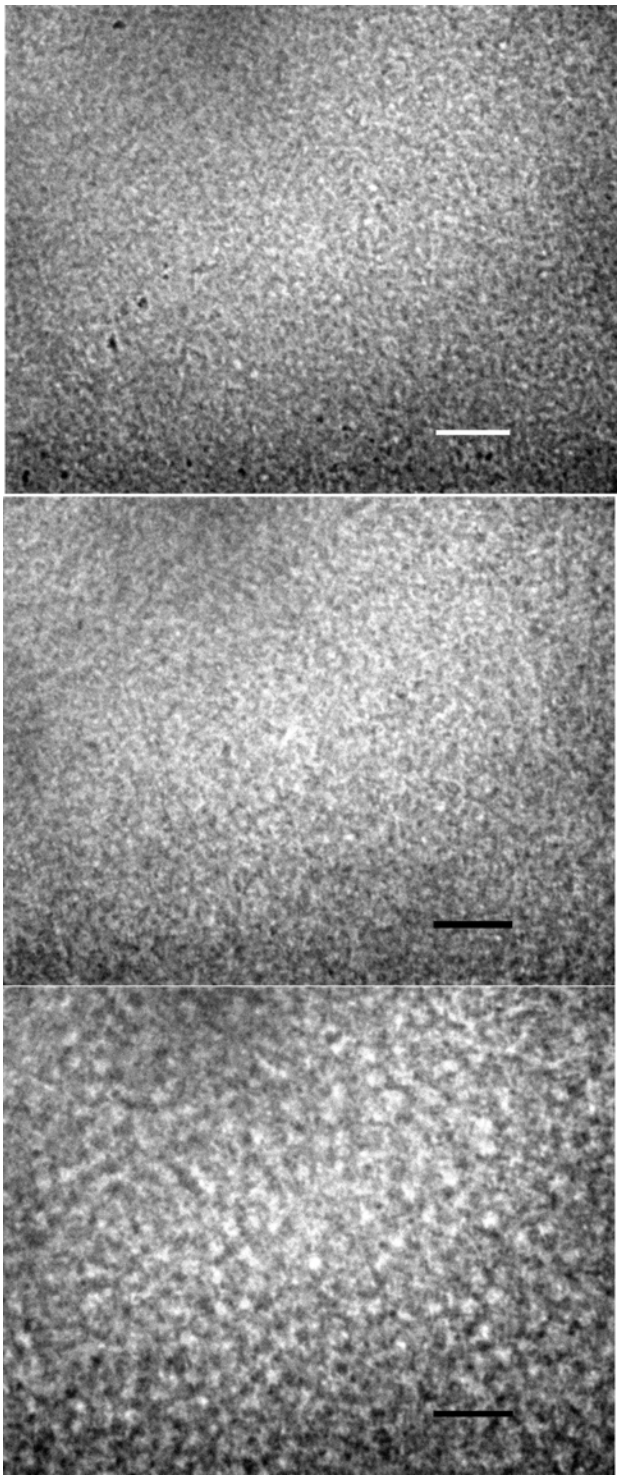

Figure A.3-2 Micrograph image of TBA-*p*NIPAm mixture sample at 35 °C. Doped microgel melts completely. (a), (b) and (c) are taken from bottom, middle and top of the sample, respectively. Scale bar =10 μm.

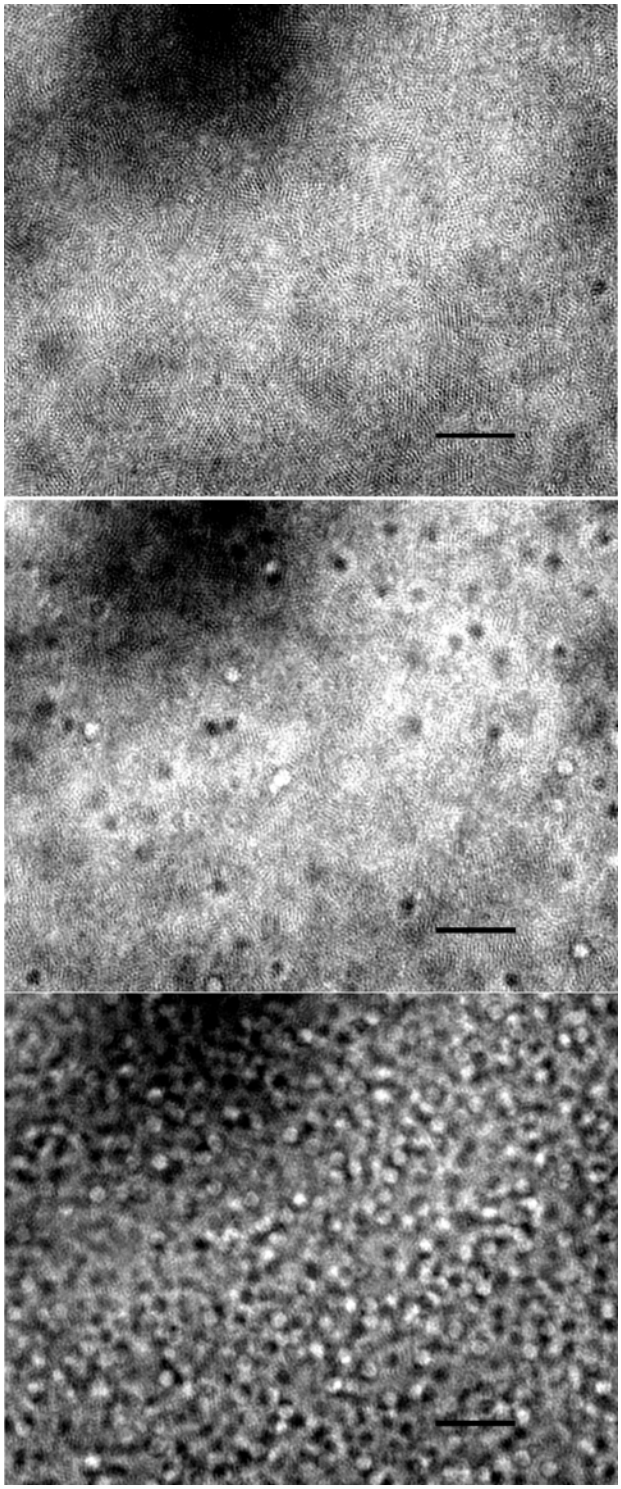

Figure A.3-3 Micrograph image of TBA-*p*NIPAm mixture sample after thermal gradient. (a), (b) and (c) are taken from bottom, middle and top of the sample, respectively. Scale bar =10 μm.

Figure A.3-4 shows the series of z-sectioning images taken from AFA-TBA doped *p*NIPAm microgel crystals after heating and cooling. The left, top image is obtained from the bottom of the doped microgel; the right, bottom image is taken from the top of the doped crystal. The distance between first and last image is ~ 64 μm. Thus, the distance between each image is ~ 2 μm. The series of z-sectioning images clearly show that more TBA microgels are on top of the mixture sample after melting and cooling.

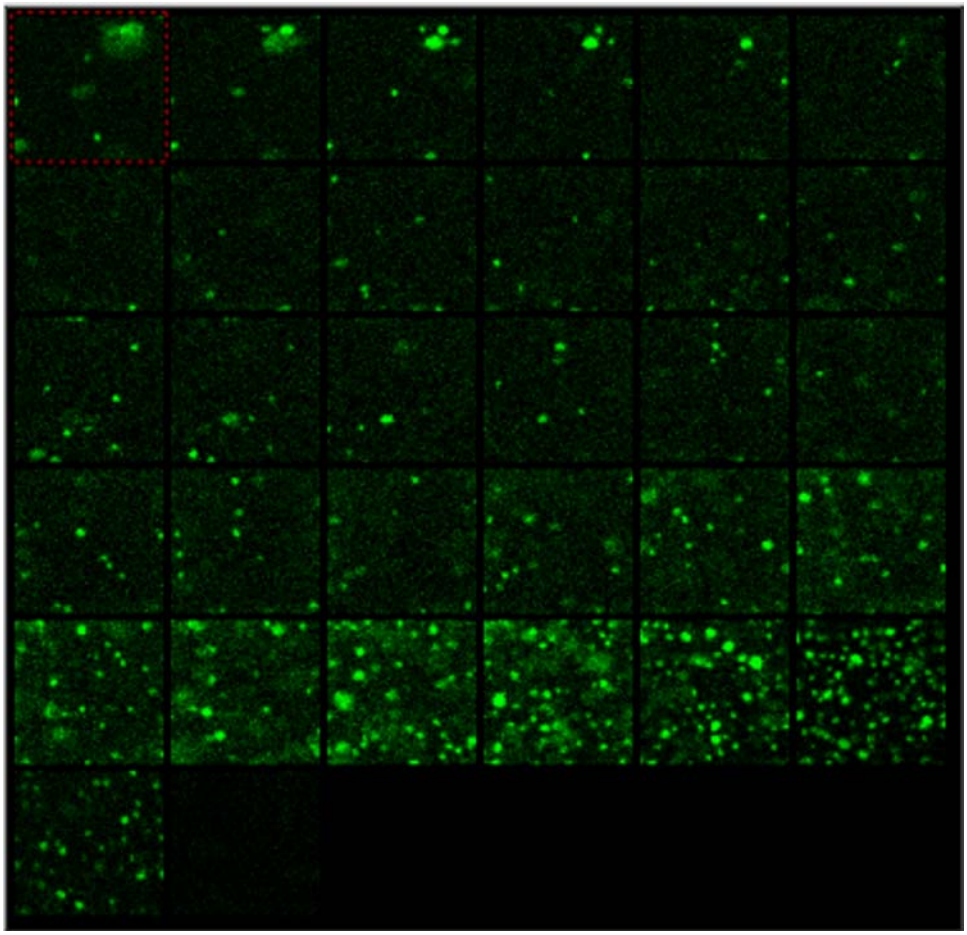

Figure A.3-4 Series of optical sections obtained by confocal laser scanning microscopy of AFA-TBA doped *p*NIPAm microgel crystals. Bright green particles are from AFA-TBA microgels. The image size is 25 × 25 × ~64 μm^3.

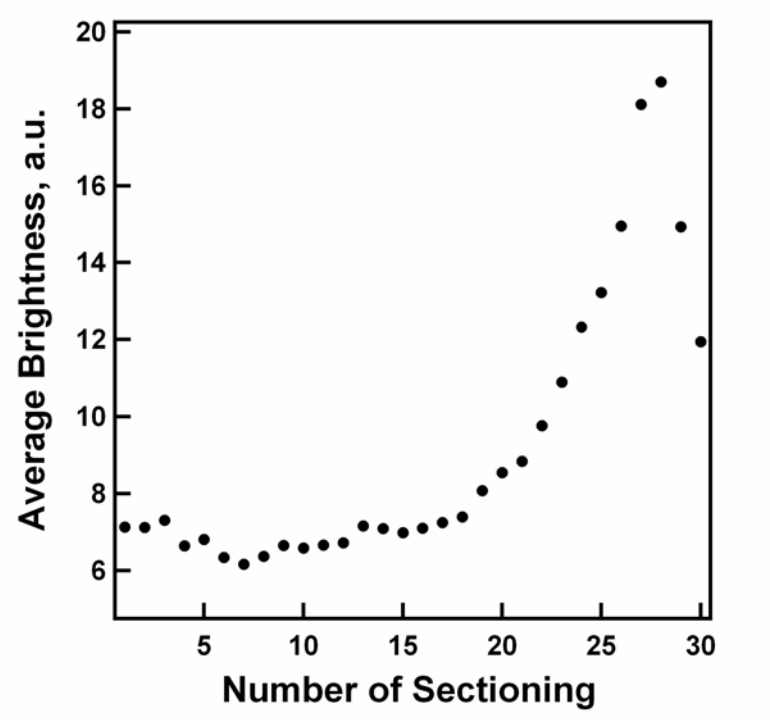

Figure A.3-5 The average brightness of each image vs. sectioning.

To show the AFA-TBA microgel distribution in a quantative way, average brightness of each sectioning is calculated by IDL analysis. The average brightness plot in figure A.3-5 again shows that the majority of TBA microgels are at the top. This result is reminiscent of Brazil nut effect observed from granular mixtures. There are reports of experiments on vertically shaken binary granular mixtures that separate into their components due to the external excitation. This well-known phenomenon, where large particles rise to the top of the mixture, is called the Brazil nut effect.[4,5] For granular mixtures, vertical shaking or vibration are used as external excitations. One can think of the convection induced by thermal a gradient may contribute to the particle segregation. Here, the convection would push the larger TBA microgels upward, while the smaller *p*NIPAm microgels would fill the void volume underneath the TBA microgel. Since it is hard to determine the density and size of the TBA and *p*NIPAm microgels at the moment

when the particle segregation occurs, it is not safe to say that Brazil nut effect is the particle segregation mechanism observed here.

Next, different microgel mixtures were prepared and tested to gain a better understanding of what causes the particle segregation shown in figure A.3-4. Table A.3-1 summarizes the doped microgels and observation after heating and cooling.

Table A.3-7. Doped microgel dispersions and the observation after heating and cooling

Sample	Dopant (diameter in nm)	Major component (diameter in nm)	After heating and cooling
1	3 mol% TBA (1.12 μm)	2% BIS *p*NIPAm (626)	TBA rose to top
2	2% BIS *p*NIPAm (632 nm)	2% BIS *p*NIPAm (334)	No change
3	5% BIS *p*NIPAm (592 nm)	2% BIS *p*NIPAm (334)	No change
4	*P*NIPAm-*co*-AAc* (636 nm)	2% BIS *p*NIPAm (626)	No change
5	PS (0.51 μm)	2% BIS *p*NIPAm (626)	No change
6	PS (1.0 μm)	2% BIS *p*NIPAm (626)	PS sank to bottom

* : Fluorescein amine was incorporated to this microgels by post polymerization.

First, the same flavor of microgels with different densities and sizes are synthesized and a two-component sample was prepared in the same manner as TBA doped *p*NIPAm microgels dispersions. 632 nm 2% BIS *p*NIPAm doped 334 nm 2% BIS pNIPAm (sample # 2) and 5% BIS *p*NIPAm doped 2% BIS pNIPAm (sample #3) were prepared. Fluorescence micrograph images (not shown here) showed no particle segregation after heating and cooling.

Second, AFA-*p*NIPAm-*co*-AAc doped *p*NIPAm microgel mixture (sample # 4) was tested. Here, AFA-*p*NIPAm-*co*-AAc microgels are larger and lighter than *p*NIPAm

microgels and the LCST is similar to TBA microgels. Here, it was not clear that particle segregation occurred after heating and cooling due to photo-bleaching. It seemed to me that there was no change after heating and cooling.

Third, non-responsive colloidal, green fluorescence labeled polystyrene (PS), doped pNIPAm microgel crystals were tested. Very small amounts of 0.51 μm radius PS (sample # 5) and 1.0 μm radius PS (sample # 4) were mixed with the 626 nm radius *p*NIPAm microgels. Since these PS latex particles are fluorescence-labeled, it is easy to distinguish PS particles under a fluorescence microscope. DIC and fluorescence microscope images revealed that both PS doped *p*NIPAm form crystalline phase at room temperature and PS particles distribute homogeneously in the *p*NIPAm microgels. When the mixture was heated, both doped crystals completely turned to fluid phase at 31 °C due to deswelling of *p*NIPAm and the PS particles were floating in fluid phase *p*NIPAm microgel dispersion. After the crystals melted completely, the thermal gradient was applied and the doped crystals were observed under a microscope. Both DIC and fluorescence micrograph images revealed that the samples did not show change in 0.51 μm PS particle distribution. However, for 1.0 μm PS doped *p*NIPAm, PS particles sank after applying the thermal gradient. This observation is reminiscent of those related to reverse Brazil nut problem.[6-9] Here, when the density/radius ratio exceeds a certain level, larger and heavier particles sank. It is hard to know accurate the density of *p*NIPAm and PS was; but one can estimate that PS particle have higher density than *p*NIPAm.

3.1 Conclusions

In this chapter, 3% TBA microgel doped *p*NIPAm microgel crystal showed interesting microgel segregation after heating and cooling the sample. Larger and probably lighter TBA particles rose to the top after melting and recrystallization. The Brazil nut effect was proposed to explain the particle redistribution. To test the microgel segregation may be caused for the same mechanism as Brazil nut effect, doped microgels made from different size and/or density microgels were prepared and the same experiments were performed as TBA doped *p*NIPAm crystals. Larger *p*NIPAm doped *p*NIPAm microgel, *p*NIPAm-*co*-AAc doped *p*NIPAm microgel mixtures were prepared and tested. None of the binary mixtures showed change after heating and cooling the mixtures samples. PS doped *p*NIPAm crystals were prepared to perform the same experiments as TBA doped *p*NIPAm crystals. After heating and cooling, PS particles similar size to *p*NIPAm particles did not show segregation; and an experiment with larger PS particles where they sank to the bottom could be explained by reverse Brazil nut problem.

At this point, it is not clear what causes TBA microgels to rise during cooling. To understand the microgel segregation mechanism, 1) density and size of microgels in dispersion at a specific temperature need to be calculated, 2) larger and heavier microgel doped crystals need to be tested. Here, the density to size ratio is under normal Brazil nut problem conditions.

Besides the particle segregation, it is interesting that TBA microgel in TBA doped *p*NIPAm crystals changed its optical properties at higher temperature than TBA microgel's LCST. Also, it seems to me that TBA doped *p*NIPAm crystals melt at higher

temperature than pure *p*NIPAm crystals or PS doped *p*NIPAm crystals. It would be interesting to investigate the recrystallization processes of doped crystals after melting.

References

(1) Synthesis and characterization of ph-responsive copolymer microgels with tunable volume phase transition temperatures, J. D. Debord and L. A. Lyon *Langmuir* **2003**, *19*, 7662.

(2) Color-tunable colloidal crystals from soft hydrogel nanoparticles, J. D. Debord, S. Eustis, S. B. Debord, M. T. Lofye and L. A. Lyon *Adv. Mater.* **2002**, *14*, 658.

(3) Influence of particle volume fraction on packing in responsive hydrogel colloidal crystals, S. B. Debord and L. A. Lyon *J. Phys. Chem. B* **2003**, *107*, 2927.

(4) Brazil-nut effect: Size separation of granular particles, M. E. Moebius, B. E. Lauderdale, S. R. Nagel and H. M. Jaeger *Nature* **2001**, *414*, 270.

(5) Why the brazil buts are on top: Size segregation of particulate matter by shaking, A. Rosato, K. J. Strandberg, F. Prinz and R. H. Snowndsen *Phys. Rev. Lett.* **1987**, *58*, 1038.

(6) Variational approach to hard sphere segregation under gravity, J. A. Both and D. C. Hong *Phys. Rev. Lett.* **2002**, *88*, 124301.

(7) Reverse brazil nut problem: Competition between percolation and condensation, D. C. Hong, P. V. Quinn and S. Luding *Phys. Rev. Lett.* **2001**, *86*, 3423.

(8) Does the reverse brazil nut problem exist?, G. A. Canul-Chay, P. A. Belmont, Y. Nahmad-Molinari and J. C. Ruiz-Suarez *Phys. Rev. Lett.* **2002**, *89*, 189601/1.

(9) Reversing the brazil-nut effect: Competition between percolation and condensation, A. P. J. Breu, H. M. Ensner, C. A. Kruelle and I. Rehberg *Phys. Rev. Lett.* **2003**, *90*, 014302/1.